EPIGENETIC ALTERATIONS ASSOCIATED WITH CTCF EXPRESSION IN PROSTATE CANCER

by

Nathan Allan Damaschke

A dissertation submitted in partial fulfillment

of the requirements for the degree of

Doctor of Philosophy

(Cancer Biology)

at the

UNIVERSITY OF WISCONSIN-MADISON

2017

Date of final oral examination: 12/12/2016

The dissertation is approved by the following members of the Final Oral Committee:

David Jarrard, Professor, Urology
Wei Xu, Professor, Oncology
Paul Marker, Professor, Pharmaceutical Sciences
John Svaren, Professor, Comparative Biosciences
Michael Gould, Professor, Oncology

ABSTRACT

Epigenetic Alterations Associated with CTCF Expression in Prostate Cancer

Nathan Allan Damaschke

Under the supervision of Dr. David F. Jarrard

At the University of Wisconsin-Madison

CCCTC-Binding Factor (CTCF), an 11-zinc finger DNA-binding protein, functions in a variety of chromatin and transcriptional regulation events. CTCF exhibits DNA methylation sensitive binding, but little is known about the functional consequence of altered CTCF levels on epigenetic regulation or the pattern of altered CTCF in prostate cancer. Decreased CTCF expression causes loss of imprinting at the *IGF2/H19* imprint control region, a common epigenetic alteration seen with aging in the prostate. Our studies analyzed the contribution of aberrant CTCF function to prostate cancer development and progression. Using a mouse model that abolishes CTCF insulator activity at the *Igf2/H19* imprint control region, we demonstrated that increased IGF2 levels via loss of imprinting increases the frequency of prostatic intraepithelial neoplasia. Increased IGF2 lead to increased intracellular signaling, of phosphorylated Extracellular Signal-Regulated Kinase 1/2 (p-ERK) and phosphorylated RAC-alpha serine/threonine-protein kinase (p-AKT), and proliferation. In human prostate tissues, we observed a similar correlation between these markers and increased IGF2, supporting these findings relevance in human disease.

We characterized the expression of CTCF and other proteins involved in CTCF function in human prostate samples. These studies demonstrated that decreased CTCF expression was prevalent in disease and the expression of proteins which interact with CTCF are also frequently altered. We found prostate cancer samples exhibit decreased Chromodomain Helicase DNA Binding Protein 8 (CHD8), a protein that complexes with CTCF in transcriptional regulation. Altered CHD8 expression was found to correlate with a number of patient clinical characteristics, including disease recurrence. These findings suggest CHD8 may contain clinical value as a biomarker, an area of critical importance in prostate cancer treatment and diagnosis.

Finally, we investigated the epigenetic impact of decreased CTCF expression in prostate cancer. We found human prostate cancer samples with CTCF genomic copy number loss display frequent hypermethylation at CTCF binding sites. We modeled decreased CTCF expression *in vitro* and showed knockdown leads to DNA methylation alterations genome-wide. With this model, we recapitulated the human prostate cancer findings, that decreased CTCF expression leads to increased DNA methylation at CTCF binding sites. Furthermore, decreased CTCF was found to transcriptionally regulate genes involved in stress response pathways, demonstrating its role as a tumor suppressor and suggesting epigenetic alteration of stress response pathways is important for CTCF mediated disease development.

We conclude that decreased CTCF expression is an important step for prostate cancer development and progression through epigenetic alteration of the neoplasia promoting *IGF2* gene and DNA methylation alterations genome-wide.

ACKNOWLEDGEMENTS

This thesis could not have been completed without the guidance and help of many wonderful people both inside and outside of the Jarrard Lab. My utmost gratitude goes to my supervisor Dr. David Jarrard for his support and guidance during my tenure in his laboratory. His untiring confidence in those around him led me to believe in my abilities and use them to their fullest extent. With his encouragement, I have learned a number of techniques and skills that will be absolutely invaluable to my future as a scientist. His willingness to brainstorm out loud with me helped me to learn how to approach and attack the questions at hand. I will never forget and always value the time spent under his guidance.

I would like to thank all of my committee members: Dr. John Svaren, Dr. Wei Xu, Dr. Paul Marker, and Dr. Michael Gould. Their insightful inputs helped to push my projects forward. They encouraged me to broaden my knowledge base and pursue opportunities I may have otherwise overlooked, including reaching out to collaborators that were instrumental in completing these projects.

I highly value the opinions of every committee member and would like to specifically thank them individually. Dr. John Svaren was always willing to participate in scientific discussion and brainstorming sessions, he provided invaluable advice and suggestions that I believe significantly improved the quality of this thesis research. Dr. Paul Marker often brought a new perspective, which encouraged me to think about the problem at hand from a different angle, in addition he urged me to keep thinking about the future and the next steps. I thank Dr. Wei Xu for her thoughtful advice and encouragement both scientifically and in aiding in the navigation to complete my degree and take the next steps in my pursuit

of science. I thank Dr. Michael Gould for his always insightful comments, his experience in science and on campus helped open new doors for addressing research questions and collaborations.

I would like to thank all the members of the Jarrard laboratory that have come, gone, or stayed over the years. They are an exemplary group for the team approach to scientific research. An immense thank you to those who worked closely with me on these projects, including Amanda Krueger, Jennifer Wagner, Dr. Sachin Bhusari, Dr. Michael Blute, Tianyu Yao, and Mele Avilla, without them this work would not have been possible. In particular, I would like to thank Dr. Bing Yang for all of her help and advice during my tenure in the lab. I hold an indescribable amount of respect and admiration for Bing. She is a model scientist that I can only hope to emulate in the future. Her hard working attitude has always encouraged me to never stop attempting to solve the problem at hand.

I am grateful to many other people at the University of Wisconsin for their help and collaborative efforts. Including Wei Huang and Sally Drew of the Translational Pathology Lab, Dr. Weixiong Zhong for his pathologic expertise, and Dr. Avtar Roopra and Dr. Sunduz Keles for their help and advice in bioinformatics and statistical analysis.

Finally, my heartfelt gratitude is extended to all of my family and friends for enduring with me and encouraging me throughout this process. My parents, Jeff and Jeanne, have always motivated me to pursue my dreams and have been my biggest role models. They have always shown me no problem is too large to tackle and that hard work pays off. I would be nothing without their love, support, and encouragement. Lastly, my everlasting gratitude to my partner and best friend Ally. She has encouraged me with every step, every day. Her hard work and unwavering support motivated me, even in the toughest of times, to never give up.

TABLE OF CONTENTS

LIST OF TABLES AND FIGURES

ABBREVIATIONS

5-azadC	5-aza-2'-deoxycytidine
5hmC	5-hydoxymethyl cytosine
5mC	5-methyl cytosine
AKT	RAC-alpha serine/threonine-protein kinase
AREAS	Age-Related Epigenetic Alterations inducing Susceptibility
ASM	allele-specific methylation
BORIS	Brother Of The Regulator Of Imprinted Sites
Bp	base pairs
BPH	benign prostatic hyperplasia
cDNA	complementary deoxyribonucleic acid
CGI	cytosine-phospho-guanine island
CHD8	Chromodomain Helicase DNA Binding Protein 8
ChIP	chromatin immunoprecipitation
CN	copy number
CNA	copy number alteration
CpG	cytosine-phospho-guanine
CTCF	CCCTC-Binding Factor
DMR	differentially methylated region
DNA	deoxyribonucleic acid
DNMT	DNA methyltrasnferase
Dox	doxycycline
ERK	extracellular regulated protein kinase
EZH2	Enhancer of Zeste Homolog 2

FBS	fetal bovine serum
GC	guanine-cytosine
GO	gene ontology
GSEA	gene set enrichment analysis
GSTP1	Glutathione S-Transferase Pi 1
ICR	imprint control region
IGF2	Insulin-like Growth Factor 2
IHC	immunohistochemistry
Kb	kilobase
kDA	kilodalton
LOI	loss of imprinting
MAPK	Mitogen-activated Protein Kinase
MeDIP	Methylated deoxyribonucleic acid immunoprecipitation
mRNA	messenger ribonucleic acid
NF-κB	nuclear factor kappa-light-chain-enhancer of activated B Cells
NKX3.1	NK3 Homeobox 1
p-AKT	phosphorylated-AKT
PCa	prostate cancer
p-ERK	phosphorylated-ERK
PIN	prostatic intraepithelial neoplasia
qPCR	quantitative polymerase chain reaction
RNA	ribonucleic acid
TCGA	The Cancer Genome Atlas
TFBS	transcription factor binding site

Chapter I

General Introduction

Parts of this chapter have been adapted from:

Damaschke NA, Yang B, Bhusari S, Svaren JP, Jarrard DF. Prostate 2013;73:1721-30

Introduction

Prostate cancer is a significant cause of death among males in the United States. Despite its prevalence, many unknowns exist pertaining to the molecular mechanisms contributing to prostate cancer development and progression. One of the most perplexing unknown is how age contributes to prostate cancer. Advancing age is significant risk factor for prostate cancer development. Increasing research demonstrates epigenetic alterations are experienced in aging human tissues (1,2). The accumulation of epigenetic changes has been postulated to contribute to the age-related incidence of a number of diseases, including prostate cancer.

Mechanistically, the reasons why epigenetic changes occur with age is undefined. It is unknown whether these alterations occur at random or if specific intracellular factors are involved dictating epigenetic change. One clue to this question is the fact that a number of epigenetic alterations commonly occur in the human prostate (3), suggesting a potential regulatory factor. One such alteration is a loss of the Insulin-like Growth Factor 2 (*IGF2*) gene imprint, which has been attributed to altered CCCTC-binding Factor (CTCF) expression and binding patterns (4). These findings implicate CTCF as a potential regulator of age and cancer related epigenetic alterations.

The Prostate and Prostate Cancer

The prostate is a glandular organ situated at the base of the bladder involved in sexual function in mammals. Initiation of prostate development occurs in late embryogenesis and continues to grow until the completion of puberty (5). The fully developed human prostate is located at the base of the bladder, surrounding the urethra. The currently accepted concept of human prostate anatomy describes the prostate as consisting of three zones. The central zone, surrounding the ejaculatory ducts, the

transition zone, surrounding the urethra, and the peripheral zone, the largest area of the prostate located closest to the rectum (6). The peripheral zone is the site in which a large majority of prostate cancers develop.

Prostate cancer (PCa) is the most common cancer male cancer in the U.S. and the second leading cause of cancer deaths (7). Older age is a significant risk factor, with histologic PCa being found in 60% of men by the age of 70 (8). Histologically, similarities are found between prostate cancer and other epithelial cancers. In the normal prostate, glands consist of luminal columnar epithelial cells and a layer of basal cells with rare neuroendocrine cells. Luminal epithelial cells are most commonly identified as the proliferative cell type in neoplasia and cancers in the prostate (9). Interestingly, PCa is often multifocal, in a single prostate several distinct foci of prostatic intraepithelial neoplasia (PIN) and cancer can be found in radical prostatectomy specimens (10), suggesting a field of susceptibility develops in the prostate encouraging tumor formation.

Prostate Cancer and Epigenetics

Interest has arisen in an epigenetic basis underlying this susceptibility of the prostate and other aging-related cancers, including cancers of the colon and breast. Monozygotic twins studies have been instrumental in demonstrating epigenetic changes occur during aging as a result of both stochastic processes and environmental exposures (2). The accumulation of these alterations with age may promote fields of susceptibility to oncogenic triggers in aging organs that eventually give rise to cancer. This is one aspect of the ‘field effect’ that is manifested in the known multifocality observed in radical prostatectomy specimens (10). A number of genetic and epigenetic changes throughout the histologically normal aging prostate have recently been identified.

Epigenetics refers to functionally relevant genomic information, other than the DNA

sequence, that is heritable during cell division (11). There are several major types of epigenetic modifications including DNA methylation, genomic imprinting, and histone modifications. Altered epigenetic marks modify chromatin structure and alter gene expression without the requirement for changing DNA sequence (12). These epigenetic modifications are crucial during embryonic development. More recently it has been recognized that aberrant epigenetic reprogramming can lead to altered gene expression associated with cancer development and progression (13).

An epigenetic field effect, or field defect, within the context of cancer is often thought of as resulting from the presence of a tumor. However, recent evidence suggests these changes may occur with age and potentially even precede the formation of cancer. We have termed these changes *A*ge-*R*elated *E*pigenetic *A*lterations inducing *S*usceptibility (AREAS) (3). These age-related changes may be widespread throughout the prostate and can result in gene expression changes that induce or are selected for in the subsequent tumor.

DNA Methylation in Aging and Cancer

DNA methylation was the first epigenetic mark to be implicated in human cancer (11). Alterations of DNA methylation in cancer and aging are typically characterized as global hypomethylation and regional hypermethylation. Methylation occurs at cytosine bases, typically CpG dinucleotides. CpG dinucleotides tend to cluster in regions called CpG islands (CGI), which can be defined as stretches of DNA (>200 bases) with a GC content greater than 50% and an observed:expected ratio of more than 0.6 (14). CpG dinucleotides occur in only ~1% in the mammalian genome, however 60% of human promoters are associated with CGI's in a mostly unmethylated state (15). DNA hypermethylation refers to the gain of methylation at sites that are typically unmethylated and occurs mainly at CGIs.

CGI hypermethylation is often associated with gene silencing, achieved by blocking DNA binding proteins, such as transcriptional regulators, that result in decreased transcription. Methylated DNA also acts as a recruitment site for methyl-CpG-binding domain (MBD) proteins that can elicit a chromatin silencing response when bound (16).

DNA methylation also occurs at sites outside CGIs including island shores (defined as up to 2 kb outside of CGIs), gene bodies, and gene poor areas including repetitive sequences, retrotransposons, and intergenic regions. Human tumor cells often experience a global hypomethylation, despite hypermethylation at specific sites, as a result of hypomethylation at repetitive elements and CpG rich-satellites (17). Hypomethylation in repetitive sequences and retrotransposons, found in gene poor areas, commonly occurs in PCa and may contribute to metastatic tumor heterogeneity (18). Their properly methylated state protects genomic integrity by blocking reactivation of these endoparasitic sequences (16,17).

Previous analyses of global methylation levels have been conducted in the prostate comparing advancing pathologic conditions. In general, more severe conditions experience greater global hypomethylation. Bedford *et al.* found 5-methylcytosine (5mC) content of prostatic DNA significantly decreased from normal (4.01% $\pm$ 0.11) to BPH (3.62% $\pm$ 0.14), and further decreases in metastatic PCa (3.29% $\pm$ 0.24) (19). Other studies have also found more extensive methylation loss in high grade and metastatic cancers (18,20). Additionally, DNA hypomethylation is also found in the cancer precursor lesions, prostatic intraepithelial neoplasia (PIN), when compared to normal prostate tissue suggesting methylation alterations may precede frank cancer (20,21).

A characterization of global methylation patterns in the aging peripheral prostate has not yet been performed. However, given the clinical similarities between the colon and

prostate, including the prevalence with aging and multifocality, studies of colon tissues may be informative. In the colon, global demethylation with aging correlates with increased genomic damage, and precedes cancer development (22). Furthermore, patients with more extensive hypomethylation in normal colon tissue are predisposed to the development of multiple tumors (23). Some have hypothesized hypomethylation is more important to the progression of PCa and not particularly a consequence of aging in the prostate (18). Research examining hypomethylation in the aging human prostate is required to definitively test this.

Genome-wide methylation studies and DNA methylation microarray sets are useful tools for the characterization of site specific methylation changes and have been used to document methylation changes in the prostate (24). One of the first hypermethylation events demonstrated in human aging involved hypermethylation at the estrogen receptor gene promoter in normal colon tissue that was subsequently selected for in the colon cancers studied (25). Other gene hypermethylation events in the colon with aging include *N33, MYOD, P16(INK4A), MLH1,* and *DAPK* (26,27). Of these genes, *MYOD*, *P16(INK4A),* and *MLH1* have all been implicated as tumor-suppressor genes, further, *MLH1* has been implicated in DNA mismatch repair. These studies have shown gene silencing by promoter hypermethylation events can have functional relevance in age-related tumorigenesis.

One of the few papers to exclusively examine DNA methylation in aging prostate tissues was performed by Kwabi-Addo *et al* (28). They analyzed 9 genes known to be hypermethylated in PCa in the peripheral prostate tissues of men without cancer. They found increased promoter methylation with aging in 5 of these genes (*RARβ2, RASSF1A, GSTP1, NKX2-5,* and *ESR1*). This frequent finding of hypermethylation with aging in loci altered with cancer (56%) is striking and suggests AREAS may occur more commonly than

anticipated. In another study, Henrique *et al.* found *APC* and *RARβ2* were more frequently hypermethylated with aging in normal prostate samples from patients assessed across a narrow age range (50-72y) (29). Frequent *RARβ2* silencing by epigenetic events may desensitize prostate cells to retinoic acid (RA) treatment. In response, RA treatment coupled with epigenetic modulators have demonstrated promise as viable treatments (30). This specific case demonstrates how epigenetic modulators may be required to sensitize tumors to certain therapeutic interventions.

In prostate tissues taken from men *with cancer*, several genes undergo increased methylation with aging in the normal appearing tissue. Some genes analyzed in these studies were previously found to precede disease including *NKX2-5*, and *GSTP1* (28,31). Others that demonstrate a positive association with age include *TIG1, CDH12, EGFR5, MCAM, SLIT2* (31), ESR1 (31,32), and DLC-1 (33). Vasiljevic *et al.* noted a moderate effect of age common to increasing methylation of all genes analyzed in their study (31). The functional consequence and mechanism of these methylation changes involved with aging and cancer have not been investigated to date.

In an effort to compare aging histologically normal tissue in men with and without cancer, our lab performed a genome-wide analysis of DNA methylation changes in normal peripheral prostate tissue at 385,000 loci based on the ENCODE18 genomic sequence(34). There were 615 significantly differentially methylated probes in tumor associated tissues found. The majority (87%) of loci demonstrated hypomethylation and the remainder hypermethylation. Notably, these arrays were not focused on promoter CGIs and reflected more global changes in methylation. This pattern of methylation fits the idea that global decreases in methylation parallel hypermethylation at CpG islands. A closer look at some of the more significantly altered probes associated with CGIs indicate many of these

changes occurred at the edges or periphery of the islands consistent with data that DNA methylation spreads from the edges of CGIs inward (35).

This study also examined whether the DNA methylation defect was found adjacent to tumors suggesting a peritumor effect, or at a distance (>1cm) raising the possibility of a more widespread field defect encompassing the peripheral prostate. The loci used for mapping the extent of this field defect did not degrade with increased distance to the main tumor focus suggesting a spatially widespread field of cancer susceptibility consistent with an age-related phenomenon. Methylation changes, both hyper- and hypomethylation, have been found in the colon with aging that are postulated to increase cancer risk (25,36,37). Further data will determine whether a similar aging-dependent field of susceptibility also occurs in the prostate. Interestingly, not all genes altered in the prostate were enriched for in the associated tumors. This may suggest that some changes (e.g. *FGF-1*) are important in the initiation of PCa that are not selected for as the tumor develops. This study also identified several changes associated only with the development of high-grade cancer. This suggests a unique biologic background may give rise to these more aggressive variants. These changes may be important in identifying not only the disease at an earlier timepoint, but also the genesis of high grade cancer.

Recently, the epigenetic and cancer fields have seen a growing interest into 5-hydroxymethylcytosine (5hmC). 5mC found in CpG dinucleotides can be converted to 5hmC by the Ten-eleven translocation 1-3 (TET1-3) enzymes (38). In general, 5hmC presence correlates with tissue differentiation, with terminally differentiated cells containing higher 5hmC content than tissue stem/progenitor cells (39). The conversion of 5mC to 5hmC by TET enzymes is thought to be part of a stepwise mechanism in the demethylation of the target cytosine (38,40). A study classifying 5hmC levels in various tissues found that

carcinoma of the prostate, breast, and colon all had a significant reduction in 5hmC levels by immunohistochemistry (39). Of interest, small low grade lesions also contained significant reduction in 5hmC levels suggesting it may be an early step in prostate tumorigenesis (39). TET activity may be downregulated by environmental stressors, providing a link between 5hmC, aging and cancer development (41).

Genomic Imprinting

Genomic imprinting is an epigenetic mechanism in which individual alleles are silenced based on the parent of origin. Imprinted alleles are established with blastocyst formation, and disruption results in a lethal phenotype (42,43). Expression occurs in a developmental and tissue-specific manner. Imprinted genes generally reside in clusters and roughly 100 human genes have been identified thus far (42). It is postulated that this grouping allows coordinated control by imprinting centers also known as imprint control regions (ICRs) (44). Imprinting deregulation was initially recognized in childhood syndromes including Prader-Willi, Angelman, Beckwith-Wiedermann (BWS), and Silver-Russell (42). In BWS a loss of imprinting (LOI) at the *Igf2/H19* and *KCNQ1-KCNQ10T1* domains leads to fetal and postnatal overgrowth along with a much higher incidence of cancer (45). These diseases provide evidence that the proper regulation of imprinting is required for normal growth and maturation.

The *Insulin-like Growth Factor 2 (IGF2)* gene and its 3' neighbor *H19* on 11p15 comprise one of the most widely studied ICRs. The role of DNA methylation and the insulator gene CTCF have been characterized in establishing the imprinted allele (Figure 1A). *IGF2* is a potent growth factor and loss of *IGF2* imprinting in normal tissues has been casually associated with an increased cancer incidence in the colon (46,47). *IGF2* is known to act upon epithelial cells predominantly in a paracrine fashion due to its higher expression in stromal cells. However, evidence for autocrine loops in cultured human prostate cells

has been demonstrated (48). LOI of *IGF2* has also been found in other types of adult cancers including gastric (49), ovarian (50), and esophageal (51). The spatially distinct relationship of disease in the prostate presents a unique scenario. Initially, biallelic expression of the *IGF2* gene was shown in both cancerous and associated histologically normal tissue in the peripheral prostate, but not in BPH of the transition zone, which is centrally located and embryologically distinct (52). We have found that this LOI marks a widespread field effect throughout the peripheral prostate that may contribute to the multifocality of the disease (53). In mice and in humans, a clear erosion of the *IGF2* imprint can be seen with aging in the prostate (4). In the mouse this change is not seen in other tissues such as the kidney, liver, or the adjacent seminal vesicle. These data provide evidence that AREAS may underlie the predisposition of the prostate for cancer formation.

The *Igf2/H19* locus demonstrates how DNA methylation and insulator proteins, such as CTCF, are both required to maintain imprinting status. Our studies indicate CTCF binding decreases at the *Igf2/H19* ICR in the aging mouse prostate (4). As a genomic insulator, CTCF binds widely throughout the genome and is implicated in epigenetic homeostasis (54). This involvement with both imprinting and epigenetic processes makes CTCF an important candidate for the dysregulation of genes seen in aging and PCa.

Loss of Imprinting and Carcinogenesis

These studies and many others establish a link between LOI and carcinogenesis. The understanding of when and how these changes occur is still evolving. Mutations in imprinted genes are rare and would only explain a focal cancer development. Environmental stressors or inherent susceptibility, or a combination of the two may better explain the widespread relaxation of an imprint within a tissue. Environmental exposures may induce epigenetic changes or elicit signaling anomalies leading to widespread reprogramming at imprinted regions.

Similar to DNA methylation, imprinting marks, such as the differentially methylated *Igf2/H19* imprint control region, can be altered by oxidative stress and diet. A mouse model of oxidative stress generated by deletion of superoxide dismutase (*SOD*) show a decrease in DNA methylation at the *Igf2* promoter and CTCF binding site 3 in the ICR (55). These increases correlated with a 2-fold decrease in *Igf2* expression at 12 months. Changes in *Igf2* expression are consistent with other studies and may be due to the sensitivity of the *Igf2/H19* region to *de novo* methylation (56). Other known factors that modulate the *Igf2* imprint, such as CTCF, also represent a potential mechanism underlying changes with oxidative and other stress.

Igf2 is a well-studied imprinted locus, however other imprinted genes are also susceptible to changes in methylation. Holm *et al.* used a transient demethylation model to generate mice lacking imprinting at all loci. Chimeric adult mice derived from this model demonstrate widespread LOI that resulted in increased tumorigenesis in the liver and intestine (57). A study on mouse mammary carcinogenesis demonstrated imprinted genes may play a role in AREAS development in breast cancer. The imprinted gene *Decorin* decreased with age and was associated with spontaneous tumor development (58). Changes in imprinting may also demonstrate transgenerational effects. Cui *et al.* found an association between LOI in colon tissues and a positive family or personal history of colorectal neoplasia suggesting altered imprinting may be involved in disease susceptibility (46).

Novel techniques are opening new doors in the research of imprinted genes. The use of transcriptome sequencing was used to probe imprinted genes throughout the genome (43). This early study identified six novel imprinted genes in mouse tissues. More recently, an interest in allele-specific methylation (ASM) has arisen in the development of

disease (59). Differential methylation of alleles may occur during PCa progression and is more widespread than previously thought occurring at greater than 30% of CpGs in hypermethylated or hypomethylated CGIs in one study (60). These new interests may aid in our understanding of complex disease genetics and provide new insights into aging and cancer.

Histone Modifications

Histones are fundamental building blocks for the tightly regulated chromatin packaging within the genome. The nucleosome consists of two of each of the core histones, (H2A, H2B, H3, and H4), with 147 base pairs of DNA wrapped around the octamer (61). Histones have amino-terminal tails that are subject to post-translational modifications resulting in the histone code. Acetylation and methylation are the most widely studied modifications in aging and have been implicated in transcriptional activation or repression. Acetylation is generally associated with euchromatin and an active transcription profile. Methylation of histone tails presents a more complex situation, where activation or repression is linked to the position of the residue within the histone (62). Each of these modifications affects chromatin in a different way, by either altering molecular associations of chromatin or recruiting other proteins to the chromatin.

Studies have suggested that alterations in histone modifications are important in PCa (63). Immunohistochemical analysis of primary prostatectomy tissue samples revealed an association of H3K18Ac, H3K4Me2, H4K12Ac, and H3K9Ac with increasing tumor grade (64). Remarkably, by analyzing the percentile staining of just two modifications, H3K4Me2 and H3K18Ac, patients could be grouped into lower and higher risk recurrence risk groups. In normal prostate cells active gene promoters are associated with H3 lysine 4 methylation (H3K4me2 and H3K4me3) and H3 lysine 9 acetylation (H3K9acetyl). These are replaced by repressive marks (H3K9me2, H3K9me3, and

H3K27me3) in transcriptionally silenced genes (63). H4K20me1 was shown to identify CRPC, while H4K20me2 correlated with different stages of PCa (63).

To date, no analyses have been performed on the state of histone modifications during aging in the prostate. Decreases of H3K4me2 occur with aging human fibroblasts *in vitro* (65). DNA methyltranferases regulate aging in stem cells via Enhancer of zeste homolog 2 (*EZH2*), an important histone methylase in PCa progression (66). Studies of monozygotic twins reveal acetylation of histones H3 and H4 patterns diverge between twins with increasing age in various tissues, including lymphocytes and sketetal muscle (2). Recent evidence suggests that modulating histones may impact prostate function. In a study involving men on long term antiepileptics (e.g. valproic acid, carbamazepine, oxcarbazepine, lamotrigine, and levetiracetam) drugs known to inhibit histone deacetylases (HDACs), treatment resulted in lower PSA levels than age-matched counterparts (67). This effect was marked in older men. As HDAC inhibitors, these drugs may impact the androgen receptor with aging resulting in lower PSA levels. This study provides intriguing data suggesting a role for histone modifiers in cancer risk.

These epigenetic states pose questions about whether these marks have a causal or bystander relationship with cancer development (68). Furthermore, to date there have been no demethylases identified or other clear mechanisms that underlie the significant reduction of H4K20me1/2 or other histone methylation. The aging studies clearly indicate histone modifications may be altered by environmental factors and as such represent an area of research with regard to epigenetic cancer susceptibility.

The Role of CTCF in Genome Regulation

CTCF was initially discovered in the search for factors binding to *Myc* regulatory regions (69), discovered to bind the CCCTC DNA motif. Since its initial characterization,

CTCF has been found to participate in a variety of genome regulatory roles by binding varying DNA motifs, earning the description as a “multivalent” transcription factor. DNA recognition and binding is achieved through 11 zinc finger DNA-binding motifs. Studies have demonstrated CTCF can act as both a positive (70,71) and negative (69,72) regulator of transcription. Studies utilizing chromatin immunoprecipitation followed by DNA sequencing (ChIP-Seq) demonstrated CTCF binds widely throughout the genome. Initial ChIP-Seq experiments in resting $CD4^+$ T cells identified 26,814 DNA binding sites (73). Rapid advancements in sequencing and data processing technologies have allowed CTCF binding site characterization in a wide variety of cell types. In the prostate, LNCaP cancer cells demonstrated ~60,000 DNA binding sites genome wide (GEO: GSE33213).

The ubiquitous nature of CTCF binding activity facilitates its function as the main chromatin insulator in mammalian cells. As mentioned in the discussion of genomic imprinting, CTCF insulator activity dictates *IGF2* and *H19* gene expression through blocking of downstream enhancer sequences (74). These enhancer blocking activities have been demonstrated at a number of gene loci including the β-globin (75), *DM1* (76), T cell receptor α, and *DAD1* genes (77).

In addition to enhancer blocking insulation, CTCF also participates in barrier insulation of chromatin. Barrier insulation is the demarcation of euchromatin and heterochromatin domains. CTCFs barrier insulation is evidenced in ChIP-Seq experiments showing CTCF binding the boundaries of repressive chromatin domains marked by H3K27me3. Further, complementary patterns between repressive H3K27me3 and active H2K5ac are separated by CTCF-binding sites (78).

Most recently, significant interest has been focused on CTCF genome-wide insulation through chromatin looping activity. Studies utilizing Chromatin Confirmation

Capture assays (3C) have demonstrated CTCF interacts with Cohesins to mediate long-range chromosomal interactions such as promoter interaction with distal enhancers (79). These interactions have been shown to be important for CTCF mediated regulation of gene clusters, where regulatory sequences are far from target genes (80). It is postulated the 3-dimensional structure of chromatin leading to transcriptionally active regions, so called topologically associating domains (TADs), work to define cell type specific transcriptional landscapes (81). Several studies have demonstrated that CTCF and Cohesin are required to maintain the organization of these TADs (82-85). These works demonstrated how changes to relatively few, specific, CTCF binding sites can drastically alter expression of multiple genes. In part, explaining how relatively small differences in CTCF binding sites can dictate cell fate and transcriptional landscape.

CTCF in DNA Methylation Regulation

Ten years after its initial characterization (86), several groups simultaneously discovered CTCF exhibits methylation-sensitive binding at the *H19-IGF2* locus (74,87,88) (Figure 1A), providing the first link between CTCF and epigenetic marks. Following this observation, a number of studies focused on specific regions of the genome have shown DNA methylation and CTCF binding are inversely correlated. Some of these studies demonstrated this inverse relationship at cancer associated genes including *p53* (89), *RB* (90,91), *p16INK4A* (92), and *mi-R181C* (93). This observation was later demonstrated genome-wide, through the combination of CTCF ChIP-seq and DNA methylation analyzed by bisulfite sequencing, which showed variable CTCF binding was strongly linked to differential DNA methylation (94).

The research analyzing the inverse relationship of CTCF binding and DNA methylation suggested that the physical presence of CTCF is sufficient to block gains in

DNA methylation. However, this hypothesis has been further modified with the finding that CTCF can actively inhibit DNA methyltransferase activity through activation of Poly (ADP-ribose) polymerase 1 (PARP-1) (95). Further research demonstrated CTCF forms a complex with PARP-1 and DNMT1 at CTCF binding sites, and activated PARP-1 in this complex inhibits local DNMT activity (96). This work directly demonstrated for the first time CTCF binding sites can be actively protected from DNA methylation gains when bound by CTCF.

Environmental and Age-Related Regulation of CTCF

With increased interest in CTCF influencing epigenetic marks, our lab and others have documented a number of factors that may alter CTCF expression. Notably, we originally described decreases in CTCF associated with aging in the mouse prostate (4). In addition, our lab has noted CTCF downregulation and CTCF mediated changes in methylation at the *IGF2-H19* imprint control region following oxidative stress induction (97) and at senescence in prostate cell lines (98). Interest in CTCF regulation is increasing outside of the prostate as well. Wang *et al.* demonstrated UV stress-induced corneal epithelial cells experience CTCF downregulation (99). Cha *et al*. identified lower CTCF expression in skeletal muscle of aged mice fed long chain polyunsaturated fatty acids versus mice fed short chain polyunsaturated fatty acids (100).

These studies and others have indicated altered CTCF expression is important for disease development. However, the outcome of CTCF regulation on genetic and epigenetic processes is still not well understood. In particular, how altered CTCF expression in the prostate may contribute to disease is yet to be defined. To date, only site-specific associations have been made with CTCF directly influencing epigenetic marks. Therefore, despite these advances in our understanding of CTCF functions, it is unknown whether

CTCF is important for genome-wide epigenetic regulation. In addition, the genes that CTCF transcriptionally regulates are overall not well defined. Answering these questions has important implications as it could provide potential targets for therapeutic intervention or hold prognostic potential.

Concluding Remarks and Purpose of this Thesis

During aging, alterations in the epigenetic landscape results from endogenous and exogenous exposures. These changes affect tightly regulated imprinted regions, CpG island methylation, intergenic DNA methylation, and histone modifications. Epigenetic changes over a lifetime may accumulate in the prostate and result in the marked prevalence of the disease with aging. These accumulated changes that increase cancer incidence can be referred to as *A*ge-*R*elated *E*pigenetic *A*lterations inducing *S*usceptibility or AREAS (Figure 1B). They involve regions of the susceptible prostate that give rise to cancer. Unlike one common view of the field defect, that they represent alterations induced in normal tissues adjacent to tumors, AREAS give rise to subsequent neoplasms.

The studies constituting this thesis examined the role of CTCF mediated age-related epigenetic alterations in prostate cancer. Our previous research on *IGF2* imprinting supports a role for AREAS in the development of neoplastic lesions (4,53). We investigated the role of *Igf2* loss of imprinting in disease formation using a mouse model of LOI. Ultimately, *Igf2* imprinting is controlled by allele-specific CTCF binding, influencing methylation in the Imprint Control Region. The Jarrard Lab demonstrated that *Igf2* LOI in mice correlates with CTCF downregulation with age (4). These results point to age-related decreases in CTCF expression mediating aberrant epigenetic regulation. Therefore, we characterized the expression of CTCF and other interacting factors in human prostate tissues to determine if these proteins are frequently altered in prostate cancer. This study

and others provide evidence that decreased CTCF expression frequently occurs in cancer development. Therefore, we investigated the role of CTCF downregulation and its effects on genome-wide DNA methylation and transcriptional alterations in the prostate.

References

1. Talens RP, Christensen K, Putter H, Willemsen G, Christiansen L, Kremer D*, et al.* Epigenetic variation during the adult lifespan: cross-sectional and longitudinal data on monozygotic twin pairs. Aging Cell **2012**:no-no
2. Fraga MF, Ballestar E, Paz MF, Ropero S, Setien F, Ballestar ML*, et al.* Epigenetic differences arise during the lifetime of monozygotic twins. Proc Natl Acad Sci U S A **2005**;102:10604-9
3. Damaschke NA, Yang B, Bhusari S, Svaren JP, Jarrard DF. Epigenetic susceptibility factors for prostate cancer with aging. Prostate **2013**;73:1721-30
4. Fu VX, Dobosy JR, Desotelle JA, Almassi N, Ewald JA, Srinivasan R*, et al.* Aging and cancer-related loss of insulin-like growth factor 2 imprinting in the mouse and human prostate. Cancer Res **2008**;68:6797-802
5. Powers GL, Marker PC. Recent advances in prostate development and links to prostatic diseases. Wiley Interdiscip Rev Syst Biol Med **2013**;5:243-56
6. Timms BG. Prostate development: a historical perspective. Differentiation **2008**;76:565-77
7. Siegel R, Naishadham D, Jemal A. Cancer statistics, 2012. CA: A Cancer Journal for Clinicians **2012**;62:10-29
8. Haas GP, Sakr WA. Epidemiology of prostate cancer. CA Cancer J Clin **1997**;47:273-87
9. Tomlins SA, Mehra R, Rhodes DR, Cao X, Wang L, Dhanasekaran SM*, et al.* Integrative molecular concept modeling of prostate cancer progression. Nat Genet **2007**;39:41-51
10. Epstein JI, Carmichael MJ, Partin AW, Walsh PC. Small high grade adenocarcinoma of the prostate in radical prostatectomy specimens performed for nonpalpable disease: pathogenetic and clinical implications. J Urol **1994**;151:1587-92
11. Feinberg AP, Tycko B. The history of cancer epigenetics. Nat Rev Cancer **2004**;4:143-53
12. Suvà ML, Riggi N, Bernstein BE. Epigenetic reprogramming in cancer. Science **2013**;339:1567-70
13. Berdasco M, Esteller M. Hot topics in epigenetic mechanisms of aging: 2011. Aging Cell **2012**;11:181-6
14. Wang Y, Leung FC. An evaluation of new criteria for CpG islands in the human genome as gene markers. Bioinformatics **2004**;20:1170-7
15. Straussman R, Nejman D, Roberts D, Steinfeld I, Blum B, Benvenisty N*, et al.* Developmental programming of CpG island methylation profiles in the human genome. Nat Struct Mol Biol **2009**;16:564-71
16. Lopez-Serra L, Esteller M. Proteins that bind methylated DNA and human cancer: reading the wrong words. Br J Cancer **2008**;98:1881-5
17. Esteller M. Cancer epigenomics: DNA methylomes and histone-modification maps. Nat Rev Genet **2007**;8:286-98
18. Yegnasubramanian S, Haffner MC, Zhang Y, Gurel B, Cornish TC, Wu Z*, et al.* DNA hypomethylation arises later in prostate cancer progression than CpG island hypermethylation and contributes to metastatic tumor heterogeneity. Cancer Res **2008**;68:8954-67

19. Bedford MT, van Helden PD. Hypomethylation of DNA in pathological conditions of the human prostate. Cancer Res **1987**;47:5274-6
20. Yang B, Sun H, Lin W, Hou W, Li H, Zhang L*, et al.* Evaluation of global DNA hypomethylation in human prostate cancer and prostatic intraepithelial neoplasm tissues by immunohistochemistry. Urol Oncol **2011**
21. Cho NY, Kim JH, Moon KC, Kang GH. Genomic hypomethylation and CpG island hypermethylation in prostatic intraepithelial neoplasm. Virchows Arch **2009**;454:17-23
22. Suzuki K, Suzuki I, Leodolter A, Alonso S, Horiuchi S, Yamashita K*, et al.* Global DNA demethylation in gastrointestinal cancer is age dependent and precedes genomic damage. Cancer Cell **2006**;9:199-207
23. Kamiyama HSKMTKKMYOSKYJSJKASKFPM. DNA demethylation in normal colon tissue predicts predisposition to multiple cancers. Oncogene **2012**;31:5029-37
24. Kobayashi Y, Absher DM, Gulzar ZG, Young SR, McKenney JK, Peehl DM*, et al.* DNA methylation profiling reveals novel biomarkers and important roles for DNA methyltransferases in prostate cancer. Genome Res **2011**;21:1017-27
25. Issa JP, Ottaviano YL, Celano P, Hamilton SR, Davidson NE, Baylin SB. Methylation of the oestrogen receptor CpG island links ageing and neoplasia in human colon. Nat Genet **1994**;7:536-40
26. Ahuja N, Li Q, Mohan AL, Baylin SB, Issa JP. Aging and DNA methylation in colorectal mucosa and cancer. Cancer Res **1998**;58:5489-94
27. Kawakami K, Ruszkiewicz A, Bennett G, Moore J, Grieu F, Watanabe G*, et al.* DNA hypermethylation in the normal colonic mucosa of patients with colorectal cancer. Br J Cancer **2006**;94:593-8
28. Kwabi-Addo B, Chung W, Shen L, Ittmann M, Wheeler T, Jelinek J*, et al.* Age-related DNA methylation changes in normal human prostate tissues. Clin Cancer Res **2007**;13:3796-802
29. Henrique R, Jerónimo C, Teixeira MR, Hoque MO, Carvalho AL, Pais I*, et al.* Epigenetic heterogeneity of high-grade prostatic intraepithelial neoplasia: clues for clonal progression in prostate carcinogenesis. Mol Cancer Res **2006**;4:1-8
30. Pili R, Salumbides B, Zhao M, Altiok S, Qian D, Zwiebel J*, et al.* Phase I study of the histone deacetylase inhibitor entinostat in combination with 13-cis retinoic acid in patients with solid tumours. Br J Cancer **2012**;106:77-84
31. Vasiljević N, Wu K, Brentnall AR, Kim DC, Thorat MA, Kudahetti SC*, et al.* Absolute quantitation of DNA methylation of 28 candidate genes in prostate cancer using pyrosequencing. Dis Markers **2011**;30:151-61
32. Li LC, Shiina H, Deguchi M, Zhao H, Okino ST, Kane CJ*, et al.* Age-dependent methylation of ESR1 gene in prostate cancer. Biochem Biophys Res Commun **2004**;321:455-61
33. Guan M, Zhou X, Soulitzis N, Spandidos DA, Popescu NC. Aberrant methylation and deacetylation of deleted in liver cancer-1 gene in prostate cancer: potential clinical applications. Clin Cancer Res **2006**;12:1412-9
34. Yang B, Bhusari S, Kueck J, Weeratunga P, Wagner J, Leverson G*, et al.* Methylation profiling defines an extensive field defect in histologically normal prostate tissues associated with prostate cancer. Neoplasia **2013**;15:399-408
35. Jones PA, Takai D. The role of DNA methylation in mammalian epigenetics. Science **2001**;293:1068-70

36. Horii J, Hiraoka S, Kato J, Harada K, Kuwaki K, Fujita H*, et al.* Age-related methylation in normal colon mucosa differs between the proximal and distal colon in patients who underwent colonoscopy. Clin Biochem **2008**;41:1440-8
37. Hiraoka S, Kato J, Horii J, Saito S, Harada K, Fujita H*, et al.* Methylation status of normal background mucosa is correlated with occurrence and development of neoplasia in the distal colon. Hum Pathol **2010**;41:38-47
38. Tahiliani M, Koh KP, Shen Y, Pastor WA, Bandukwala H, Brudno Y*, et al.* Conversion of 5-methylcytosine to 5-hydroxymethylcytosine in mammalian DNA by MLL partner TET1. Science **2009**;324:930-5
39. Haffner MC, Chaux A, Meeker AK, Esopi DM, Gerber J, Pellakuru LG*, et al.* Global 5-hydroxymethylcytosine content is significantly reduced in tissue stem/progenitor cell compartments and in human cancers. Oncotarget **2011**;2:627-37
40. Branco MR, Ficz G, Reik W. Uncovering the role of 5-hydroxymethylcytosine in the epigenome. Nat Rev Genet **2012**;13:7-13
41. Chia N, Wang L, Lu X, Senut MC, Brenner C, Ruden DM. Hypothesis: environmental regulation of 5-hydroxymethylcytosine by oxidative stress. Epigenetics **2011**;6:853-6
42. Horsthemke B. Mechanisms of imprint dysregulation. Am J Med Genet C Semin Med Genet **2010**;154C:321-8
43. Babak T, Deveale B, Armour C, Raymond C, Cleary MA, van der Kooy D*, et al.* Global survey of genomic imprinting by transcriptome sequencing. Curr Biol **2008**;18:1735-41
44. Reik W, Walter J. Genomic imprinting: parental influence on the genome. Nat Rev Genet **2001**;2:21-32
45. McGrath J, Solter D. Completion of mouse embryogenesis requires both the maternal and paternal genomes. Cell **1984**;37:179-83
46. Cui H, Cruz-Correa M, Giardiello FM, Hutcheon DF, Kafonek DR, Brandenburg S*, et al.* Loss of IGF2 imprinting: a potential marker of colorectal cancer risk. Science **2003**;299:1753-5
47. Woodson K, Flood A, Green L, Tangrea JA, Hanson J, Cash B*, et al.* Loss of insulin-like growth factor-II imprinting and the presence of screen-detected colorectal adenomas in women. J Natl Cancer Inst **2004**;96:407-10
48. Figueroa JA, Lee AV, Jackson JG, Yee D. Proliferation of cultured human prostate cancer cells is inhibited by insulin-like growth factor (IGF) binding protein-1: evidence for an IGF-II autocrine growth loop. J Clin Endocrinol Metab **1995**;80:3476-82
49. Zuo QS, Yan R, Feng DX, Zhao R, Chen C, Jiang YM*, et al.* Loss of imprinting and abnormal expression of the insulin-like growth factor 2 gene in gastric cancer. Mol Carcinog **2011**;50:390-6
50. Hiura H, Okae H, Kobayash H, Miyauchi N, Sato F, Sato A*, et al.* High-throughput detection of aberrant imprint methylation in the ovarian cancer by the bisulphite PCR-Luminex method. BMC Med Genomics **2012**;5:8
51. Zhao R, DeCoteau JF, Geyer CR, Gao M, Cui H, Casson AG. Loss of imprinting of the insulin-like growth factor II (IGF2) gene in esophageal normal and adenocarcinoma tissues. Carcinogenesis **2009**;30:2117-22
52. Jarrard DF, Bussemakers MJ, Bova GS, Isaacs WB. Regional loss of imprinting of the insulin-like growth factor II gene occurs in human prostate tissues. Clin Cancer Res **1995**;1:1471-8

53. Bhusari S, Yang B, Kueck J, Huang W, Jarrard DF. Insulin-like growth factor-2 (IGF2) loss of imprinting marks a field defect within human prostates containing cancer. Prostate **2011**;71:1621-30
54. Herold M, Bartkuhn M, Renkawitz R. CTCF: insights into insulator function during development. Development **2012**;139:1045-57
55. Bhusari SS, Dobosy JR, Fu V, Almassi N, Oberley T, Jarrard DF. Superoxide dismutase 1 knockdown induces oxidative stress and DNA methylation loss in the prostate. Epigenetics **2010**;5:402-9
56. Biniszkiewicz D, Gribnau J, Ramsahoye B, Gaudet F, Eggan K, Humpherys D*, et al.* Dnmt1 overexpression causes genomic hypermethylation, loss of imprinting, and embryonic lethality. Mol Cell Biol **2002**;22:2124-35
57. Holm TM, Jackson-Grusby L, Brambrink T, Yamada Y, Rideout WM, Jaenisch R. Global loss of imprinting leads to widespread tumorigenesis in adult mice. Cancer Cell **2005**;8:275-85
58. Gu Y, Zhang S, Wu Q, Xu S, Cui Y, Yang Z*, et al.* Differential expression of decorin, EGFR and cyclin D1 during mammary gland carcinogenesis in TA2 mice with spontaneous breast cancer. J Exp Clin Cancer Res **2010**;29:6
59. Aryee MJ, Liu W, Engelmann JC, Nuhn P, Gurel M, Haffner MC*, et al.* DNA methylation alterations exhibit intraindividual stability and interindividual heterogeneity in prostate cancer metastases. Sci Transl Med **2013**;5:169ra10
60. Lin PC, Giannopoulou EG, Park K, Mosquera JM, Sboner A, Tewari AK*, et al.* Epigenomic alterations in localized and advanced prostate cancer. Neoplasia **2013**;15:373-83
61. Travers AA, Vaillant C, Arneodo A, Muskhelishvili G. DNA structure, nucleosome placement and chromatin remodelling: a perspective. Biochem Soc Trans **2012**;40:335-40
62. Kouzarides T. SnapShot: Histone-modifying enzymes. Cell **2007**;128:802
63. Behbahani TE, Kahl P, von der Gathen J, Heukamp LC, Baumann C, Gütgemann I*, et al.* Alterations of global histone H4K20 methylation during prostate carcinogenesis. BMC Urol **2012**;12:5
64. Seligson DB, Horvath S, Shi T, Yu H, Tze S, Grunstein M*, et al.* Global histone modification patterns predict risk of prostate cancer recurrence. Nature **2005**;435:1262-6
65. O'Sullivan RJ, Kubicek S, Schreiber SL, Karlseder J. Reduced histone biosynthesis and chromatin changes arising from a damage signal at telomeres. Nat Struct Mol Biol **2010**;17:1218-25
66. So AY, Jung JW, Lee S, Kim HS, Kang KS. DNA methyltransferase controls stem cell aging by regulating BMI1 and EZH2 through microRNAs. PLoS One **2011**;6:e19503
67. Stettner M, Krämer G, Strauss A, Kvitkina T, Ohle S, Kieseier BC*, et al.* Long-term antiepileptic treatment with histone deacetylase inhibitors may reduce the risk of prostate cancer. Eur J Cancer Prev **2012**;21:55-64
68. Balakrishnan L, Milavetz B. Decoding the histone H4 lysine 20 methylation mark. Crit Rev Biochem Mol Biol **2010**;45:440-52
69. Lobanenkov VV, Nicolas RH, Adler VV, Paterson H, Klenova EM, Polotskaja AV*, et al.* A novel sequence-specific DNA binding protein which interacts with three regularly spaced direct repeats of the CCCTC-motif in the 5'-flanking sequence of the chicken c-myc gene. Oncogene **1990**;5:1743-53

70. Yang Y, Quitschke WW, Vostrov AA, Brewer GJ. CTCF is essential for up-regulating expression from the amyloid precursor protein promoter during differentiation of primary hippocampal neurons. J Neurochem **1999**;73:2286-98
71. Vostrov AA, Quitschke WW. The zinc finger protein CTCF binds to the APBbeta domain of the amyloid beta-protein precursor promoter. Evidence for a role in transcriptional activation. J Biol Chem **1997**;272:33353-9
72. Lutz M, Baniahmad A, Renkawitz R. Modulation of thyroid hormone receptor silencing function by co-repressors and a synergizing transcription factor. Biochem Soc Trans **2000**;28:386-9
73. Jothi R, Cuddapah S, Barski A, Cui K, Zhao K. Genome-wide identification of in vivo protein-DNA binding sites from ChIP-Seq data. Nucleic Acids Res **2008**;36:5221-31
74. Bell AC, Felsenfeld G. Methylation of a CTCF-dependent boundary controls imprinted expression of the Igf2 gene. Nature **2000**;405:482-5
75. Farrell CM, West AG, Felsenfeld G. Conserved CTCF insulator elements flank the mouse and human beta-globin loci. Mol Cell Biol **2002**;22:3820-31
76. Filippova GN, Thienes CP, Penn BH, Cho DH, Hu YJ, Moore JM*, et al.* CTCF-binding sites flank CTG/CAG repeats and form a methylation-sensitive insulator at the DM1 locus. Nat Genet **2001**;28:335-43
77. Magdinier F, Yusufzai TM, Felsenfeld G. Both CTCF-dependent and -independent insulators are found between the mouse T cell receptor alpha and Dad1 genes. J Biol Chem **2004**;279:25381-9
78. Cuddapah S, Jothi R, Schones DE, Roh TY, Cui K, Zhao K. Global analysis of the insulator binding protein CTCF in chromatin barrier regions reveals demarcation of active and repressive domains. Genome Res **2009**;19:24-32
79. Hou C, Dale R, Dean A. Cell type specificity of chromatin organization mediated by CTCF and cohesin. Proc Natl Acad Sci U S A **2010**;107:3651-6
80. Xu Z, Wei G, Chepelev I, Zhao K, Felsenfeld G. Mapping of INS promoter interactions reveals its role in long-range regulation of SYT8 transcription. Nat Struct Mol Biol **2011**;18:372-8
81. Ong CT, Corces VG. CTCF: an architectural protein bridging genome topology and function. Nat Rev Genet **2014**;15:234-46
82. Zuin J, Dixon JR, van der Reijden MI, Ye Z, Kolovos P, Brouwer RW*, et al.* Cohesin and CTCF differentially affect chromatin architecture and gene expression in human cells. Proc Natl Acad Sci U S A **2014**;111:996-1001
83. Nora EP, Lajoie BR, Schulz EG, Giorgetti L, Okamoto I, Servant N*, et al.* Spatial partitioning of the regulatory landscape of the X-inactivation centre. Nature **2012**;485:381-5
84. Sofueva S, Yaffe E, Chan WC, Georgopoulou D, Vietri Rudan M, Mira-Bontenbal H*, et al.* Cohesin-mediated interactions organize chromosomal domain architecture. EMBO J **2013**;32:3119-29
85. Seitan VC, Faure AJ, Zhan Y, McCord RP, Lajoie BR, Ing-Simmons E*, et al.* Cohesin-based chromatin interactions enable regulated gene expression within preexisting architectural compartments. Genome Res **2013**;23:2066-77
86. Lobanenkov Vv NRHAVVPHKEMPAVGGH. A novel sequence-specific DNA binding protein which interacts with three regularly spaced direct repeats of the CCCTC-motif in the 5'-flanking sequence of the chicken c-myc gene. Oncogene **1990**;5:1743-53

87. Hark AT, Schoenherr CJ, Katz DJ, Ingram RS, Levorse JM, Tilghman SM. CTCF mediates methylation-sensitive enhancer-blocking activity at the H19/Igf2 locus. Nature **2000**;405:486-9
88. Kanduri C, Pant V, Loukinov D, Pugacheva E, Qi CF, Wolffe A*, et al.* Functional association of CTCF with the insulator upstream of the H19 gene is parent of origin-specific and methylation-sensitive. Curr Biol **2000**;10:853-6
89. Soto-Reyes E, Recillas-Targa F. Epigenetic regulation of the human p53 gene promoter by the CTCF transcription factor in transformed cell lines. Oncogene **2010**;29:2217-27
90. De La Rosa-Velázquez IA, Rincón-Arano H, Benítez-Bribiesca L, Recillas-Targa F. Epigenetic regulation of the human retinoblastoma tumor suppressor gene promoter by CTCF. Cancer Res **2007**;67:2577-85
91. Dávalos-Salas M, Furlan-Magaril M, González-Buendía E, Valdes-Quezada C, Ayala-Ortega E, Recillas-Targa F. Gain of DNA methylation is enhanced in the absence of CTCF at the human retinoblastoma gene promoter. BMC Cancer **2011**;11:232
92. Witcher M, Emerson BM. Epigenetic silencing of the p16(INK4a) tumor suppressor is associated with loss of CTCF binding and a chromatin boundary. Mol Cell **2009**;34:271-84
93. Ayala-Ortega E, Arzate-Mejía R, Pérez-Molina R, González-Buendía E, Meier K, Guerrero G*, et al.* Epigenetic silencing of miR-181c by DNA methylation in glioblastoma cell lines. BMC Cancer **2016**;16:226
94. Wang H, Maurano MT, Qu H, Varley KE, Gertz J, Pauli F*, et al.* Widespread plasticity in CTCF occupancy linked to DNA methylation. Genome Res **2012**;22:1680-8
95. Guastafierro T, Cecchinelli B, Zampieri M, Reale A, Riggio G, Sthandier O*, et al.* CCCTC-binding factor activates PARP-1 affecting DNA methylation machinery. J Biol Chem **2008**;283:21873-80
96. Zampieri M, Guastafierro T, Calabrese R, Ciccarone F, Bacalini MG, Reale A*, et al.* ADP-ribose polymers localized on Ctcf-Parp1-Dnmt1 complex prevent methylation of Ctcf target sites. Biochem J **2012**;441:645-52
97. Yang B, Wagner J, Damaschke N, Yao T, Wuerzberger-Davis SM, Lee MH*, et al.* A novel pathway links oxidative stress to loss of insulin growth factor-2 (IGF2) imprinting through NF-κB activation. PLoS One **2014**;9:e88052
98. Fu VX, Schwarze SR, Kenowski ML, LeBlanc S, Svaren J, Jarrard DF. A Loss of Insulin-like Growth Factor-2 Imprinting Is Modulated by CCCTC-binding Factor Down-regulation at Senescence in Human Epithelial Cells. J Biol Chem **2004**;279:52218-26
99. Wang Y, Lu L. Activation of oxidative stress-regulated Bcl-3 suppresses CTCF in corneal epithelial cells. PLoS One **2011**;6:e23984
100. Cha SH, Fukushima A, Sakuma K, Kagawa Y. Chronic docosahexaenoic acid intake enhances expression of the gene for uncoupling protein 3 and affects pleiotropic mRNA levels in skeletal muscle of aged C57BL/6NJcl mice. J Nutr **2001**;131:2636-42

Figure 1. IGF2 Imprinting and Age-related Epigenetic Alterations Inducing Susceptibility (AREAS) in the Prostate.

A, Schematic of *Igf2-H19* imprint regulation. The imprinted *IGF2/H19* locus contains an intergenic imprint control region (ICR) along with shared enhancers that collectively coordinate gene expression. Normal imprinting in this region is characterized by CpG methylation on the paternal allele (lower) within the ICR. This CpG methylation blocks CTCF, a chromatin insulator, binding to IGF2 and facilitates enhancer binding to the IGF2 promoter leading to expression of the gene. CTCF binds hypomethylated CpGs on the maternal allele (upper) at the ICR blocking enhancer binding to the IGF2 promoter and silencing of gene expression. Aging is associated with decreased CTCF levels and altered methylation at the ICR. ***B,*** Specific epigenetic alterations, including loss of imprinting, gene methylation, and histone modifications, are either stable (1) or erode (2) over time in the epithelium (or stroma) of the prostate that does not develop cancer. Alternately, in the prostate gland that develops cancer epigenetic alterations occurring during aging result in gene expression changes that confer a selective advantage to early neoplastic changes (3). These changes represent a field of susceptibility and may be accelerated by environmental insults. These epigenetic changes that occur in aging tissues are frequently selected for in tumors (4). Other cancer specific epigenetic alterations arise within the tumor and are age-independent (5).

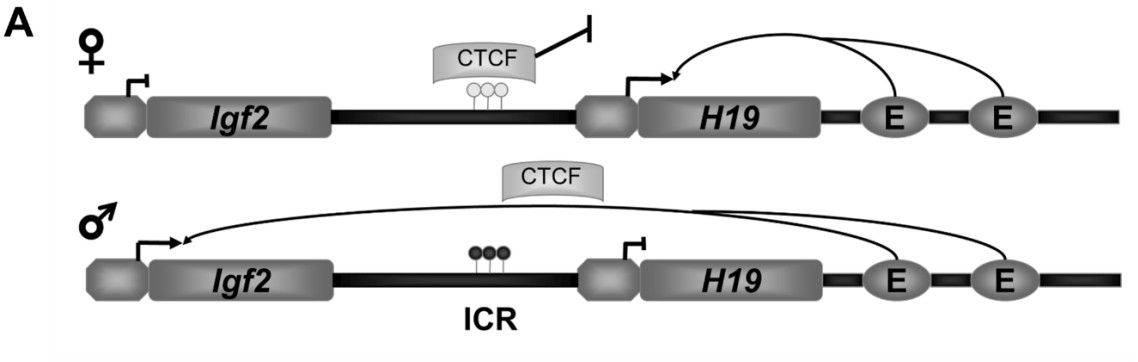
A
♀
CTCF
Igf2
H19
E
E
CTCF
♂
Igf2
H19
E
E
ICR

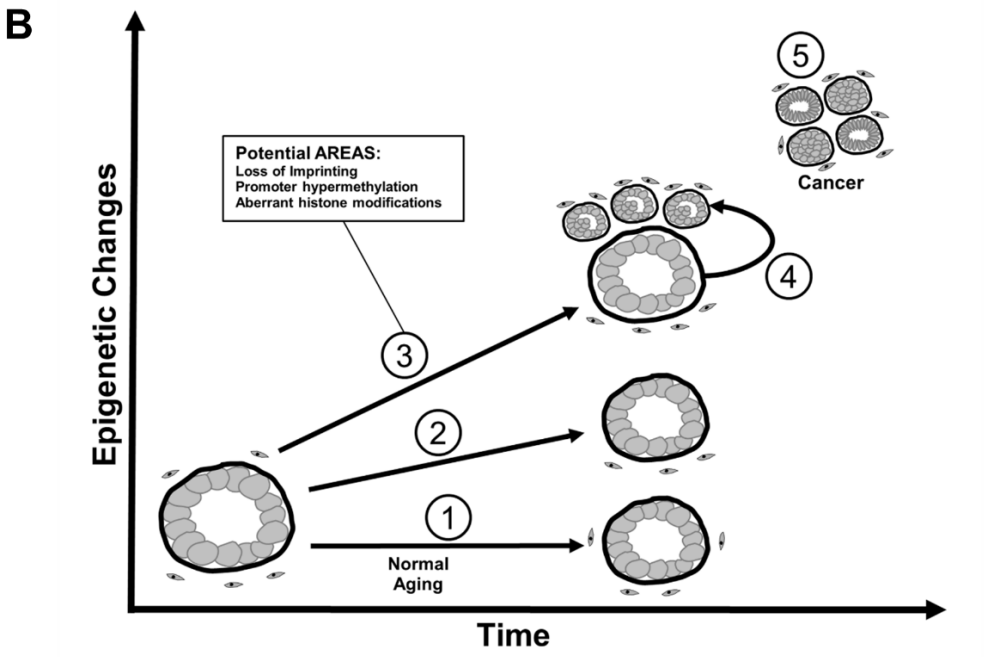
B
Epigenetic Changes
Potential AREAS:
Loss of Imprinting
Promoter hypermethylation
Aberrant histone modifications
5
Cancer
4
3
2
1
Normal
Aging
Time

Chapter II

Igf2 Loss of Imprinting Engineered using CTCF Binding Site Mutations Promotes Widespread Neoplastic Growth in the Prostate

Nathan A. Damaschke and David F. Jarrard

NA Damaschke, B Yang, S Bhusari, W Zhong, ML Blute Jr., W Huang, and DF Jarrard, Cancer Research. *In revisions*.

Abstract

Loss of imprinting (LOI) is an epigenetic event where allele-specific restriction of gene expression is relaxed. The gene locus encoding the paracrine growth factor Insulin-like Growth Factor 2 (*IGF2*) commonly experiences LOI during aging and cancer development in human prostate tissues (Can Res 2008). However, the contribution of *IGF2* LOI to malignant development in the prostate is not well understood. In this study, we utilized a mouse model with CTCF binding site mutations at the *Igf2-H19* imprint control region that abolishes CTCF insulator activity resulting in biallelic *Igf2* expression and closely mimics increased expression levels seen with aging-induced LOI. We find *Igf2* LOI is associated with an increased prevalence and severity of the prostate cancer precursor, prostatic intraepithelial neoplasia (PIN). Crossing with a prostate specific *Nkx3.1* knockout model, an early finding in human cancer, results in increased frequency of PIN lesions in an additive fashion. Quantitative immunohistochemistry (IHC) revealed increased MAPK/ERK signaling and epithelial proliferation in LOI affected mouse prostates. IHC on human prostate tissue arrays demonstrate increased IGF2 positively correlates with p-ERK (R=0.264, $P = 0.035$) and p-AKT (R=0.883, $P < 1e-7$) expression in benign tissues. In this study, we demonstrate that a known age-related epigenetic alteration, *Igf2* LOI, alone is sufficient to increase rates of neoplastic disease. These findings suggest *Igf2* LOI plays an essential role in the widespread neoplastic formation that characterizes the multifocal nature of human prostate cancer through upregulation of cancer-associated signaling pathways.

Introduction

Prostate cancer (PCa) is the most commonly diagnosed cancer in the male U.S. population, and the second most common cause of death in aging men (1) . Several etiologic factors, including diet and aging, have been strongly implicated in the development of this disease (2). Nearly 80% of men age 80y develop PCa based on autopsy findings (3). In addition, numerous foci of cancer are often found upon histopathological examination confirming the multifocal nature of PCa (3). How these epidemiologic factors contribute to the initiation and progression of PCa at the molecular level remains elusive and is an important key in understanding and preventing this disease.

Accumulating data supports an age-related erosion of the epigenome in the predisposition of the prostate to cancer (2). To date, one of the few alterations implicated in aging non-cancerous peripheral prostate tissue and in associated prostate tumors is the finding of a loss in the typical imprint of the Insulin-like growth factor 2 gene (*IGF2*) (4). Genomic imprinting is an epigenetic modification that leads to the differential expression (i.e. only from one allele) of a gene based on parental origin. *IGF2*, a paracrine and autocrine regulator of cell proliferation is tightly regulated and maintains a strict imprint pattern in adult tissues. Alterations in *IGF2* regulation, via a loss of imprinting (i.e. biallelic expression) have been demonstrated to occur in the human prostate with aging (4,5). Whether *IGF2* LOI directly underlies proliferative changes in the aging prostate remains an unanswered question.

IGF2 shares structural similarity to insulin, and possesses mitogenic activity (6). IGF2 stimulation of the Insulin/IGF-1 receptors leads to activation of a variety of cell signaling cascades including PI3K/AKT and MAPK/ERK pathways (6). The *IGF2* gene is located within the *IGF2-H19* imprinted locus, which includes a differentially methylated

region (DMR) and shared downstream enhancers. Imprinted expression is achieved via allele-specific methylation at the differentially methylated region (DMR), dictating CTCF insulator activity and ultimately directing enhancer association with either *IGF2* or *H19* promoter sequences, driving their expression.

The homeobox gene *NKX3.1* is continuously expressed in the epithelium during prostate development and in adulthood, but is commonly downregulated early in prostate cancer development (7). Human *NKX3.1* exists at chromosome 8p21, a region that frequently undergoes loss of heterozygosity (LOH) early in prostate carcinogenesis (8,9). It is also regulated in part by PTEN, a gene mutated in 30% of primary prostate cancers (10). Nkx3.1 mutant mice develop prostatic hyperplasia and dysplasia yet fail to progress to frank cancers (7,11). Restoration of NKX3.1 expression in PTEN deficient cells reverts their phenotype and the progression of prostate cancer in the *Pten* null mouse (12), suggesting a key early role for NKX3.1 in prostate cancer.

IGF2 loss of imprinting (LOI) has been implicated in a range of human disease following its original description in Wilm's Tumors (13). In humans, *IGF2* LOI has been demonstrated in prostate (4), ovarian (14), esophageal (15), breast (16), and colon cancers (17). In addition to tumors of the prostate, *IGF2* LOI is seen in histologically normal human peripheral prostate tissue and was more extensive in prostates with associated cancer (4,5). Various animal models leading to *IGF2* overexpression have demonstrated increased risk of malignancy including mammary, lung, and colon cancers (6). However, these models often alter *H19* expression, which may also play a role in tumorigenesis (18,19), or use transgenic overexpression of *IGF2* resulting in levels not normally seen with aging (20,21). A mouse with point mutations within CTCF binding sites at the *H19* ICR results in biallelic *Igf2* expression without altering *H19* expression (22). Using this animal model, the role of

biallelic Igf2 expression on neoplastic development was assessed in the prostate. Furthermore, we test whether a synergistic/additive effect is seen with *Nkx3.1* loss, an early alteration in prostate cancer development.

Materials and Methods

Maintenance (MOI) and loss of imprinting (LOI) mice generation and Nkx3.1 crosses

All mouse experiments were performed under a UW-IACUC approved IRB protocol. A mouse model of *Igf2* LOI previously generated by Pant *et al*. contains mutations in three of the four CTCF target sites within the *Igf2-H19* imprint control region (ICR) changing the core sequence from GTGG to ATAT (142* mutation) (22,23). This sequence change deletes essential CTCF contact points while preserving the CpGs responsible for the methylation-sensitive CTCF targeting. Maternal transmission of 142* mutation results in offspring exhibiting Igf2 LOI ($H19^{+/-}$) thereby expressing the normally silenced allele. Mice carrying the 142* mutation were backcrossed on a C57Bl/6J background for 7 generations.

A prostate specific *Nkx3.1* knockout mouse containing a targeted gene disruption of the *Nkx3.1* homeodomain and carboxy-terminal protein sequences that generates a null mutation were used (7). These mice have been maintained on a hybrid 129/SvlmJ and C57Bl/6J background. To create experimental mice with their *Igf2* imprint maintained on the *Nkx3.1* knockout background, 142* mice were bred with *Nkx3.1* knockout mice to create male breeders ($H19^{-/-}$;$Nkx3.1^{+/-}$). These male breeders ($H19^{-/-}$;$Nkx3.1^{+/-}$) were bred with female $H19^{+/+}$,$Nkx3.1^{+/-}$ and the subsequent male offspring carry *Nkx3.1* mutation at varying rates (+/+, +/-, -/-) and inherit the 142* mutation paternally. Their maternal imprint is maintained, resulting in normal *Igf2* expression levels. To generate Igf2 LOI mice, $H19^{-/-}$ $Nkx3.1^{+/-}$ female breeders were created and bred with $H19^{+/+}$;$Nkx3.1^{+/-}$ male mice. These offspring inherit characteristic *Nkx3.1* mutations, but maternally inherit the mutant *H19* ICR allele. However, the male offspring express both *Igf2* alleles since *Igf2* silencing is lost with

the 142* mutation on the maternal allele (Figure 1A). Mice were aged to 6, 12, and 18 months before tissue collection.

Analysis of Igf2 LOI via FluPE (Fluorescent Primer Extension Assay)

C57Bl/6(cast H19-p57), a C57Bl/6 congenic strain heterozygous for distal chromosome 7 sequences from *Mus* castaneus were used to analyze *Igf2* LOI status in 142* mice prostates. Male mice homozygous for M. castaneus alleles (H19-p57) were bred with female 142* mutant heterozygous mice ($H19^{+/-}$). *Igf2* LOI in male mice aged 2 months were analyzed using FluPE assay as previously described (4).

Analysis of Prostate Tissue Pathology

Prostate tissues were scored for Prostatic Intraepithelial Neoplasia (PIN) based on criteria as described by Park *et al.* (24). Low grade PIN lesions (PIN 1/2) consist of foci with few layers of atypical cells, pale cytoplasm and abundant heterochromatic nuclei, but containing minimal pleomorphism. Intermediate grade PIN lesions (PIN 3) consist of larger foci that do not fill the lumen of the ducts but exhibit cribiform, papillary, or tufting patterns. Glandular structure is compromised with poor orientation of atypical cells. Nuclei exhibit pleomorphism and heterochromasia with abundant pale cytoplasmic staining. High grade PIN lesions (PIN 4) consist of atypical cells filling the lumen of the ducts, nuclear and cytoplasmic patterns are similar to intermediate grade PIN, however increasingly severe pleomorphism and hyperchromasia are seen. Inflammatory responses are marked by lymphocyte invasion.

Histologic analyses of mouse prostate tissues were performed on male mice at 6, 12, and 18 months of age. Upon tissue collection ventral (VP) and dorsolateral prostate (DLP) tissues were formalin-fixed and paraffin embedded. H&E stained slides were

analyzed on a blinded basis independently by W.Z. and M.L.B. Prostate tissues of experimental animals were first analyzed for the highest scoring PIN lesion seen in serial FFPE H&E stained tissue sections (Table 1). H&E slides were then scanned and, in a blinded fashion, the total number of normal and PIN (of any grade) affected glands were scored for each prostate. Sections from the same animal were averaged to obtain a percentage of PIN affected glands.

cDNA preparation and quantitative PCR

Total RNA was extracted from OCT embedded or flash frozen tissues using the PerfectPure RNA Tissue Kit (5prime) as described by the manufacturer. RNA was DnaseI treated during extraction, cDNA was synthesized from 500 ng of total RNA using Omniscript RT reagents (Qiagen) and both oligo(dT) and random hexamers. Samples without reverse transcriptase served as negative control to detect gDNA contamination. Quantitative PCR (qPCR) was performed with PerfeCta SYBR Green FastMix (Quanta Biosciences) on a CFX96 (Bio-Rad). A geometric mean using *Gapdh*, *18s*, and *Actb* was used for reference. All primer sequences are available on request.

Quantitative Automated Immunohistochemistry

Tissue microarrays were constructed using mouse DLP tissues to quantitatively analyze protein expression in prostate tissues. Preparation of slides and antigen retrieval methods have been previously described (25). Two dual stains were performed on sequential sections, IGF2 (LS-B9544; LSBio, Seattle, WA) versus p-ERK (#4370, Cell Signaling, Danvers, MA) and IGF2 versus p-AKT (#4060, Cell Signaling, Danvers, MA). KI67 (ab15580; Abcam, Cambridge, UK) and TUNEL (Cat#: 12156792910, Roche, Basel, Switzerland) staining was performed on additional sections. Stained slides were scanned

as previously described (25). Human tissue microarrays (hTMA) constructed as previously described (25) containing duplicate cores of 48 benign prostate tissues (from radical prostatectomy specimens), 74 PCa tissues, and 22 metastatic samples from PCa patients were used for IHC analysis. Two triple stains were performed on hTMA slides using IGF2/p-ERK/E-cadherin (Ventana #790-4497; Roche, Basel, Switzerland) antibodies and IGF2/p-AKT/E-cadherin antibodies. E-cadherin antibodies were used to segment epithelial and stromal compartments in human prostate tissues. Cellular protein for individual cores was quantitated using the VECTRA^{TM} imaging system according to manufacturer's protocols (Caliper Life Sciences, Hopkinton, MA). InForm 1.2^{TM} software was used to segment epithelium vs. stroma and nuclear vs. cytoplasmic tissue compartments. Cores from the same patient were averaged to give a more precise estimate. Cores with <5% epithelial component or loss of tissue were excluded from the analysis.

Statistical Analysis

Statistical analyses were performed with the use of GraphPad Prism 5.0 Software and Excel 2016 (Microsoft). Quantitative IHC, mRNA expression, and histologic analyses were compared using the Student's t-test when assumptions are met (normal distribution and equality of variance), or the Wilcoxon rank sum test where appropriate. Categorical data was compared using Fisher's Exact. *P* values of <0.05 were considered as significant.

Results

142* Mutant (LOI) Mice Exhibit Biallelic and Increased Igf2 Expression in the Prostate

Our previous work had demonstrated that biallelic Igf2 expression occurs in the aging mouse and human prostate and this finding in the histologically normal prostate tissue was linked to the presence of human cancer (4). Construction of a mouse model with mutated CTCF binding sites at the *H19-Igf2* imprint control region leads to a premature biallelic Igf2 expression (22). Figure 1A demonstrates the breeding schema employed for the current study. Allele-specific expression was initially analyzed in experimental mouse prostates at 2 months of age by Fluorescent Primer Extension Assay (FluPE). Wildtype mice exhibit monoallelic *Igf2* expression indicating maintenance of imprinting (MOI) in both the ventral prostate (VP) and dorsolateral prostate (DLP) tissues. In contrast, the normally silenced *Igf2* allele is expressed when the 142* mutation is inherited maternally (LOI) resulting in biallelic *Igf2* expression (Figure 1B). In kidney, liver, bladder, and testis, control mice maintain *Igf2* imprinting while LOI mice exhibit biallelic expression in these tissues (data not shown).

To determine if LOI translates into changes in *Igf2* gene expression, mRNA was analyzed in experimental mice using quantitative real-time PCR. Experiments focused on the mouse DLP due to its anatomic similarities to the human peripheral prostate, the site of PCa development, and the previous association of LOI with aging in this prostatic region (4). At 6 months of age, *Igf2* mRNA expression is 2.7 fold higher in LOI mouse prostates when compared to controls ($P = 0.02$) (Figure 1C). Expression of *H19*, a downstream tumor suppressor gene, was not significantly altered in LOI mice (Supplementary Figure S1A), an advantage in utilizing the 142* mice that specifically target CTCF binding.

In LOI animals biallelic expression of *Igf2* occurs in all tissues tested. Body weight measurements taken throughout experimental mice lifetimes (Figure 1D) demonstrate heavier mice at weaning (21 days of age) compared to MOI (12.3g vs. 10.7g, P=0.016). LOI mice are 14% heavier (on average) throughout their lifetime with the largest differences seen at 6 and 7 months of age (20%, both P<0.001). Similar results were seen in *Nkx3.1+/-* and *Nkx3.1-/-* animals containing LOI (Supplementary Figure S1B-C).

NKX3.1 mutant mice, a homeobox 1 family member frequently inactivated early in PCa development (26), was bred onto MOI and LOI Igf2 backgrounds to examine whether a synergistic effect of increased androgen receptor (AR) and AKT signaling on neoplastic potential occurs in these mice prostates (**Fig. 1A**). Immunohistochemical analysis for IGF2 on tissue microarrays constructed from mouse prostate tissues confirmed the mRNA results. A significant increase in IGF2 protein was observed in all LOI genotypes including *LOI;Nkx3.1*$^{+/+}$, *LOI;Nkx3.1*$^{+/-}$, and *LOI;Nkx3.1*$^{-/-}$ mice **(Fig. 1E-G)** compared to genotype matched MOI animals. MOI mice for all three Nkx3.1 genotypes exhibit increases in Igf2 expression with older age as previously demonstrated (4).

Loss of Igf2 Imprinting Increases Rates of Prostatic Intraepithelial Neoplasia

Prostatic intraepithelial neoplasia (PIN) is a marker of early neoplastic disease in humans and is used as a histologic surrogate in rodent models for neoplasia (24). Increased PIN in the context of *Nkx3.1* knockout (27) and other genetically engineered mouse models has been described (24). Tissues were analyzed for the presence and prevalence of PIN lesions using validated grading criteria established by Park *et al* (24) (Figure 2A-F). The number of mice with low (PIN 1 and 2) versus intermediate/high grade (PIN 3 and 4) lesions were quantified based upon the most severe lesion within the prostate (Table 1). When examining all genotypes, the presence of any PIN lesion in *Igf2* LOI

prostates occurred with modestly increased frequency when all genotypes and ages were compared to MOI mice (77% vs 89%; MOI, LOI respectively, P=0.088; Fisher's Exact). However, significantly higher rates of IG/HGPIN was found in LOI animals compared to MOI animals (62% vs. 42%; respectively, P=0.004; Fisher's Exact). As shown in Table 1 and Figure 2G**,** LOI mice with both *Nkx3.1* alleles intact (*LOI;Nkx3.1*$^{+/+}$) display a 10-30% increased incidence of any PIN over 6, 12, and 18 months. LOI heterozygous *Nkx3.1* (*LOI;Nkx3.1*$^{+/-}$) mice exhibit increased frequency of PIN formation at 6, 12, and 18 months (35%, 21%, and 17% increases respectively) compared to their MOI counterparts. *Nkx3.1*$^{-/-}$ rates of PIN are higher than other *Nkx3.1*$^{+/+}$ genotypes, but the impact of biallelic *Igf2* expression on PIN incidence in this genotype was not different. Therefore, *Igf2* LOI mice develop IG/HGPIN lesions more commonly than MOI animals on multiple genetic backgrounds.

Loss of Igf2 Imprinting Increases the Multifocality of Prostatic Intraepithelial Neoplasia

On histologic analysis, LOI prostates displayed the increased presence of multifocal PIN similar to a widespread field effect seen in human disease (2). To quantify this observation, the number of PIN affected glands (any PIN) out of total glands (PIN glands/Total glands) within each prostate was determined (Figure 3A-C). LOI mice with a wildtype *Nkx3.1* background exhibit increased prevalence of PIN lesions at 6 months compared to *MOI;Nkx3.1*$^{+/+}$ (11%$\pm$2.3 vs. 29%$\pm$3.5; MOI, LOI respectively, P = 0.002) and at later time points (Figure 3A). LOI in prostate tissues from *Nkx3.1*$^{+/-}$ mice also demonstrate an increased prevalence of PIN glands at all ages examined compared to MOI (Figure 3B). In *Nkx3.1* homozygous knockout animals (*Nkx3.1*$^{-/-}$) (Figure 3C) significantly

higher frequencies of PIN lesions were seen in *LOI* mice at 6 months ($P = 0.009$), however the frequency of PIN lesions in this genotype did not differ at later time points.

A comparison across all genotypes at 6 months of age demonstrates the additive effects of Nkx3.1 mutation and *Igf2* LOI on PIN formation (Figure 3D). This effect is clearly demonstrated when comparing *Nkx3.1*$^{-/-}$ mice to their age and imprint status-matched controls. *MOI;Nkx3.1*$^{-/-}$ developed a significantly higher percentage of PIN affected glands than *MOI;Nkx3.1*$^{+/+}$ ($P < 0.001$) and *MOI;Nkx3.1*$^{+/-}$ ($P = 0.006$) animals. *LOI;Nkx3.1*$^{-/-}$ animals also yield significantly higher percentage of PIN than *LOI;Nkx3.1*$^{+/+}$ ($P = 0.004$) and *LOI;Nkx3.1*$^{+/-}$ ($P = 0.016$) animals, while also exhibiting higher percentage of PIN than *MOI;Nkx3.1*$^{-/-}$ ($P = 0.009$). Thus, the *Nkx3.1* background leads to an increased frequency of PIN lesions throughout the gland when compared to wildtype animals while an additive effect on PIN formation is observed in the presence of LOI. *Nkx3.1* and LOI together did not result in the formation of invasive cancer within the time points examined.

Proliferation and p-ERK is Significantly Elevated in Mice Exhibiting Increased PIN

IGF2 signaling occurs by binding to the Insulin-like growth factor 1 (IGF1R) or Insulin Receptors (IR). Signaling via these receptors activates unique and shared downstream pathways including PI3K/AKT and MAPK/ERK leading to cell growth and proliferation (28). Using tissue microarrays constructed from mouse prostates, VECTRA was used to independently quantitate proliferation rates by measuring percent KI67 immunohistochemical staining. Biallelic *Igf2* expression on any *Nkx3.1* genotype results in a significant increase in the percentage of KI67 positive cells at 6, 12 and 18 months of age ($P = 0.027$, $P = 0.043$, $P = 0.019$ respectively) compared to MOI. (Figure 4A). No synergistic increase in proliferation was found when both phenotypes, the *LOI;Nkx3.1*$^{-/-}$ mice, were compared to *Nkx3.1*$^{+/+}$.

To uncover the activated signaling pathways boosting proliferation and PIN formation in *Igf2* LOI animals we assessed p-AKT, and p-ERK by quantitative IHC using VECTRA image analysis. IHC demonstrates p-ERK staining occurs primarily in the glandular epithelium, therefore analysis focused on the epithelial compartment (Figure 4B-C). *Igf2* LOI was associated with elevated p-ERK in both *Nkx3.1*$^{+/+}$ (Figure 4D) and *Nkx3.1*$^{+/-}$ mice (Figure 4E). No significant change in p-ERK staining was detected in *LOI;Nkx3.1*$^{-/-}$ mice despite a significant increase in proliferation (Supplementary Figure S2A). To further investigate, an analysis of p-AKT was performed that revealed significantly elevated p-AKT levels at 6 and 12 months in *LOI;Nkx3.1*$^{-/-}$ mice vs. *MOI;Nkx3.1*$^{-/-}$ (Figure 4F) but not in *Nkx3.1*$^{+/+}$ and *Nkx3.1*$^{+/-}$ (p-AKT staining, Supplementary Fig. S2B-C). In sum, *Igf2* LOI induces ERK signaling primarily, but with loss of *Nkx3.1* function, p-AKT activation becomes prominent.

Igf2 LOI Leads to Increased Transcription of MAPK/ERK Effector and Proliferation Related Genes

IGF2 exhibits structural similarity to insulin, with the ability to elicit signaling through both the insulin–like growth factor 1 receptor (IGF1R) and insulin receptor (IR). Ligand binding to these growth receptors results in context dependent signaling through PI3K/AKT and MAPK pathways (6). As demonstrated (Figure 3), upregulation of p-ERK levels occurred predominantly in *LOI;Nkx3.1*$^{+/+}$ mice, but in *LOI;Nkx3.1*$^{-/-}$ prostates AKT signaling significantly increases. We performed further transcriptional analyses to determine potential MAPK/ERK effector genes associated with the increased proliferation in LOI mouse prostates. Using 12mo *Nkx3.1*$^{+/+}$ prostate specimens the effect of biallelic expression was compared to MOI by qPCR for immediate early genes (IEGs) which are activated in response to growth factor stimuli (29). *C-Fos* transcription is significantly

elevated in LOI prostates (2-fold, *P* = 0.003) indicating increased activated MAPK signaling (Figure 5A). Phosphorylation of c-FOS and c-JUN by MAPK results in the formation of the AP-1 transcription factor complex. Increased *FosL1* (*Fra-1*) mRNA in LOI prostates (1.5-fold, *P* = 0.009) confirms active AP-1 which is required for *FosL1* transcription (30). MAPK signaling results in transcription of cell cycle-related genes including C*yclin D* which is also increased in LOI mouse prostates compared to MOI (2.1 fold, *P* = 0.003).

In addition to MAPK/ERK related gene transcription, we analyzed a DNA replication gene set previously shown to be induced with *Igf2* LOI in mice (Figure 5B) (18). Of these genes, G0/G1 associated genes *Mcm5* (1.48 fold, *P* = 0.009), *Mcm3* (1.56 fold, *P* = 0.012), *Cdc6* (2.25-fold, *P* = 0.001), and *Chaf1a* (1.73-fold, *P* = 0.005) were significantly upregulated in LOI prostates (non-significant difference in *Lig1, Tiam2, Axin1,* and *NF-κB* subunits p50 and p65), supporting the enrichment of proliferating cells as identified by KI67 staining (Figure 4E).

IGF2 Protein Expression Correlates with p-AKT and p-ERK in Nontumor Human Prostate Tissue from Radical Prostatectomy Specimens

To determine the relevance of these findings to human prostate disease we examined IGF2, p-AKT, and p-ERK protein levels using a human tissue microarray (hTMA) containing benign prostate tissues (BPT) and cancer. Our animal studies revealed increased IGF2 expression results in induction of both p-ERK and p-AKT signaling. Therefore, we performed a correlation analysis between IGF2 and p-ERK and p-AKT to establish a potential link between these proteins (Figure 5C-D). A significant positive correlation exists between increased IGF2 and p-ERK in BPT (Pearson R = 0.26, *P* = 0.035) (Figure 5C). IGF2 and p-AKT exhibited an even more marked positive correlation (Pearson R = 0.88; *P* < 1.0E-7) (Figure 5D). Notably, these correlations were less pronounced in

primary PCa tissues, although higher IGF2 and p-AKT protein expression was noted (Supplementary Figure S3). Loss of IGF2 imprinting is a common finding in benign human tissues removed at cancer surgery (4,31). While this approach did not examine *IGF2* imprint status, the underlying increased IGF2 expression noted results supports our animal model findings that higher *Igf2* expression is associated with increased p-AKT and p-ERK signaling.

Discussion

The human prostate develops cancer remarkably frequently with aging (3) yet a clear genetic etiology has not been identified. In parallel, *Igf2* LOI is more extensive in the normal peripheral prostate tissue of patients that develop prostate cancer compared to age-matched controls, and furthermore an erosion of this allelic imprinting occurs with aging in mouse and human prostates (4). In the current study we show *Igf2* loss of imprinting alone plays a role in the development of prostatic disease using a mouse model of *Igf2* LOI that mimics the biallelic, increased *Igf2* levels seen in the peripheral prostate during aging (4,32). Biallelic expression of *Igf2,* induced by mutation of CTCF binding sites within the intergenic imprint control region, resulted in widespread PIN in the mouse prostate. Significant upregulation of p-ERK signaling associates with increased epithelial cell proliferation. We concurrently test *Nkx3.1* deletion, a common early molecular alteration in established prostate cancer (27), and find LOI;*Nkx3.1*$^{+/-}$ animals developed significantly more extensive PIN in an additive fashion, but not frank cancer. These novel epigenetic results support a model in which the widespread multifocal development of neoplasia in the peripheral human prostate is dependent on the presence of *Igf2* LOI. This observation explains, in part, the remarkable predisposition of the human prostate for the development of cancer with aging.

Igf2 exerts its mitogenic effects by signaling through the IGF1 receptor, insulin receptor, or heterodimeric hybrid receptors, which bind *Igf2* with differing affinity (33). The MAPK/ERK and PI3K/AKT pathways are the predominant intracellular signaling pathways affected by IGF2 stimulation (Figure 5C). Interrogation of these pathways by quantitative IHC revealed strong upregulation of p-ERK signaling with *Igf2* LOI. Conversely, in mice harboring a complete loss of *Nkx3.1*, the alternate and competing pathway, p-AKT is increased. This is consistent with *in vitro* studies showing that in NKX3.1 deficiency, the

repressive effect on AR signaling is lost and p-AKT upregulated (12). These results may be explained by the differential dosage sensitivity to NKX3.1 loss seen in certain genes, where *Nkx3.1*$^{-/-}$ prostates exhibit a drastically altered transcriptional profile compared to less significant differences between *Nkx3.1*$^{+/+}$ and *Nkx3.1*$^{+/-}$ animals (34). Other studies show homozygous inactivation of *Nkx3.1* results in increased AKT signaling (12) and activated AKT signaling is implicated in the negative regulation of MAPK/ERK signaling (35).

We examined the relationship of IGF2 and these downstream signaling markers, p-ERK and p-AKT, in human prostate samples using automated quantitative image analysis. Interestingly, p-AKT exhibited a very strong correlation with IGF2 in benign prostate tissues with a less pronounced, but signfiicant p-ERK correlation (Figure 5C-D). This stronger relationship between IGF2 and p-AKT signaling in humans might be due to species-specific differences. A recent report demonstrated *IGF2* LOI correlates with increased p-AKT in human colorectal cancer tissues (38). Alternatively, the histologically normal prostate specimens analyzed here originated from prostates containing cancer, and potentially harbor epigenetic alterations as part of a well-described field effect (36,37) encouraging signaling through p-AKT. In sum, these data support our animal model findings in which animals expressing greater levels of IGF2 through LOI lead to increases in p-ERK or p-AKT signaling.

Using KI67 immunohistochemistry, the current work demonstrates significantly increased levels of epithelial-specific proliferation in mouse prostates containing *Igf2* LOI (Figure 4A). Kaneda *et al.* previously found *Igf2* LOI in the murine colon induces increased expression of proliferation related-genes (18). This mouse model achieved *Igf2* LOI in the colon through genomic deletion of the ICR and *H19* gene sequences, a potentially confounding factor given the emerging role of H19 long noncoding sequences in cancer

development and progression (39). The animal model used in the current study has clear advantages namely achieving *Igf2* LOI while leaving *H19* sequences and expression intact (Supplementary Figure S1A) (22). Despite these model differences we find, by RT-qPCR, a similar set of cell-cycle related genes to be upregulated with *Igf2* LOI alone. In addition, we demonstrate upregulation of transcriptional markers of activated p-ERK signaling (Figure 5A) emphasizing the role of this epigenetic alteration in driving proliferation. A recent report analyzing the field effect in prostate cancer demonstrated a number of genes induced in normal appearing, cancer-adjacent tissues that are predictive of worse clinical outcomes (36). Among these prognostic genes were *KI67*, *FOS*, and *CHAF1A*, all significantly altered with *Igf2* LOI in this study. This suggests that the *IGF2* LOI found in the field effect, commonly seen in human cancer, may hold prognostic value in normal prostate tissues, such as negative biopsy specimens.

One potential issue with the 142* mouse model of *Igf2* LOI in the study of prostatic disease is the *Igf2* LOI experienced in all tissues of these animals. The effects of systemic LOI were indeed apparent in these animals, including increased bodyweight (Figure 1D; Supplementary Figure S1B and S1C) at all ages and liver enlargement in older animals. However, this model has specific advantages over studies previously conducted in other organ systems. Compared to transgenic models that experience 20- to 30-fold increases in serum *Igf2* (42) and large increases in tissue levels (20,40), our animals experience ~2.5 fold increase in *Igf2* expression, physiologically similar to the levels seen with aging (4) and in tumors (41). Other animal models have achieved physiologic levels of *Igf2* LOI, but these require deletion of the *Igf2-H19* ICR and/or the *H19* gene (18). Our LOI animals also do not develop invasive cancer. We tested whether *Nkx3.1* loss acts in a synergistic fashion to generate tumors, but this was not found to occur. *Igf2* LOI has been studied for its

contribution to cancer development but typically requires other strong genetic alterations to form tumors, such as ApcMin/+ in the colon (43), SV-40 large T-antigen in the liver (44), and Wilm's Tumor 1 (*Wt1*) in Wilm's tumor models (45).

Ultimately, PCa is an age-related disease that is marked by multiple foci of cancer. Mirroring this observation, *IGF2* loss of imprinting progresses in an age-related manor, and can be found throughout the peripheral prostate (4,31). Herein, we provide evidence for the first time that *Igf2* LOI encourages early prostatic neoplasia. Furthermore, underlying increased disease was an induction of proliferation mediated by increased MAPK/ERK signaling. Taken together, *Igf2* LOI acts as a promoter of disease formation by increasing the fitness of affected cells, subsequently raising the possibility of further adverse genomic events. Ultimately, *Igf2* LOI may be an important biomarker for future disease risk and the development of this epigenetic alteration may provide a reversible target for chemoprevention. Recent research suggests metformin may dampen IGF axis signaling through negative regulation of p-ERK (47,48) and is currently being investigated as a prevention agent for early prostate cancer (49). Screening for *Igf2* LOI, or potentially p-ERK or p-AKT signaling induction in patients with negative biopsies may provide important future opportunities for identifying these chemoprevention targets.

Acknowledgements

This study was supported by NIH/NCI 5R01CA097131 (PI: Jarrard) and ND was supported by an NCI training grant (T32 CA009135). The author(s) thank the University of Wisconsin Translational Research Initiatives in Pathology laboratory, in part supported by the UW Department of Pathology and Laboratory Medicine and UWCCC grant P30 CA014520, for use of its facilities and services.

References

1. Siegel RL, Miller KD, Jemal A. Cancer statistics, 2015. CA Cancer J Clin **2015**;65:5-29

2. Damaschke NA, Yang B, Bhusari S, Svaren JP, Jarrard DF. Epigenetic susceptibility factors for prostate cancer with aging. Prostate **2013**;73:1721-30

3. Guileyardo JM, Johnson WD, Welsh RA, Akazaki K, Correa P. Prevalence of latent prostate carcinoma in two U.S. populations. J Natl Cancer Inst **1980**;65:311-6

4. Fu VX, Dobosy JR, Desotelle JA, Almassi N, Ewald JA, Srinivasan R*, et al.* Aging and Cancer-Related Loss of Insulin-like Growth Factor 2 Imprinting in the Mouse and Human Prostate. Cancer Res **2008**;68:6797-802

5. Jarrard DF, Bussemakers MJ, Bova GS, Isaacs WB. Regional loss of imprinting of the insulin-like growth factor II gene occurs in human prostate tissues. Clin Cancer Res **1995**;1:1471-8

6. Livingstone C. IGF2 and cancer. Endocr Relat Cancer **2013**;20:R321-39

7. Bhatia-Gaur R, Donjacour AA, Sciavolino PJ, Kim M, Desai N, Young P*, et al.* Roles for Nkx3.1 in prostate development and cancer. Genes Dev **1999**;13:966-77

8. He WW, Sciavolino PJ, Wing J, Augustus M, Hudson P, Meissner PS*, et al.* A novel human prostate-specific, androgen-regulated homeobox gene (NKX3.1) that maps to 8p21, a region frequently deleted in prostate cancer. Genomics **1997**;43:69-77

9. Voeller HJ, Augustus M, Madike V, Bova GS, Carter KC, Gelmann EP. Coding region of NKX3.1, a prostate-specific homeobox gene on 8p21, is not mutated in human prostate cancers. Cancer Res **1997**;57:4455-9

10. Dahia PL. PTEN, a unique tumor suppressor gene. Endocr Relat Cancer **2000**;7:115-29

11. Abdulkadir SA, Magee JA, Peters TJ, Kaleem Z, Naughton CK, Humphrey PA*, et al.* Conditional loss of Nkx3.1 in adult mice induces prostatic intraepithelial neoplasia. Mol Cell Biol **2002**;22:1495-503

12. Lei Q, Jiao J, Xin L, Chang CJ, Wang S, Gao J*, et al.* NKX3.1 stabilizes p53, inhibits AKT activation, and blocks prostate cancer initiation caused by PTEN loss. Cancer Cell **2006**;9:367-78

13. Ogawa O, Eccles MR, Szeto J, McNoe LA, Yun K, Maw MA*, et al.* Relaxation of insulin-like growth factor II gene imprinting implicated in Wilms' tumour. Nature **1993**;362:749-51

14. Murphy SK, Huang Z, Wen Y, Spillman MA, Whitaker RS, Simel LR*, et al.* Frequent IGF2/H19 domain epigenetic alterations and elevated IGF2 expression in epithelial ovarian cancer. Mol Cancer Res **2006**;4:283-92

15. Zhao R, DeCoteau JF, Geyer CR, Gao M, Cui H, Casson AG. Loss of imprinting of the insulin-like growth factor II (IGF2) gene in esophageal normal and adenocarcinoma tissues. Carcinogenesis **2009**;30:2117-22

16. Hartmann LC, Sellers TA, Frost MH, Lingle WL, Degnim AC, Ghosh K*, et al.* Benign breast disease and the risk of breast cancer. N Engl J Med **2005**;353:229-37

17. Cui H, Cruz-Correa M, Giardiello FM, Hutcheon DF, Kafonek DR, Brandenburg S*, et al.* Loss of IGF2 imprinting: a potential marker of colorectal cancer risk. Science **2003**;299:1753-5

18. Kaneda A, Wang CJ, Cheong R, Timp W, Onyango P, Wen B*, et al.* Enhanced sensitivity to IGF-II signaling links loss of imprinting of IGF2 to increased cell proliferation and tumor risk. Proc Natl Acad Sci U S A **2007**;104:20926-31

19. Haley VL, Barnes DJ, Sandovici I, Constancia M, Graham CF, Pezzella F*, et al.* Igf2 pathway dependency of the Trp53 developmental and tumour phenotypes. EMBO Mol Med **2012**;4:705-18

20. Bates P, Fisher R, Ward A, Richardson L, Hill DJ, Graham CF. Mammary cancer in transgenic mice expressing insulin-like growth factor II (IGF-II). Br J Cancer **1995**;72:1189-93

21. Moorehead RA, Sanchez OH, Baldwin RM, Khokha R. Transgenic overexpression of IGF-II induces spontaneous lung tumors: a model for human lung adenocarcinoma. Oncogene **2003**;22:853-7

22. Pant V, Mariano P, Kanduri C, Mattsson A, Lobanenkov V, Heuchel R*, et al.* The nucleotides responsible for the direct physical contact between the chromatin insulator protein CTCF and the H19 imprinting control region manifest parent of origin-specific long-distance insulation and methylation-free domains. Genes Dev **2003**;17:586-90

23. Kanduri C, Pant V, Loukinov D, Pugacheva E, Qi CF, Wolffe A*, et al.* Functional association of CTCF with the insulator upstream of the H19 gene is parent of origin-specific and methylation-sensitive. Curr Biol **2000**;10:853-6

24. Park JH, Walls JE, Galvez JJ, Kim M, Abate-Shen C, Shen MM*, et al.* Prostatic intraepithelial neoplasia in genetically engineered mice. Am J Pathol **2002**;161:727-35

25. Huang W, Hennrick K, Drew S. A colorful future of quantitative pathology: validation of Vectra technology using chromogenic multiplexed immunohistochemistry and prostate tissue microarrays. Hum Pathol **2013**;44:29-38

26. Vocke CD, Pozzatti RO, Bostwick DG, Florence CD, Jennings SB, Strup SE*, et al.* Analysis of 99 microdissected prostate carcinomas reveals a high frequency of allelic loss on chromosome 8p12-21. Cancer Res **1996**;56:2411-6

27. Kim MJ, Bhatia-Gaur R, Banach-Petrosky WA, Desai N, Wang Y, Hayward SW*, et al.* Nkx3.1 mutant mice recapitulate early stages of prostate carcinogenesis. Cancer Res **2002**;62:2999-3004

28. Pollak M. Insulin and insulin-like growth factor signalling in neoplasia. Nat Rev Cancer **2008**;8:915-28

29. Whitmarsh AJ. Regulation of gene transcription by mitogen-activated protein kinase signaling pathways. Biochim Biophys Acta **2007**;1773:1285-98

30. Bergers G, Graninger P, Braselmann S, Wrighton C, Busslinger M. Transcriptional activation of the fra-1 gene by AP-1 is mediated by regulatory sequences in the first intron. Mol Cell Biol **1995**;15:3748-58

31. Bhusari S, Yang B, Kueck J, Huang W, Jarrard DF. Insulin-like growth factor-2 (IGF2) loss of imprinting marks a field defect within human prostates containing cancer. Prostate **2011**;71:1621-30

32. Bonnet P, Reiter E, Bruyninx M, Sente B, Dombrowicz D, de Leval J*, et al.* Benign prostatic hyperplasia and normal prostate aging: differences in types I and II 5 alpha-reductase and steroid hormone receptor messenger ribonucleic acid (mRNA) levels, but not in insulin-like growth factor mRNA levels. J Clin Endocrinol Metab **1993**;77:1203-8

33. Samani AA, Yakar S, LeRoith D, Brodt P. The role of the IGF system in cancer growth and metastasis: overview and recent insights. Endocr Rev **2007**;28:20-47

34. Magee JA, Abdulkadir SA, Milbrandt J. Haploinsufficiency at the Nkx3.1 locus. A paradigm for stochastic, dosage-sensitive gene regulation during tumor initiation. Cancer Cell **2003**;3:273-83

35. Mendoza MC, Er EE, Blenis J. The Ras-ERK and PI3K-mTOR pathways: cross-talk and compensation. Trends Biochem Sci **2011**;36:320-8

36. Magi-Galluzzi C, Maddala T, Falzarano SM, Cherbavaz DB, Zhang N, Knezevic D*, et al.* Gene expression in normal-appearing tissue adjacent to prostate cancers are predictive of clinical outcome: evidence for a biologically meaningful field effect. Oncotarget **2016**;7:33855-65

37. Yang B, Bhusari S, Kueck J, Weeratunga P, Wagner J, Leverson G*, et al.* Methylation profiling defines an extensive field defect in histologically normal prostate tissues associated with prostate cancer. Neoplasia **2013**;15:399-408

38. Belharazem D, Magdeburg J, Berton AK, Beissbarth L, Sauer C, Sticht C*, et al.* Carcinoma of the colon and rectum with deregulation of insulin-like growth factor 2 signaling: clinical and molecular implications. J Gastroenterol **2016**;51:971-84

39. Raveh E, Matouk IJ, Gilon M, Hochberg A. The H19 Long non-coding RNA in cancer initiation, progression and metastasis - a proposed unifying theory. Mol Cancer **2015**;14:184

40. Rao G, Pedone CA, Del Valle L, Reiss K, Holland EC, Fults DW. Sonic hedgehog and insulin-like growth factor signaling synergize to induce medulloblastoma formation from nestin-expressing neural progenitors in mice. Oncogene **2004**;23:6156-62

41. Ravenel JD, Broman KW, Perlman EJ, Niemitz EL, Jayawardena TM, Bell DW*, et al.* Loss of imprinting of insulin-like growth factor-II (IGF2) gene in distinguishing specific biologic subtypes of Wilms tumor. J Natl Cancer Inst **2001**;93:1698-703

42. Rogler CE, Yang D, Rossetti L, Donohoe J, Alt E, Chang CJ*, et al.* Altered body composition and increased frequency of diverse malignancies in insulin-like growth factor-II transgenic mice. Journal of Biological Chemistry **1994**;269:13779-84

43. Hassan AB, Howell JA. Insulin-like growth factor II supply modifies growth of intestinal adenoma in Apc(Min/+) mice. Cancer Res **2000**;60:1070-6

44. Christofori G, Naik P, Hanahan D. A second signal supplied by insulin-like growth factor II in oncogene-induced tumorigenesis. Nature **1994**;369:414-8

45. Hu Q, Gao F, Tian W, Ruteshouser EC, Wang Y, Lazar A*, et al.* Wt1 ablation and Igf2 upregulation in mice result in Wilms tumors with elevated ERK1/2 phosphorylation. J Clin Invest **2011**;121:174-83

46. Kim MJ, Cardiff RD, Desai N, Banach-Petrosky WA, Parsons R, Shen MM*, et al.* Cooperativity of Nkx3.1 and Pten loss of function in a mouse model of prostate carcinogenesis. Proc Natl Acad Sci U S A **2002**;99:2884-9

47. Klubo-Gwiezdzinska J, Jensen K, Costello J, Patel A, Hoperia V, Bauer A*, et al.* Metformin inhibits growth and decreases resistance to anoikis in medullary thyroid cancer cells. Endocr Relat Cancer **2012**;19:447-56

48. Cao H, Dong W, Qu X, Shen H, Xu J, Zhu L*, et al.* Metformin Enhances the Therapy Effects of Anti-IGF-1R mAb Figitumumab to NSCLC. Sci Rep **2016**;6:31072

49. Morales DR, Morris AD. Metformin in cancer treatment and prevention. Annu Rev Med **2015**;66:17-29

Table 1: Prostatic Intraepithelial Neoplasia (PIN) Occurrence in Experimental Animals

	Maintenance of Imprinting				Loss of Imprinting			
Nkx3.1(+/+)	**Total**	**NL**	**LG**	**IG/HG**	**Total**	**NL**	**LG**	**IG/HG**
6 Months	16	4	10	2	13	1	5	7
12 Months	15	4	6	5	12	3	4	5
18 Months	11	2	5	4	16	0	6	10
	42	10 (24%)	21 (50%)	11 (26%)	41	4 (10%)	15 (37%)	22 (54%)
Nkx3.1(+/-)								
6 Months	11	1	7	3	12	2	3	7
12 Months	11	2	4	5	13	1	5	7
18 Months	10	3	3	4	16	2	4	10
	32	6 (19%)	14 (44%)	12 (38%)	41	5 (12%)	12 (29%)	24 (59%)
Nkx3.1(-/-)								
6 Months	11	0	4	7	10	0	2	8
12 Months	10	0	3	7	15	0	3	12
18 Months	11	0	3	8	14	0	5	9
	32	0 (0%)	10 (31%)	22 (69%)	39	0 (0%)	10 (26%)	29 (74%)

*NL (normal), LG (Low grade PIN), IG (Intermediate grade), HG (High grade). The highest scoring lesion in each mouse prostate was determined.

Figure 1. Biallelic expression of Igf2 in 142* mice.

A, Breeding schemes for generation of maintenance (monoallelic *Igf2*) and loss of imprinting (biallelic *Igf2*) mice. Maternal transmission of 142* mutation (H19-ICR +/-) results in biallelic expression in offspring by abolishing CTCF insulator activity at the normally silenced maternal allele. Paternal transmission leads to the typical monoallelic expression. ***B,*** Ventral prostate (VP) and Dorsolateral prostate (DLP) tissues were analyzed for maintenance of imprinting (MOI) and loss of imprinting (LOI) in mice and maternal and paternal allelic expression was quantitated using FluPE as described in methods. MOI mice maintain expression from a single allele, while LOI mice exhibit biallelic expression. ***C,*** *Igf2* mRNA expression measured by qPCR in mouse prostates (**P*<0.05, mean±SD; n = 6 each group). ***D*****,** Body weights of experimental animals were recorded throughout their lifetime. LOI animals expressing biallelic *Igf2* were persistently heavier throughout their life (mean±95% CI; ***P*<0.01, **P*<0.05). ***E, F, G,*** *Igf2* protein expression was quantitatively analyzed on tissue microarrays constructed from mouse prostate tissues. *Igf2* protein expression was significantly elevated in LOI animals with ***(E)*** *Nkx3.1*$^{+/+}$ (*P*=0.001, *P*=0.015, *P*=0.012; 6, 12, 18 months)**,** ***(F)*** *Nkx3.1*$^{+/-}$ (*P*=0.002, *P*=0.02, *P*=0.04; 6, 12, 18 months) and ***(G)*** *Nkx3.1*$^{-/-}$ (*P*<0.001, *P*=0.029, *P*=0.043; 6, 12, 18 months)**,** backgrounds across all ages (**P*<0.05, columns represent Mean±SD; n > 8 for each group).

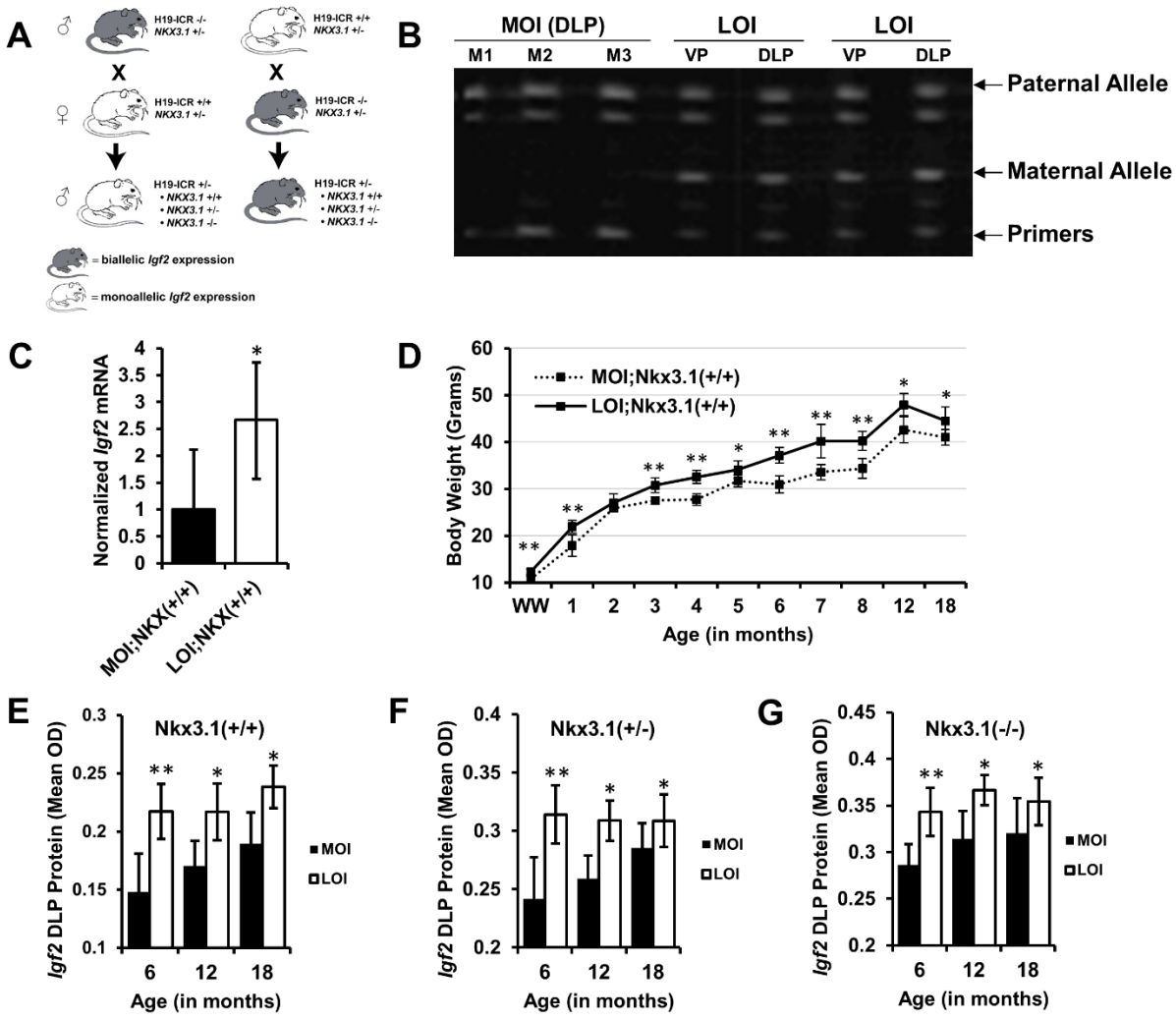
A
H19-ICR -/-
NKX3.1 +/-
H19-ICR +/+
NKX3.1 +/-
X
X
H19-ICR +/+
NKX3.1 +/-
H19-ICR -/-
NKX3.1 +/-
H19-ICR +/-
• NKX3.1 +/+
• NKX3.1 +/-
• NKX3.1 -/-
H19-ICR +/-
• NKX3.1 +/+
• NKX3.1 +/-
• NKX3.1 -/-
= biallelic Igf2 expression
= monoallelic Igf2 expression
B
MOI (DLP)
LOI
LOI
M1
M2
M3
VP
DLP
VP
DLP
Paternal Allele
Maternal Allele
Primers
C
Normalized Igf2 mRNA
MOI;NKX(+/+)
LOI;NKX(+/+)
D
Body Weight (Grams)
MOI;Nkx3.1(+/+)
LOI;Nkx3.1(+/+)
WW
Age (in months)
E
Nkx3.1(+/+)
Igf2 DLP Protein (Mean OD)
MOI
LOI
Age (in months)
F
Nkx3.1(+/-)
Igf2 DLP Protein (Mean OD)
MOI
LOI
Age (in months)
G
Nkx3.1(-/-)
Igf2 DLP Protein (Mean OD)
MOI
LOI
Age (in months)

Figure 2. Histopathology of PIN lesions and demonstration of increased prevalence of PIN in LOI mice.

H&E stained FFPE mouse prostate tissues matched by *Nkx3.1* status (horizontally) and *Igf2* imprint status (vertically) at 12 mo. PIN grading was performed as described by Park et al. (25) and low (PIN 1 and 2) versus intermediate/high grade (PIN 3 and 4) lesions were based on the most severe lesion within the prostate. ***A,*** In normal *MOI;Nkx3.1*$^{+/+}$ prostate tissues, glands are lined with columnar epithelial cells and exhibit uniform staining of cytoplasmic and nucleic structures (400X Inset). Low grade (LG) PIN lesions ***(B,C)*** were seen in all genotypes surveyed, marked by nuclear pleomorphism and mild disorganization of cell layers projecting into the lumen. More severe PIN lesions ***(D, E, F)*** contain predominantly cribriform patterns, with increasing severity seen with *Nkx3.1* deletion. ***G,*** LOI prostates display increased prevalence and severity of PIN lesions. Multiple adjacent glands are affected with similar grade PIN in LOI animals.

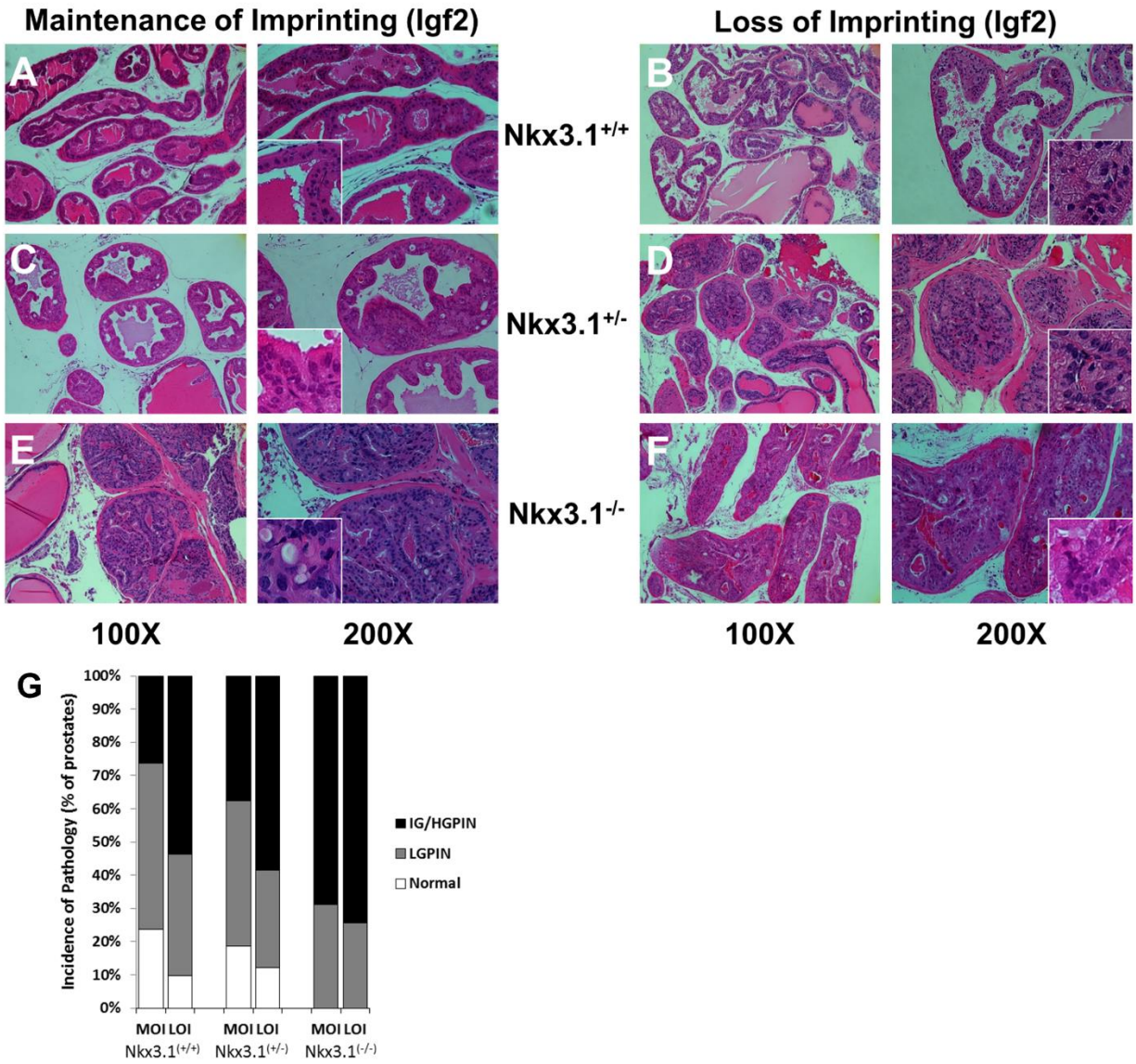
Maintenance of Imprinting (Igf2)
Loss of Imprinting (Igf2)
A
B
C
D
E
F
Nkx3.1+/+
Nkx3.1+/-
Nkx3.1-/-
100X
200X
100X
200X
G
Incidence of Pathology (% of prostates)
100%
90%
80%
70%
60%
50%
40%
30%
20%
10%
0%
MOI LOI
Nkx3.1(+/+)
MOI LOI
Nkx3.1(+/-)
MOI LOI
Nkx3.1(-/-)
IG/HGPIN
LGPIN
Normal

Figure 3. Igf2 LOI results in an increased multifocality within PIN affected prostate glands.

H&E stained sections of mouse prostate tissue were quantified for the number of normal and PIN appearing glands. Proportions of PIN affected glands were compared in **(*A*)** *Nkx3.1*$^{+/+}$, **(*B*)** *Nkx3.1*$^{+/-}$, and **(*C*)** *Nkx3.1*$^{-/-}$ mice. ***A*,** *LOI;Nkx3.1*$^{+/+}$ animals present significantly greater PIN affected glands at 6 and 18 months, at 12 months similar differences were apparent but non-significant. ***B,*** *LOI;Nkx3.1*$^{+/-}$ animals present significantly greater PIN affected glands at all ages (6, 12, 18 mo). ***C,*** *Nkx3.1*$^{-/-}$ animals exhibit a significantly increased proportion of PIN affected glands at 6 months, but non-significant differences at 12 and 18 months. ***D,*** Frequency of PIN lesions increase with *Nkx3.1* mutation and in the presence of LOI in an additive fashion (**P*<0.05, ***P*<0.01).

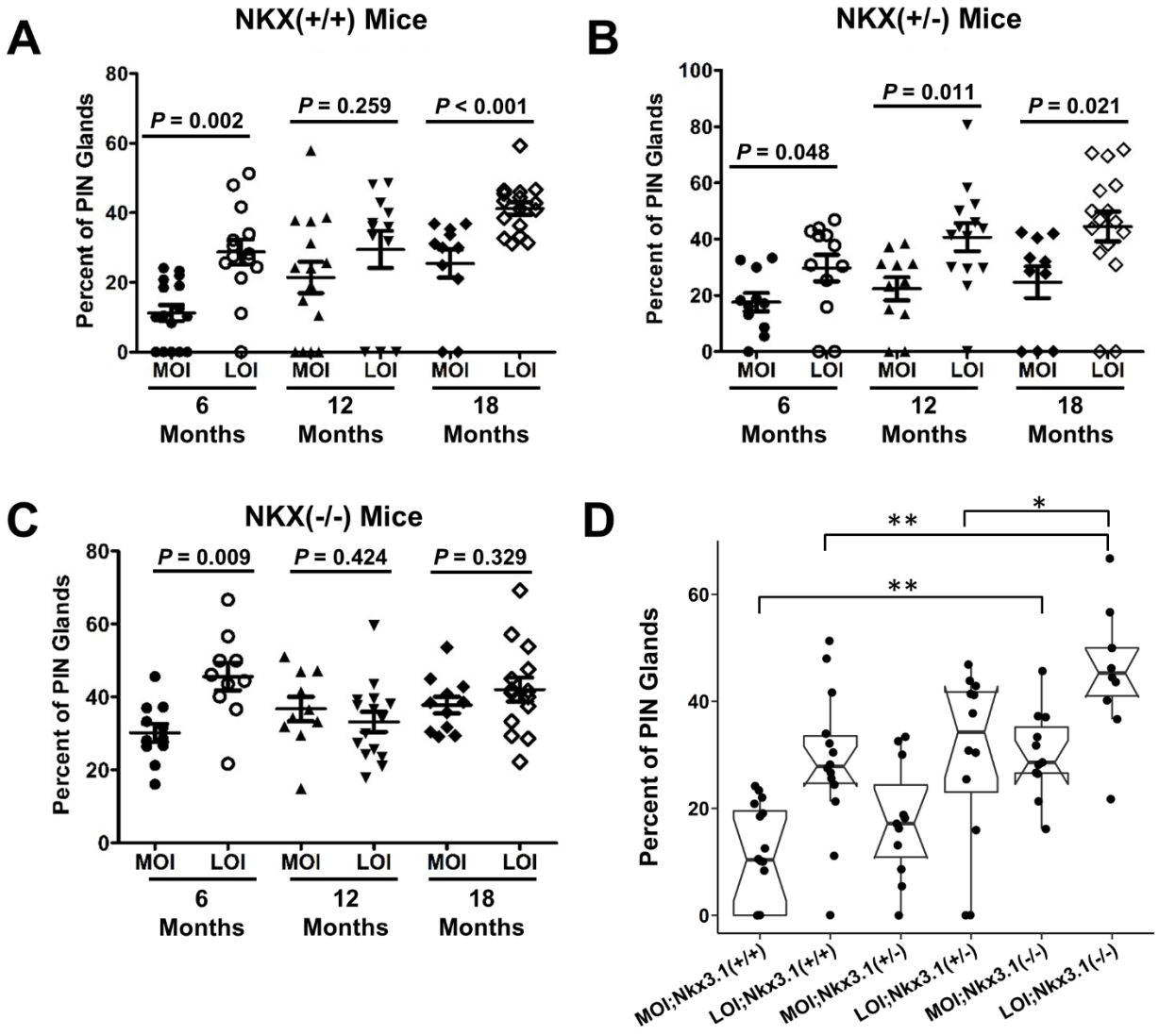
A
NKX(+/+) Mice
Percent of PIN Glands
P = 0.002
P = 0.259
P < 0.001
MOI
LOI
6 Months
12 Months
18 Months
B
NKX(+/-) Mice
P = 0.048
P = 0.011
P = 0.021
C
NKX(-/-) Mice
P = 0.009
P = 0.424
P = 0.329
D
**
*
**
MOI;Nkx3.1(+/+)
LOI;Nkx3.1(+/+)
MOI;Nkx3.1(+/-)
LOI;Nkx3.1(+/-)
MOI;Nkx3.1(-/-)
LOI;Nkx3.1(-/-)

Figure 4. Igf2 LOI animals display increased proliferation and phosphorylated ERK expression.

Tissue microarrays constructed from mouse prostate tissues were IHC stained for Ki-67 and *Igf2* downstream signaling markers. ***A,*** *Igf2* LOI resulted in significantly higher rates of prostate epithelial cell proliferation (Ki-67) ((***P*<0.01, **P*<0.05; columns represent mean±95% CI). Protein expression levels were quantified by Vectra analysis and average levels of p-ERK staining analyzed by age and genotype. Representative p-ERK staining (brown) in **(*B*)** MOI and **(*C*)** LOI prostate tissues from 12 mo *Nkx3.1*$^{+/+}$ mice. ***D,*** *LOI;Nkx3.1*$^{+/+}$ prostate tissues showed significantly elevated levels of p-ERK staining at 6, 12, and 18 months (P=0.013, P=0.004 , P=0.012 respectively) . ***E,*** Levels of p-ERK were increased at 6 (*P*=0.028) and 12 months (*P*=0.016) in *LOI;Nkx3.1*$^{+/-}$ mice compared to their age matched counterparts. ***F,*** Expression of p-AKT significantly increased in *LOI*;*Nkx3.1*$^{-/-}$ prostate tissues at 6 (*P*=0.038) and 12 (*P*=0.02) months. Figures 4D, 4E, 4F, columns represent mean±95% CI; ***P*<0.01; **P*<0.05.

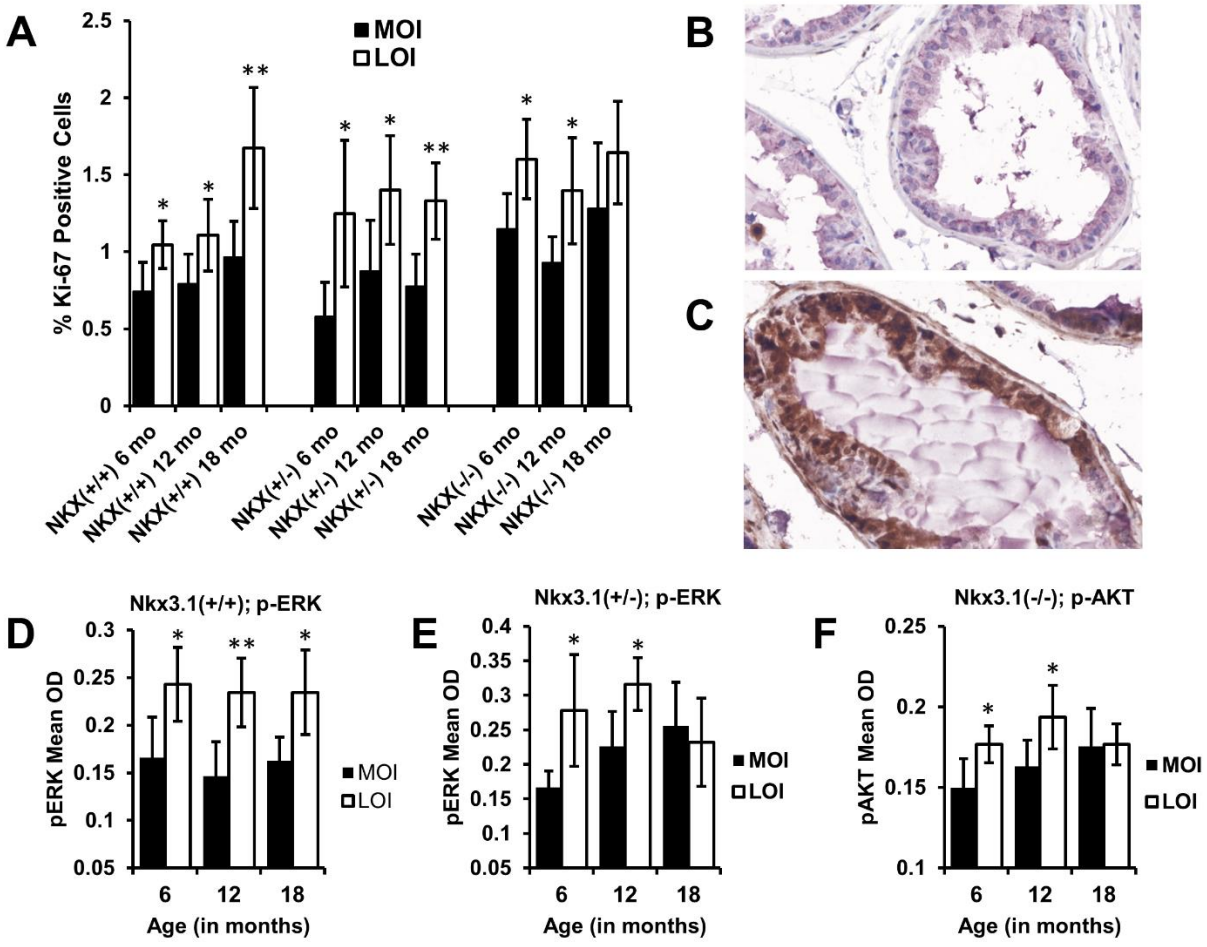
A
% Ki-67 Positive Cells
MOI
LOI
NKX(+/+) 6 mo
NKX(+/+) 12 mo
NKX(+/+) 18 mo
NKX(+/-) 6 mo
NKX(+/-) 12 mo
NKX(+/-) 18 mo
NKX(-/-) 6 mo
NKX(-/-) 12 mo
NKX(-/-) 18 mo
B
C
D
Nkx3.1(+/+); p-ERK
pERK Mean OD
Age (in months)
E
Nkx3.1(+/-); p-ERK
F
Nkx3.1(-/-); p-AKT
pAKT Mean OD

Figure 5. Transcription of p-ERK target and proliferation related genes are increased in Igf2 LOI prostates, IGF2 correlates with p-ERK and p-AKT in human prostate tissues.

Gene transcription was analyzed in *MOI;Nkx3.1*$^{+/+}$ (n=7) and *LOI;Nkx3.1*$^{+/+}$ (n=8) mouse prostate tissues. ***A*****,** Increased expression of p-ERK target genes Cyclin D1 (P=0.003), *c-Fos* (P=0.003), and *Fosl1* (P=0.009) was demonstrated in LOI prostates. ***B*****,** Increased expression of proliferation associated genes *Mcm5* (P=0.009), *Mcm3* (P=0.012), *Cdc6* (P=0.001), and *Chaf1a* (P=0.005) was also detected in LOI prostates (***P*<0.01, **P*<0.05; columns represent mean±SD). ***C,*** Quantitative IHC in human prostate tissues demonstrates a significant correlation between IGF2 and p-ERK expression in benign prostate tissues (BPT). ***D,*** IGF2 and p-AKT protein expression strongly correlate in human benign prostate tissues. Correlation coefficient and *P*-value calculated using Pearson's product moment correlation (BPT, n=48). ***E*****,** In LOI affected prostates containing at least one *Nkx3.1* allele, proliferation is predominantly mediated via MAPK/ERK signaling (red arrows). In contrast, *Nkx3.1* negatively regulates AKT signaling in *Nkx3.1*$^{+/n}$ animals, and *Nkx3.1*$^{-/-}$ prostates exhibit increased p-AKT.

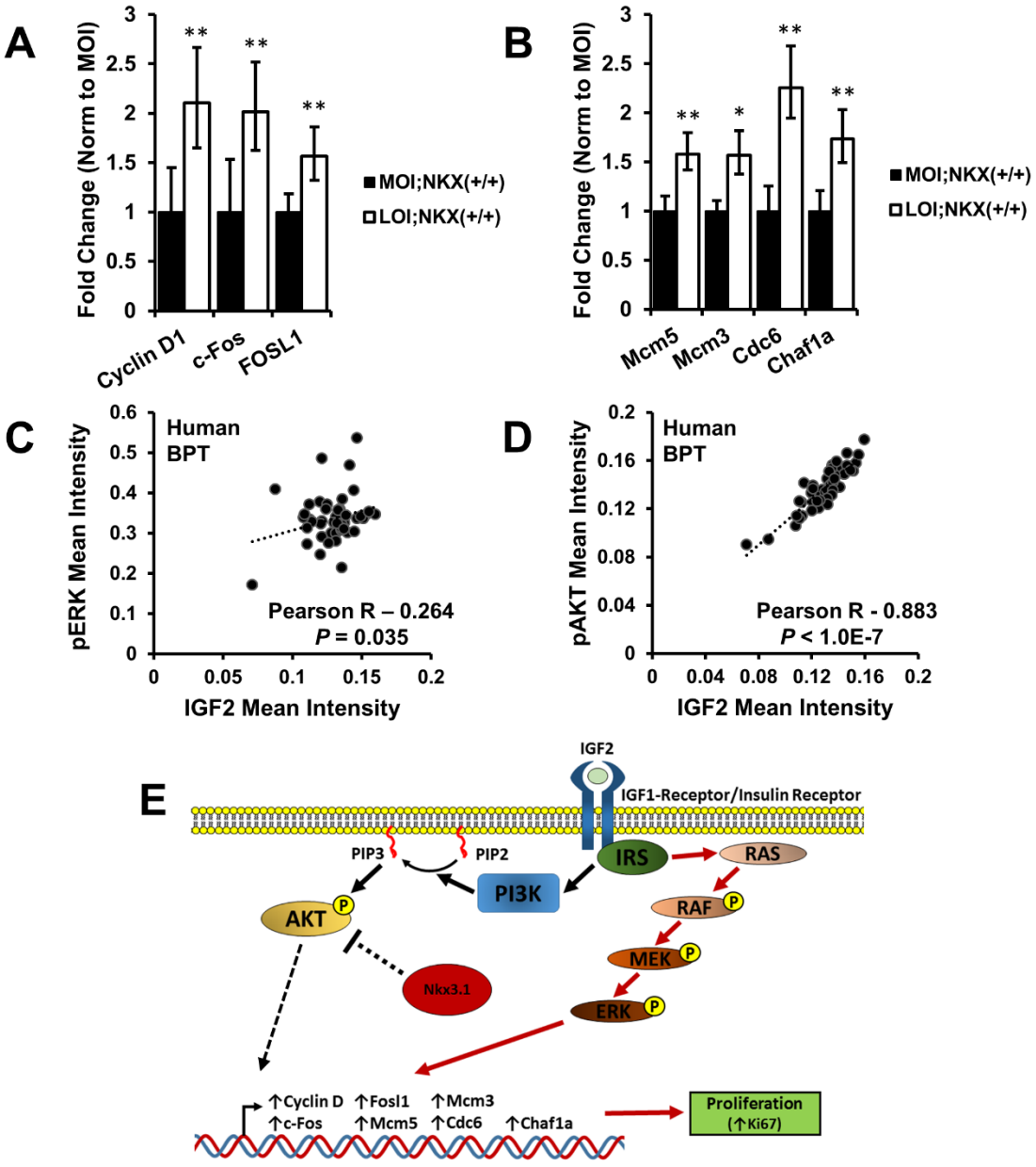
A
Fold Change (Norm to MOI)
3
2.5
2
1.5
1
0.5
0
**
**
**
MOI;NKX(+/+)
LOI;NKX(+/+)
Cyclin D1
c-Fos
FOSL1
B
Fold Change (Norm to MOI)
**
*
**
**
MOI;NKX(+/+)
LOI;NKX(+/+)
Mcm5
Mcm3
Cdc6
Chaf1a
C
pERK Mean Intensity
Human
BPT
Pearson R – 0.264
P = 0.035
IGF2 Mean Intensity
D
pAKT Mean Intensity
Human
BPT
Pearson R - 0.883
P < 1.0E-7
IGF2 Mean Intensity
E
IGF2
IGF1-Receptor/Insulin Receptor
PIP3
PIP2
IRS
RAS
PI3K
AKT
RAF
MEK
ERK
Nkx3.1
↑Cyclin D
↑c-Fos
↑Fosl1
↑Mcm5
↑Mcm3
↑Cdc6
↑Chaf1a
Proliferation
(↑Ki67)

Supplementary Figure S1. Prostatic H19 expression and bodyweight measurements of experimental mice.

A, Long non-coding RNA *H19* expression is unaltered in MOI vs. LOI mouse prostate tissues as detected by qPCR (Mean±SD, n=6 each group. ***B and C,*** Similar to *Nkx3.1*$^{+/+}$ animals, **(B)** *LOI;Nkx3.1*$^{+/-}$ and **(C)** *LOI;Nkx3.1*$^{-/-}$ animals were significantly heavier through their lifetime than their *Nkx3.1* genotype matched MOI counterparts. Measurements represent mean±SD with **P* < 0.05.

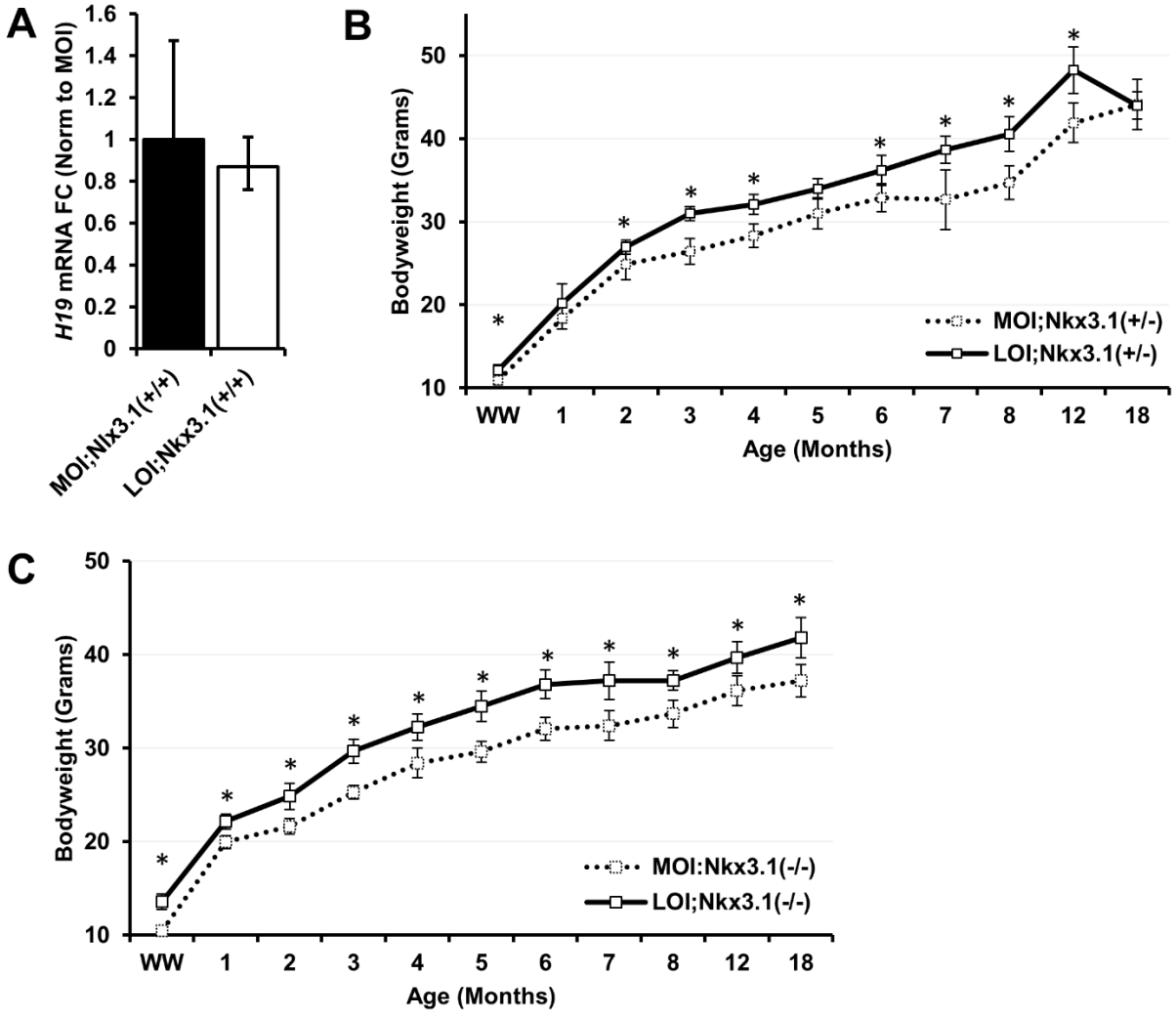
A
H19 mRNA FC (Norm to MOI)
1.6
1.4
1.2
1
0.8
0.6
0.4
0.2
0
MOI;Nkx3.1(+/+)
LOI;Nkx3.1(+/+)
B
Bodyweight (Grams)
50
40
30
20
10
WW
1
2
3
4
5
6
7
8
12
18
Age (Months)
MOI;Nkx3.1(+/-)
LOI;Nkx3.1(+/-)
C
Bodyweight (Grams)
50
40
30
20
10
WW
1
2
3
4
5
6
7
8
12
18
Age (Months)
MOI:Nkx3.1(-/-)
LOI;Nkx3.1(-/-)

Supplementary Figure S2. Phosphorylated AKT and Apoptosis IHC.

Tissue microarrays constructed from mouse prostate tissue were IHC stained for p-AKT and Tunel (Apoptosis). ***A,*** No significant changes were in p-ERK expression were detected in *Nkx3.1*$^{-/-}$ mouse prostates. ***B and C,*** No significant changes were detected in p-AKT expression in **(B)** *Nkx3.1*$^{+/+}$ and **(C)** *Nkx3.1*$^{+/-}$ mouse prostate tissues. ***C,*** p-AKT expression was significantly increased in *LOI;Nkx3.1*$^{-/-}$ mouse prostate tissues at 6 months (P=0.038) and 12 months of age (P=0.027), no difference in p-AKT levels were detected at 18 months of age. ***D,*** Tunel staining performed as a marker of apoptosis analyzed by VECTRA exhibited no significant difference between age and genotyped matched MOI vs. LOI animals. All measurements represent mean$\pm$95% CI.

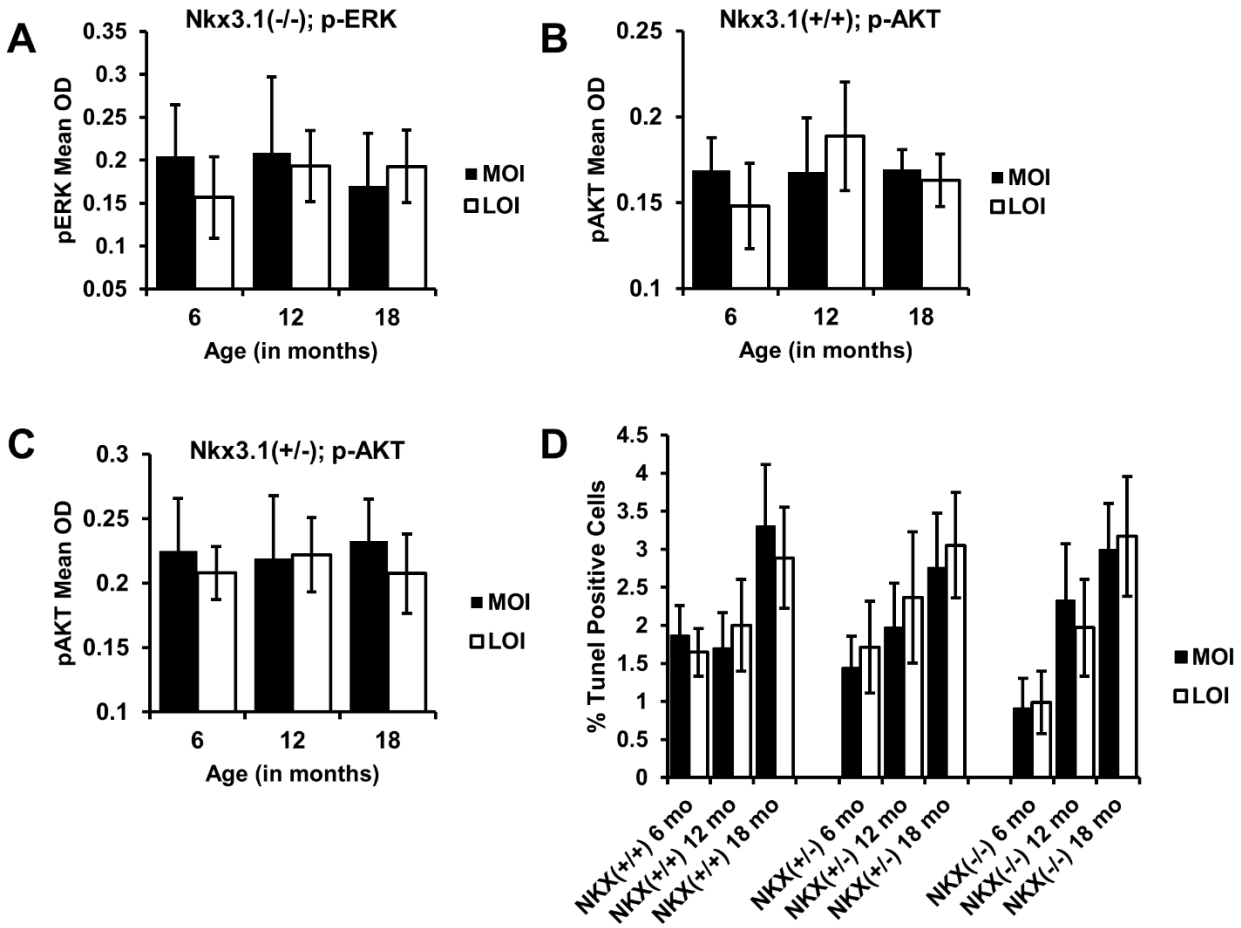
A
Nkx3.1(-/-); p-ERK
pERK Mean OD
0.35
0.3
0.25
0.2
0.15
0.1
0.05
6
12
18
Age (in months)
MOI
LOI
B
Nkx3.1(+/+); p-AKT
pAKT Mean OD
0.25
0.2
0.15
0.1
6
12
18
Age (in months)
MOI
LOI
C
Nkx3.1(+/-); p-AKT
pAKT Mean OD
0.3
0.25
0.2
0.15
0.1
6
12
18
Age (in months)
MOI
LOI
D
% Tunel Positive Cells
4.5
4
3.5
3
2.5
2
1.5
1
0.5
0
NKX(+/+) 6 mo
NKX(+/+) 12 mo
NKX(+/+) 18 mo
NKX(+/-) 6 mo
NKX(+/-) 12 mo
NKX(+/-) 18 mo
NKX(-/-) 6 mo
NKX(-/-) 12 mo
NKX(-/-) 18 mo
MOI
LOI

Supplementary Figure S3. IGF2 Expression Correlates with p-AKT and p-ERK Signaling in Human Prostate Tissues.

Protein expression levels of IGF2, p-AKT, and p-ERK were quantified by VECTRA on tissue microarrays (hTMA) containing human prostate tissues (Benign, n=48; Cancer, n=74; Metastases, n=22). ***A*****,** A significant weak positive correlation between IGF2 and p-ERK persists in cancer. ***B,*** A significant positive correlation between IGF2 and p-AKT persists in cancer. Correlation coefficient and *P*-value calculated using Pearson's product moment correlation (Cancer, n=74). ***C*****,** IGF2 expression is significantly elevated in cancer (*P* = 8.8E-10) and metastatic (*P* = 3.2E-07) tissues compared to benign. ***D,*** Phospo-AKT expression is significantly increased in cancer (*P* = 2.4E-04) and metastatic tissues (*P* = 0.0056) compared to benign. ***E,*** No significant changes in p-ERK expression were detected from benign to disease tissues. All data are mean±95% CI; ***P*<0.01.

Chapter III

CTCF and Cofactor Expression in Human Prostate Samples

Nathan A. Damaschke and David F. Jarrard

NA Damaschke, B Yang, ML Blute Jr., CP Lin, W Huang, and Jarrard DF. Neoplasia. 2014 Dec; 16(12):1018-27.

Abstract

Abnormal expression and function of chromatin regulators results in the altered chromatin structure seen in cancer. The chromatin regulator CTCF, its cofactor CHD8, and antagonistic paralogue BORIS have wide-ranging effects on gene regulation. Their concurrent expression and regulation was examined in benign, localized, and metastatic prostate cancer (PCa) arrays with extended follow-up using an automated quantitative imaging system, VECTRA™. Epithelial staining was quantified and compared against a range of clinicopathologic variables. CHD8 expression was decreased in HGPIN, localized, and metastatic PCa compared to benign ($P<0.001$). CHD8 promoter hypermethylation, assessed by Quantitative Pyrosequencing, occurred in over 45% of primary cancers in this population as well as the TGCA database. Treatment of cell lines with the demethylating agent 5-Aza-2'-deoxycytidine reactivated CHD8 expression. An interesting dichotomy for CHD8 was observed within primary cancers, with higher nuclear protein expression associated with adverse clinical outcomes including extracapsular extension ($P=0.007$), presence of metastases ($P=0.025$) and worse PSA-recurrence free survival ($P=0.048$). CHD8 outperformed Gleason score and predicted biochemical failure within intermediate grade prostate cancers. The BORIS/CTCF expression ratio increased in localized ($P=0.03$) and metastatic PCa ($P=0.006$) and was associated with higher Gleason score ($P=0.02$), increased tumor volume ($P=0.02$) and positive margins ($P=0.04$). Per cell heterogeneity of expression revealed all protein expression to be more heterogeneous in cancerous tissue (both $P<0.001$), especially high grade ($P<0.01$). In the first detailed analysis in cancer, a marked loss of CHD8 expression and increased BORIS/CTCF ratio indicate frequent disruption of CTCF and its effector genes in PCa.

Introduction

Prostate cancer (PCa) development is associated with epigenetic changes seen in both aging normal and cancerous tissues (1). The factors that direct these changes remain elusive. Polycomb-group and other proteins play a role in regulating genes through their modification of chromatin structure. Recent data suggests a critical role of these proteins, notably EZH2, in the malignant prostate phenotype (2). Three interrelated factors associated with the regulation of epigenetic marks include Chromodomain helicase DNA-binding protein 8 (*CHD8*), CCCTC-binding factor (*CTCF*), and Brother of the regulator of imprinted sites (*BORIS*). CHD8 and CTCF complex at CTCF binding sites and regulate gene expression through chromatin insulation, DNA methylation, and histone acetylation (3). Conversely, BORIS antagonizes CTCF function by competing at CTCF binding sites (4,5). Given the critical role of these chromatin-regulating genes, the co-expression of these proteins in PCa development and progression was investigated utilizing a unique quantitative, per-cell expression analysis.

CTCF is an 11-zinc finger protein with multifaceted functions. In addition to acting as a classical transcription factor, its presence regulates chromatin structure and contributes to epigenetic homeostasis through the formation of “boundary elements” between hetero- and euchromatin (6). With over 20,000 binding sites in the genome its regulatory action is complex and depends on the specific DNA sequence and interacting factors at CTCF binding sites (7). CTCF loss of function epigenetically alters numerous cancer-associated genes. In various cancers lack of CTCF activity is associated with epigenetic repression of hTERT, pRb, $p16^{INK4A}$, $p14^{ARF}$, and p53 (7). As a chromatin insulator, CTCF is known to have enhancer-blocking activity as demonstrated in the imprinted *Igf2-H19* imprint control region (8). Its function is opposed by its paralogue

BORIS, also known as CTCFL, that has extensive homology to the CTCF DNA-binding motif (9). While CTCF is thought to protect and maintain surrounding DNA methylation marks, BORIS expression coincides with the loss of CpG methylation (4,10,11). Their antagonistic function is seen at the *MAGE A1* promoter, where CTCF acts as a transcriptional repressor and BORIS leads to gene activation (5). BORIS may function as an oncogene and recent reports suggest its reactivation occurs in a variety of cancers, including the prostate (12).

The chromatin insulator function of CTCF at specific sites is dependent on CHD8, an ATP-dependent chromatin remodeling enzyme (3,13). CHD8 co-localizes and interacts with CTCF at several gene insulator sites including the *Igf2-H19* differentially methylated region (DMR), *B-globin* 5'HS5 insulator, and the c-*myc* and *BRCA1* gene promoters. The presence of both factors is required for normal genetic and epigenetic regulation (3). CHD8 loss has previously been identified in gastric and colorectal cancers (14). The CHD8-CTCF complex prevents the spread of transcriptionally inactive heterochromatin and a loss of CHD8 results in DNA hypermethylation and histone hypoacetylation near CTCF binding sites (3). Functional studies of CHD8 have shown dichotomous roles with regard to cell cycle activity. The presence of CHD8 negatively regulates β-Catenin signaling, suppresses p53-dependence (15,16), and negatively regulates HOXA2 gene expression (17). Conversely, CHD8 cooperates with androgen receptor to activate TMPRSS2 and is implicated in E2F-dependent gene transcription (18,19). The literature suggests a complex, and cryptic, role for CHD8 where losses and gains of function could have oncogenic-like gene regulation properties.

To analyze expression synchronously the VECTRA™ imaging system was employed, a quantitative tool which allows the automated selection and analysis of

expression signals within cells, cellular subsets, and compartments. This study sought to characterize the compartmental coexpression of these proteins and their clinical significance in PCa. These analyses reveal significant decreases in CHD8, in part due to hypermethylation, and increases in BORIS-CTCF ratio in PCa development. However, a dichotomy of higher CHD8 expression is associated with adverse features, including increased risk of PSA recurrence. Using this powerful imaging tool, we find the CTCF regulatory pathway is frequently altered in PCa which may help to explain common changes in CTCF effector genes in cancer.

Materials and Methods

Tissue Microarray

The University of Wisconsin Institutional Review Board (IRB) provides ethical insight to clinical projects and reviews all human research protocols in accordance with federal regulations, state laws, and local and University policies. FFPE-patient tissues used in this study were from the archive of the Department of Pathology and Laboratory Medicine, University of Wisconsin-Madison. A tissue microarray was constructed consisting of 288 duplicate cores from prostate tissues of different disease groups: 48 benign prostate tissues (BPT) (from normal, non-adjacent tissue without evidence of disease), 50 high grade intraepithelial neoplasia (HGPIN) (tissue from HGPIN tissue blocks of cancer patients in this cohort), 84 localized PCa (pT2), 62 aggressive PCa (pT3), and 44 metastatic lesions (brain, lung, bone, omentum, testis, colon, bladder, and lymph nodes).

Staining and Image Analysis

Slide preparation and antigen retrieval were conducted as previously described (20). Briefly, the slides were taken through routine deparffinization and rehydration. Two triple stains (CTCF, CHD8, and E-cadherin; CTCF, BORIS, and E-cadherin) were performed from two TMA sections with antibodies against CTCF (sc-5916; Santa Cruz Biotech, Santa Cruz, CA), CHD8 (NB100-60418; Novus Biologicals, Littleton, CO), and BORIS (sc-98982 Santa Cruz Biotech, Santa Cruz, CA). E-cadherin antibodies (Cell Signaling Technology, Beverly, MA) were used to define the epithelial compartment for better tissue segmentation.

Stained slides were loaded onto the slide scanner. Slides were scanned as previously describe(20). Cores with <5% epithelial component or loss of tissue were excluded from the analysis. Per-cell protein target signals were quantitated for individual

cores using the VECTRA™ imaging system according to manufacturer's protocols (Caliper Life Sciences, Hopkinton, MA). The inForm 1.2™ software was used to segment tissue subcellular compartments (nucleus vs. cytoplasm) and tissue compartments (epithelium vs. stroma).

Methylation analysis of CHD8 in Human Prostate Tissues

We obtained 11 paired flash frozen samples of tumor and benign adjacent tissue from radical prostatectomy samples using an approved IRB protocol. DNA was isolated and Quantitative Pyrosequencing was employed as we have previously described (21) to assess methylation across 2 CpG island regions previously suggested to be altered on methylation arrays (22). These regions were: i) 6 CpGs spanning the transcription start site (TSS) of CHD8 [Chr14:21,907,003-21,906,863] and ii) 7 CpGs encompassing a CpG island 600bp upstream of the transcription start site [Chr14:21,907,850-21,907,725]. Primers are available upon request.

Methylation Validation in The Cancer Genome Atlas Samples

To verify the patterns of methylation observed in cancer samples data was downloaded and analyzed form The Cancer Genome Atlas (TCGA) Project (https://tcga-data.nci.nih.gov/tcga/). The dataset contained methylation information for 49 solid prostate tissue normal (benign) and 336 prostate adenocarcinoma samples analyzed by the Illumina HumanMethylation450k Array. This dataset included information on the 6 CpGs analyzed at the CHD8 TSS, the 7 CpGs 600bp upstream were not analyzed by the 450k Array.

5-Aza-2'-deoxycytidine Treatment and Methylation Analyses in Cell Lines

A panel of cells was screened for low expression of CHD8. Two prostate cancer cell lines (DU145 and LNCaP)and Hela were treated with increasing doses of 5-Aza-2'-deoxycytidine

(0-100μM) for 48 hours, RNA was isolated and Quantitative PCR was performed as previously described (21). Briefly, CHD8 expression was analyzed by quantitative PCR using a CFX96 Real-time PCR detection system (Bio-Rad) and SYBR Green PCR master mix (Applied Biosystems). Primers used as previously described (23). Results were statistically compared using the t-test. DNA was generated, bisulfite treated, and Quantitative Pyrosequencing performed analyzing the same regions as the human prostate tissues above.

Statistical Analysis

Nuclear, cytoplasmic, and total expression of individual cores of various prostate tissues (benign, HGPIN, PCa, metastatic PCa) was statistically compared using Kruskal-Wallis test followed by Wilcoxon rank-sum tests. Pearson's r correlation analysis was used to quantify the relationship between CHD8/CTCF and BORIS/CTCF expressions. To compare protein expression in patient cancer samples with different clinicopathologic features (Gleason, pT stage, tumor volume, margins, SV involvement, extracapsular extension, and evidence of metastasis), Kruskal-Wallis test or Wilcoxon rank-sum test was used as appropriate, only primary tumor samples were used in this analysis. Duplicate PCa cores obtained from the same patient (73 cases) were averaged to provide a more precise estimation of protein expression in each biological replicate. Protein expression from 6 patients without clinical data was excluded from clinicopathologic analysis. Thus, 67 primary cancer patients in total were included in the clinicopathologic analysis after quality controls (Patient demographics, Table S1).

The spread and shape of per cell protein expressions for various tissues were characterized by calculating the coefficient of variation, skewness, and kurtosis. Further, these values were compared among varying pathological grades using the same non-parametric tests

as described above. The Simpson's Diversity Index (Gini-Simpson transformation) (24) was used to analyze heterogeneity as outlined by Faratian *et al.* (25). Briefly, per cell expression data of all samples was used to derive bins of equal percentages. Binning continuous expression values yield a score for each cell. Each cell from each core was then applied to the Gini-Simpson Index of diversity defined as:

$$SI = 1 - \frac{\sum n(n-1)}{N(N-1)}$$

Where n is the score of each binned cell and N is the total number of cells in each core. The SI scores for each core were then used to generate average diversity scores of Benign, HGPIN, localized PCa, and metastatic PCa.

Results

CHD8 expression is commonly decreased in localized and metastatic PCa

The CTCF-CHD8 (BORIS) system was synchronously investigated given their associations (Figure 1A) using the VECTRA™ imaging system which allows the automated selection and analysis of cells, cellular subsets (epithelial vs. stromal) and subcellular compartments (nucleus vs. cytoplasm). Nuclear levels of CHD8 were 1.5-2.5 fold higher than cytoplasmic in all samples. Total, nuclear, and cytoplasmic expression of CHD8 was significantly decreased in HGPIN, metastatic lesions, and primary PCa compared to benign prostate tissue (Figure 1B) (all $P < 0.001$, HGPIN cytoplasmic not significant). To define reduced expression, a Receiver Operating Curve (ROC) was constructed using total CHD8 expression to identify the optimal cut point that maximized the sum of sensitivity and specificity for discriminating between benign versus cancer cores. ROC analysis demonstrated excellent discrimination between benign versus cancer tissues (AUC 0.866, $P < 0.0001$) with a sensitivity and specificity of 84.3% and 76.3% respectively (Figure 1C). Using the optimal cut-off of 0.065 optical density (OD) to define decreased core expression, 118/140 (84.3%) of localized PCa , 18/46 (39.1%) of HGPIN , and 29/39 (74.4%) of metastatic lesions demonstrated reduced expression of CHD8 in contrast to only 19/80 (23.8%) of all benign cores (Fig. 1D). Therefore, decreased CHD8 expression is a common finding in PCa tissues.

Analysis of CHD8 promoter-associated CpG hypermethylation in human prostate tumor samples

CHD8 contains a promoter CpG island making CHD8 promoter-associated hypermethylation one etiology for decreased expression. One region spanning the CHD8

transcription start site (TSS) and another region 600bp upstream were analyzed. At the region 600bp upstream high levels of equivalent methylation was seen in all tumor and benign samples (data not shown). At the TSS CpG island, 5/11 (45%) of tumor samples demonstrated increased methylation across the first 4 CpG sites compared to matched benign (Figure 2A). To further assess this finding, we assessed methylation using 366 primary prostate tumors within the TGCA database. A significant increase in methylation across CpG 1-4 was also seen when tumor and normal tissues were compared (Wilcoxon Rank-sum all $P < 0.001$) (Figure 2B). In this validation dataset, 55%-67% of tumors showed increased methylation (compared to benign tissue mean) at CpGs 1-4 (data not shown).

To assess the role of methylation in controlling CHD8 transcription, a panel of cell lines was analyzed for CHD8 expression. Cell lines with lower expression of CHD8 were treated with increasing doses of 5-aza-2'-deoxycytidine (5-azadC) for 48 hrs prior to harvesting. 5-azadC resulted in a dose-dependent increase in CHD8 expression compared to DMSO alone (all $P<0.05$) for LNCaP (Figure 2C) PCa cell line. Similar treatment of DU145 did not result in increased expression of CHD8 mRNA (Supplementary Figure S1A). Analysis of CHD8 CpG methylation across the TSS showed similar levels of methylation across all 3 cell types (Supplementary Figure S1B). Additionally, all three cell types were highly methylated at a region 600 base pairs upstream of the TSS (Supplementary Figure S1C). These data indicate that DNA hypermethylation is a common finding within the CHD8 promoter region and treatment with a demethylating agent results in increased CHD8 expression.

In primary PCa, increased CHD8 is associated with adverse clinical features and outperforms Gleason Score in predicting PSA recurrence in intermediate grade tumors.

CHD8 expression was compared against a series of clinicopathologic variables including Gleason score, tumor stage, tumor volume, seminal vesicle involvement, positive margins, extracapsular extension and the presence of metastases (Table 1). Using *CHD8* as a continuous variable, a surprising increase in total and nuclear expression was associated with extracapsular extension ($P = 0.01$) and metastases ($P = 0.02$) (Table 1). The analyses did not find any associations between Gleason score or tumor volume and CHD8 expression.

Generating molecular predictors of treatment failure, especially within intermediate grade cancers is a pressing clinical need. An analysis of PSA recurrence after prostate removal, which indicates treatment failure, was performed. Patients with increased CHD8 expression exhibited an earlier PSA recurrence (P = 0.048) (Figure 3A). Gleason score provides weak separation of patients into risk categories for PSA recurrence ($P = 0.163$) (Figure 3B). Stratifying intermediate Gleason patients by CHD8 expression shows that patients with higher CHD8 expression had a greater risk of biochemical recurrence (P = 0.048) (Figure 3C). Multivariate analysis for CHD8 as an independent predictor of biochemical recurrence approached significance (HR 2.545, 95% CI 0.973-6.654; $P = 0.0568$). Therefore, although decreased in cancer compared to benign, increasing CHD8 levels in cancer cores are associated with adverse clinicopathologic variables and worse outcomes.

***BORIS*/*CTCF* expression ratio is increased in cancer samples and correlates with higher Gleason Score.**

CTCF is known to impact gene regulation through the management of chromatin organization and the maintenance of epigenetic marks (26). CTCF expression levels measured by VECTRA^{TM} were significantly decreased in metastatic PCa tumors ($P <$

0.001), but not localized PCa when compared to benign prostate tissues ($P = 0.17$) (Figure 4A). When CTCF expression within primary tumors was compared against clinicopathologic patient variables, decreased nuclear and total CTCF expression was associated with higher Gleason's Score ($P = 0.01$ and $P = 0.001$ respectively) and positive margins ($P = 0.03$ and $P = 0.043$ respectively) (Data not shown).

The CTCF paralogue, BORIS, shares a common zinc-finger DNA-binding domain with divergent N- and C- termini. BORIS and CTCF have competing effects on gene expression and epigenetic regulation (5,27). In contrast to CTCF, BORIS expression was increased in HGPIN and primary cancer cores compared to benign ($P < 0.001$ and $P = 0.002$ respectively) (Figure 4B). No clinicopathologic correlates were noted.

The competing role for BORIS/CTCF suggests the ratio of their expression may contain functional significance and greater predictive power than the expression of these proteins individually as seen in ovarian cancer (28). Analyzing all prostate tissues, a weak correlation was seen between BORIS and CTCF (Pearson's $r = 0.224$, $P < 0.001$). BORIS/CTCF levels increased significantly in cancer and metastases compared to benign ($P = 0.03$ and $P = 0.006$ respectively) (Figure 4C). High Gleason cancers have a significantly greater BORIS/CTCF ratio than both benign tissues and intermediate Gleason cancers ($P = 0.006$ and $P = 0.024$ respectively) (Figure 4D). The ratio of nuclear and total expression was calculated and found to be associated with Gleason's grade, positive surgical margins, and tumor volume (Nuclear $P = 0.04$, $P = 0.03$, $P = 0.0498$ respectively) (Table 2, for full table see supplementary data, Table S2).

Exclusion of CHD8 and/or BORIS alterations is seen in a majority of cancers

Our analysis permits a comparison of the expression of each of the chromatin regulators in the CTCF/CHD8/BORIS pathway within specific tumors. We speculated that inactivation of one gene in this pathway might exclude alterations in the other related genes in the CTCF complex. To first test this, the cBioPortal for Cancer Genomics (www.cbioportal.org/public-portal/) was queried for alterations (gene amplification, mutation, and homozygous deletion) in these 3 genes and the CTCF/CHD8/BORIS pathway was genetically altered in 15% of PCa (Supplementary Table S3). Similar low rates of concurrent alteration were seen in other cancers. This included amplification of BORIS, homozygous deletion of CTCF, and mutation of CHD8. We extended this analysis to our data by segregating gene expression into quartiles in the entire dataset using all cores (benign, HGPIN, cancer, and metastases). Expression alterations in CTCF were rarely seen and thus were not analyzed. Segregating all 73 patient tumor samples from our data into expression quartiles we found 26/73 (36%) exhibit decreased and 8/73 (11%) exhibit increased CHD8. Analyzing BORIS expression, 19/73 (26%) exhibit increases and 7/73 (10%) show decreased expression. Expressional alterations occurred in 51/73 (70%) of the tumors in total (Fig. 5A). Comparatively, alterations in both genes were rarely seen (9/73; 12%%). Odds ratio analysis indicated that these alterations showed a tendency toward mutual exclusivity (*OR* - 0.46).

CTCF, BORIS, and CHD8 expression is significantly more heterogeneous in higher grade cancers

The majority of human tumors display startling heterogeneity in many morphological and physiological features, but the ability to objectively quantitate this aspect has been lacking. VECTRA™ was utilized to assess *per cell* expression within benign and tumor cores and heterogeneity scores for each core was calculated using the Simpson's Diversity Index (SI), a formula generally used in the population sciences (24). The SI uses population size to

normalize diversity analyses to a uniform scoring system for comparison. SI analyses revealed BORIS, CHD8, and CTCF all demonstrate increased heterogeneity of protein expression in primary cancer and metastases compared to benign (all $P < 0.001$) (Fig. 5B-D respectively). Within primary PCa cores, increased heterogeneity was also seen in higher grade cancer (CHD8, $P = 0.001$, CTCF $P < 0.001$, and BORIS, $P = 0.001$). Similar increased heterogeneity was seen when the coefficient of variation was calculated for these proteins (data not shown).

Discussion

CTCF is a transcriptional regulator and member of the BORIS and CTCF gene family. It has well known insulator activity where binding to a transcriptional insulator element serves to block enhancer-promoter interactions (29) and can also act as a classical transcription factor (30). In addition, CTCF is uniquely involved in epigenetic regulation including many cell cycle and cancer specific genes (7,10). The function of CTCF is modulated at a number of levels, including at the protein level by cofactors and competitive inhibitors. This study analyzed the synchronous expression of CTCF, its cofactor CHD8, and the antagonistic CTCF paralogue BORIS using VECTRA^{TM} imaging technology. Increased heterogeneity in higher grade cancers was found and the coexpression of these chromatin regulators was largely independent of each other. A striking decrease in CHD8 expression is a major finding in the majority of primary PCa and metastatic deposits. An interesting contrast in CHD8 expression was also discovered with increased levels being associated with more adverse clinical variables and PSA recurrence-free survival. BORIS/CTCF levels also correlated with worse pathologic variables. This unique approach suggests a significant role for alterations in these chromatin factors in PCa.

There has been increased interest in the CHD family (13,14) given the finding of inactivation of other family members in disease including the recent findings of somatic mutation of CHD5 (31) and deletion of CHD1 (32). CHD8 exhibits a functional dichotomy operating in both growth inhibitory and promoting roles including chromatin remodeling, WNT signaling, CTCF insulator activity, p53-mediated apoptosis, androgen receptor mediated gene activity, and regulation of cell cycle genes (33). In the current study, the expression of CHD8 significantly decreased in HGPIN, cancer, and metastases compared to benign tissue. Using a cut-off determined by ROC analysis maximizing sensitivity and

specificity, 84% of localized and 74% of metastatic PCa tumors exhibited decreased CHD8 expression. One potential significant implication of decreased CHD8 may be a loss of the CTCF-CHD8 complex, which serves to stabilize regulation of CTCF effector genes. Ishihara *et al.* found losses of CHD8 altered DNA methylation and histone acetylation around CTCF binding sites, adjacent to heterochromatin, in HeLa and hepatoma cell lines (3).

An interesting dichotomy of expression was discovered using imaging analysis. In tumor tissues, increased CHD8 expression was associated with the presence of metastases and extracapsular extension (Table 1). Extending this analysis to examine risk of PSA recurrence after radical prostatectomy, we found that CHD8 expression served to discriminate between indolent intermediate grade cancers and those at higher risk of recurrence. Markers that predict a worse outcome for intermediate grade cancers are an area of intense clinical interest. The dichotomy in expression suggests a loss of function is important for cancer development, but progression is facilitated by higher expression. Alternatively, higher levels seen with cancer progression may indicate a nonfunctional or altered protein.

Loss of CHD8 may alter CTCF function, as well as aberrant expression of the CTCF paralogue and cancer-testis antigen BORIS. We found BORIS expression to be significantly increased in cancer compared to benign prostate tissues. Recently published findings in prostate tumor tissues and cell lines support this observation (12). The identical 11-zinc finger DNA-binding domains of CTCF and BORIS may result in sibling rivalry for binding sites but their divergent amino- and carboxy-terminal domains result in antagonistic gene regulation functions (11). Exploiting this competition, a recent study in ovarian cancer found BORIS/CTCF ratio of expression levels correlate with advanced stage and DNA

hypomethylation levels (28). An analysis of the ratio of BORIS/CTCF expression here in prostate cancer demonstrated a significant increase in cancer that correlated with higher Gleason's grade, positive surgical margins, and increased tumor volume. Aberrant BORIS expression may work alternatively or in concert with CHD8 decreases to disrupt CTCF action within the genome.

Our analysis permits a comparison of expression of each of the chromatin regulators in the CTCF/CHD8/BORIS pathway within specific tumors. By investigating the highest or lowest quartiles of expression we determined that CHD8 downregulation and BORIS upregulation occurred commonly in 56% of tumors analyzed. Furthermore, decreased CHD8 expression rarely occurred with BORIS amplification (Fig. 5A). The mechanisms underlying CTCF deregulation in disease are complex and include loss of heterozygosity, mutation, post-translational modification, and methylation at CTCF target sites. Using the cBioPortal, a similar tendency for multiple tumor types (breast, ovarian, uterine, colon) that demonstrate BORIS amplification to not contain alterations in CTCF or CHD8 was seen, suggesting if one component of the pathway is altered, others are not required (Supplementary Table S2).

We performed an analysis of CHD8 TSS hypermethylation and find this occurs in roughly 45% of tumors examined. TCGA cohorts analyzed revealed that 4 of the 6 CpGs analyzed are significantly hypermethylated in tumor samples. This confirms data seen in a recent high-throughput methylation array analysis of prostate tumors (22). Treatment of cancer cell lines with a methyltransferase inhibitor (5-azadC) resulted in increased expression of CHD8 mRNA in LNCaP indicating DNA methylation plays a role in CHD8 regulation (Figure 2C). Other mutational events or epigenetic marks, such as histone

modifications, may also play a role in reducing CHD8 expression. Therefore, epigenetic silencing of CHD8 may be one mechanism for alterations of expression.

Tumor development can be regarded as a process of Darwinian evolution. Selection forces required for the emergence of malignancies and increase genetic and epigenetic instability generate clonal populations. The VECTRA^{TM} analysis platform is a powerful objective tool for analyzing patterns of protein expression in tissues. To capitalize on this extensive quantitation, we used per cell data to analyze the heterogeneity of protein expression in tissue cores. The coefficient of variation and the Simpson's Diversity Index, a measure originally developed to measure ecological diversity, were applied to capture this aspect. We find PCa cores contain increased heterogeneity for all proteins. In addition, cancers with higher Gleason score are significantly more heterogeneous. This suggests that heterogeneity of expression translates into phenotypic diversity; this may hold potential as a biomarker in the future.

In conclusion, we demonstrate for the first time that CHD8 expression is frequently altered in PCa and its expression more accurately predicts PSA-recurrence combined with Gleason score over Gleason score alone. Interestingly, CHD8 is decreased in cancer, however higher expression is seen with more adverse clinical features. This dichotomy may be explained, in part, by the diverse functions of CHD8. The use of imaging technology allows a number of novel observations to be performed. The higher heterogeneity of protein expression seen in cancer and metastases may convey plasticity in CHD8 expression. Early decreases in CHD8 may conceivably be advantageous to tumor development, while tumor progression involves a subsequent shift to higher CHD8 within the tumor. Changes in CTCF/BORIS may accompany CHD8 expressional alterations, further contributing to neoplastic development. Frequent alterations of the CHD8/CTCF/BORIS pathway suggest

a crucial function in early PCa development. Biologically, this pathway affects chromatin and epigenetic regulation (3,10), key factors in early neoplasia. These findings warrant future study of the functional consequences of CHD8, CTCF, and BORIS expression alterations in the prostate.

Acknowledgements

This work was supported by the National Institutes of Health 5R01CA097131 [DJ], and ND was supported by the NCI Cancer Biology Training Grant T32 CA009135. We thank the University of Wisconsin Translational Research Initiatives in Pathology laboratory, in part supported by the UW Department of Pathology and Laboratory Medicine and UWCCC grant P30 CA014520, for use of its facilities and services. The results shown here are in part based upon data generated by the TCGA Research Network: http://cancergenome.nih.gov/

References

1. Damaschke NA, Yang B, Bhusari S, Svaren JP, Jarrard DF. Epigenetic susceptibility factors for prostate cancer with aging. Prostate **2013**;73:1721-30
2. Varambally S, Dhanasekaran SM, Zhou M, Barrette TR, Kumar-Sinha C, Sanda MG*, et al.* The polycomb group protein EZH2 is involved in progression of prostate cancer. Nature **2002**;419:624-9
3. Ishihara K, Oshimura M, Nakao M. CTCF-dependent chromatin insulator is linked to epigenetic remodeling. Mol Cell **2006**;23:733-42
4. Loukinov DI, Pugacheva E, Vatolin S, Pack SD, Moon H, Chernukhin I*, et al.* BORIS, a novel male germ-line-specific protein associated with epigenetic reprogramming events, shares the same 11-zinc-finger domain with CTCF, the insulator protein involved in reading imprinting marks in the soma. Proc Natl Acad Sci U S A **2002**;99:6806-11
5. Vatolin S, Abdullaev Z, Pack SD, Flanagan PT, Custer M, Loukinov DI*, et al.* Conditional expression of the CTCF-paralogous transcriptional factor BORIS in normal cells results in demethylation and derepression of MAGE-A1 and reactivation of other cancer-testis genes. Cancer Res **2005**;65:7751-62
6. Merkenschlager M, Odom DT. CTCF and cohesin: linking gene regulatory elements with their targets. Cell **2013**;152:1285-97
7. Fiorentino FP, Giordano A. The tumor suppressor role of CTCF. J Cell Physiol **2012**;227:479-92
8. Kurukuti S, Tiwari VK, Tavoosidana G, Pugacheva E, Murrell A, Zhao Z*, et al.* CTCF binding at the H19 imprinting control region mediates maternally inherited higher-order chromatin conformation to restrict enhancer access to Igf2. Proc Natl Acad Sci U S A **2006**;103:10684-9
9. Hore TA, Deakin JE, Marshall Graves JA. The evolution of epigenetic regulators CTCF and BORIS/CTCFL in amniotes. PLoS Genet **2008**;4:e1000169
10. Klenova EM, Morse HC, Ohlsson R, Lobanenkov VV. The novel BORIS + CTCF gene family is uniquely involved in the epigenetics of normal biology and cancer. Semin Cancer Biol **2002**;12:399-414
11. Pugacheva EM, Suzuki T, Pack SD, Kosaka-Suzuki N, Yoon J, Vostrov AA*, et al.* The structural complexity of the human BORIS gene in gametogenesis and cancer. PLoS One **2010**;5:e13872
12. Cheema Z, Hari-Gupta Y, Kita GX, Farrar D, Seddon I, Corr J*, et al.* Expression of the cancer-testis antigen BORIS correlates with prostate cancer. Prostate **2014**;74:164-76
13. Marfella CG, Imbalzano AN. The Chd family of chromatin remodelers. Mutat Res **2007**;618:30-40
14. Kim MS, Chung NG, Kang MR, Yoo NJ, Lee SH. Genetic and expressional alterations of CHD genes in gastric and colorectal cancers. Histopathology **2011**;58:660-8
15. Nishiyama M, Oshikawa K, Tsukada Y, Nakagawa T, Iemura S, Natsume T*, et al.* CHD8 suppresses p53-mediated apoptosis through histone H1 recruitment during early embryogenesis. Nat Cell Biol **2009**;11:172-82
16. Nishiyama M, Skoultchi AI, Nakayama KI. Histone H1 recruitment by CHD8 is essential for suppression of the Wnt-β-catenin signaling pathway. Mol Cell Biol **2012**;32:501-12

17. Yates JA, Menon T, Thompson BA, Bochar DA. Regulation of HOXA2 gene expression by the ATP-dependent chromatin remodeling enzyme CHD8. FEBS Lett **2010**;584:689-93
18. Menon T, Yates JA, Bochar DA. Regulation of androgen-responsive transcription by the chromatin remodeling factor CHD8. Mol Endocrinol **2010**;24:1165-74
19. Subtil-Rodríguez A, Vázquez-Chávez E, Ceballos-Chávez M, Rodríguez-Paredes M, Martín-Subero JI, Esteller M*, et al.* The chromatin remodeller CHD8 is required for E2F-dependent transcription activation of S-phase genes. Nucleic Acids Res **2014**;42:2185-96
20. Huang W, Hennrick K, Drew S. A colorful future of quantitative pathology: validation of Vectra technology using chromogenic multiplexed immunohistochemistry and prostate tissue microarrays. Hum Pathol **2013**;44:29-38
21. Desotelle J, Truong M, Ewald J, Weeratunga P, Yang B, Huang W*, et al.* CpG island hypermethylation frequently silences FILIP1L isoform 2 expression in prostate cancer. J Urol **2013**;189:329-35
22. Kobayashi Y, Absher DM, Gulzar ZG, Young SR, McKenney JK, Peehl DM*, et al.* DNA methylation profiling reveals novel biomarkers and important roles for DNA methyltransferases in prostate cancer. Genome Res **2011**;21:1017-27
23. Rodríguez-Paredes M, Ceballos-Chávez M, Esteller M, García-Domínguez M, Reyes JC. The chromatin remodeling factor CHD8 interacts with elongating RNA polymerase II and controls expression of the cyclin E2 gene. Nucleic Acids Res **2009**;37:2449-60
24. Peet RK. The Measurement of Species Diversity. Annual Review of Ecology and Systematics **1974**;5:285-307
25. Faratian D, Christiansen J, Gustavson M, Jones C, Scott C, Um I*, et al.* Heterogeneity mapping of protein expression in tumors using quantitative immunofluorescence. J Vis Exp **2011**:e3334
26. Phillips JE, Corces VG. CTCF: master weaver of the genome. Cell **2009**;137:1194-211
27. Hong JA, Kang Y, Abdullaev Z, Flanagan PT, Pack SD, Fischette MR*, et al.* Reciprocal binding of CTCF and BORIS to the NY-ESO-1 promoter coincides with derepression of this cancer-testis gene in lung cancer cells. Cancer Res **2005**;65:7763-74
28. Woloszynska-Read A, Zhang W, Yu J, Link PA, Mhawech-Fauceglia P, Collamat G*, et al.* Coordinated cancer germline antigen promoter and global DNA hypomethylation in ovarian cancer: association with the BORIS/CTCF expression ratio and advanced stage. Clin Cancer Res **2011**;17:2170-80
29. Bell AC, West AG, Felsenfeld G. The protein CTCF is required for the enhancer blocking activity of vertebrate insulators. Cell **1999**;98:387-96
30. Klenova EM, Nicolas RH, Paterson HF, Carne AF, Heath CM, Goodwin GH*, et al.* CTCF, a conserved nuclear factor required for optimal transcriptional activity of the chicken c-myc gene, is an 11-Zn-finger protein differentially expressed in multiple forms. Mol Cell Biol **1993**;13:7612-24
31. Robbins CM, Tembe WA, Baker A, Sinari S, Moses TY, Beckstrom-Sternberg S*, et al.* Copy number and targeted mutational analysis reveals novel somatic events in metastatic prostate tumors. Genome Res **2011**;21:47-55

32. Huang S, Gulzar ZG, Salari K, Lapointe J, Brooks JD, Pollack JR. Recurrent deletion of CHD1 in prostate cancer with relevance to cell invasiveness. Oncogene **2012**;31:4164-70
33. Sakamoto I, Kishida S, Fukui A, Kishida M, Yamamoto H, Hino S*, et al.* A novel beta-catenin-binding protein inhibits beta-catenin-dependent Tcf activation and axis formation. J Biol Chem **2000**;275:32871-8

Figure 1. Quantitative analysis of CHD8 expression.

Using the VECTRA^{TM} automated image capture and analysis nuclear, cytoplasmic and total compartments were compared. Mean intensity of cores were compared for benign, HGPIN, cancer, and metastases with 95% confidence intervals. ***A,*** Demonstrates the interactions of BORIS, CTCF, and CHD8; where BORIS and CTCF compete for similar binding sites, and CTCF and CHD8 complex at CTCF binding sites. ***B,*** Significant decreases in CHD8 expression are seen in cancer and metastases cores for total, nuclear, and cytoplasmic expression ($P < 0.001$, cytoplasmic HGPIN not significant). ***C,*** Total CHD8 expression demonstrated optimal discrimination between benign and cancer (AUC = 0.866, $P < 0.0001$) by ROC analysis, with a sensitivity and specificity of 84.3% and 76.3%. ***D,*** Using the optimum cut-off obtained by ROC analysis, 84.3% of cancer and 74.4% of metastases cores demonstrated decreased CHD8.

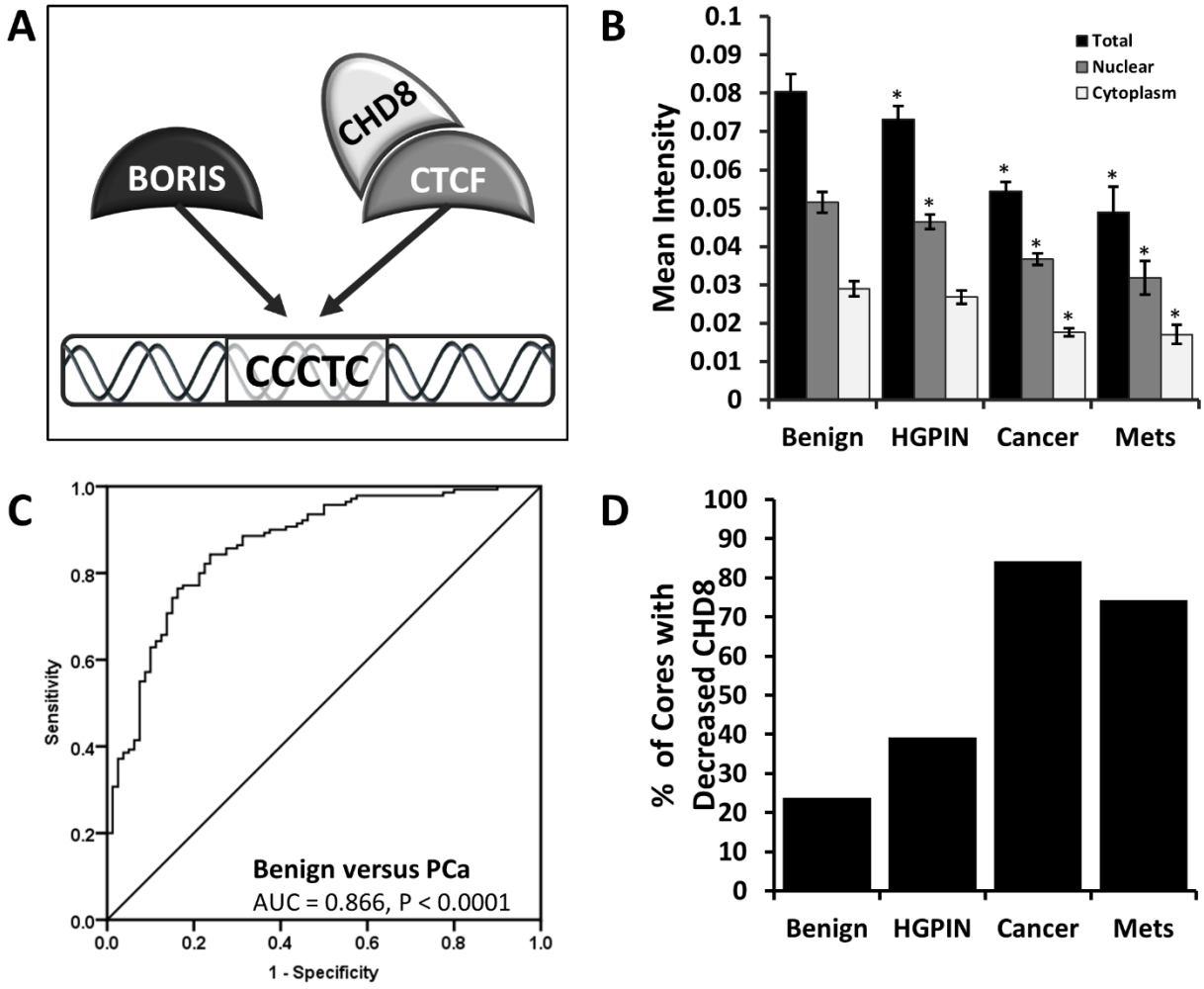
A
BORIS
CHD8
CTCF
CCCTC
B
Mean Intensity
Total
Nuclear
Cytoplasm
Benign
HGPIN
Cancer
Mets
C
Sensitivity
1 - Specificity
Benign versus PCa
AUC = 0.866, P < 0.0001
D
% of Cores with Decreased CHD8
Benign
HGPIN
Cancer
Mets

Figure 2. Methylation analysis of CHD8 in human PCa and 5-Aza-2'-deoxycytidine treatment of cancer cell lines.

DNA methylation was analyzed by Quantitative Pyrosequencing across the CHD8 transcriptional start site. ***A,*** Hypermethylation of CHD8 promoter-associated CpGs 1-4 was seen in 5/11 (45%) human tumor samples compared to matched benign. ***B,*** Significant hypermethylation was seen at 4/6 of the promoter-associated CpGs in tumors compared to benign in TCGA PRAD samples (Methylation 450K Array) (All $P < 0.001$). ***C,*** 5-azadC treatment of LNCaP cells for 48 hrs resulted in a 1.5-2.5 fold significant increase of CHD8 mRNA over treatment vehicle alone (all $P < 0.05$).

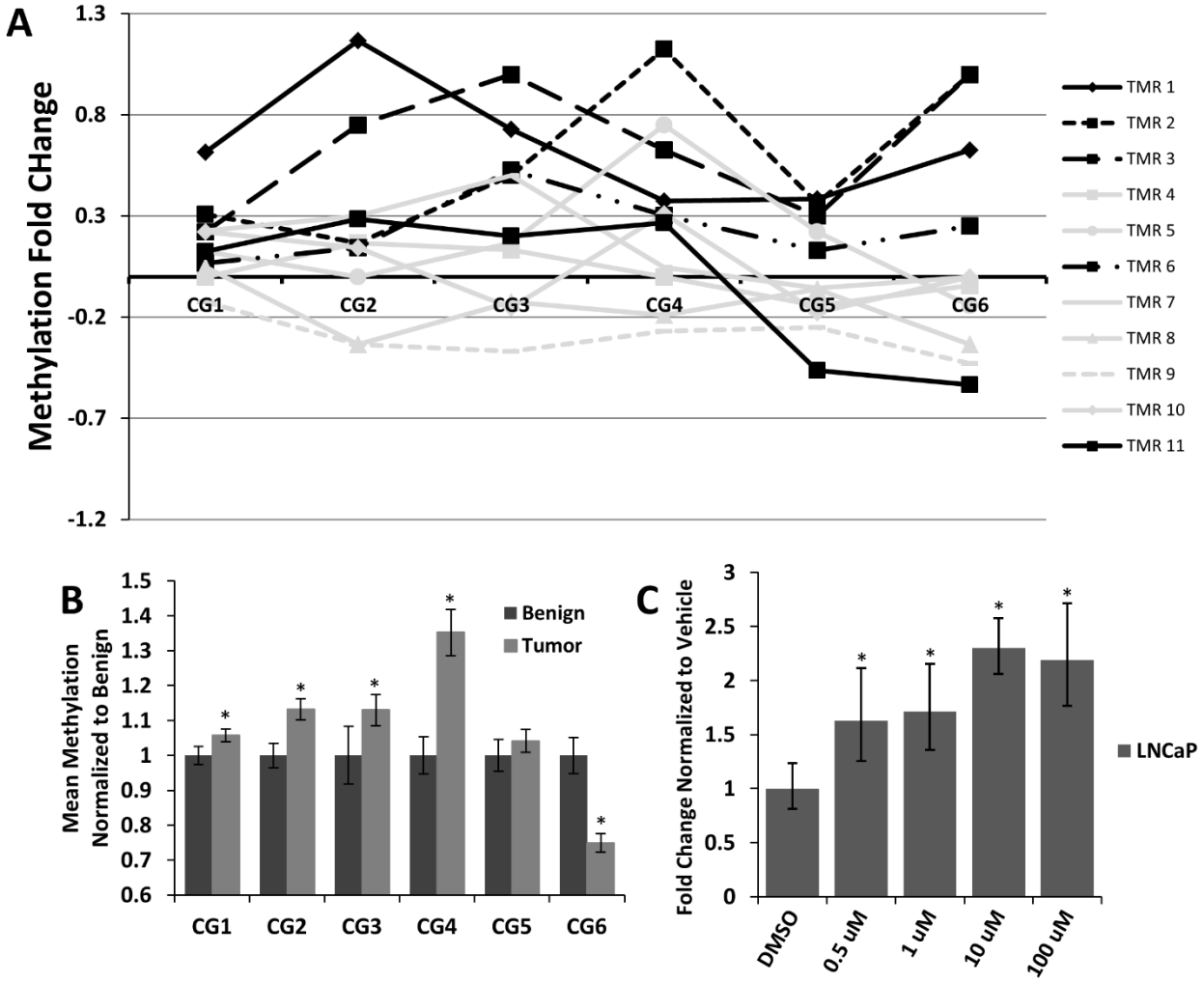
A
Methylation Fold CHange
1.3
0.8
0.3
-0.2
-0.7
-1.2
CG1
CG2
CG3
CG4
CG5
CG6
TMR 1
TMR 2
TMR 3
TMR 4
TMR 5
TMR 6
TMR 7
TMR 8
TMR 9
TMR 10
TMR 11
B
Mean Methylation Normalized to Benign
1.5
1.4
1.3
1.2
1.1
1
0.9
0.8
0.7
0.6
Benign
Tumor
CG1
CG2
CG3
CG4
CG5
CG6
C
Fold Change Normalized to Vehicle
3
2.5
2
1.5
1
0.5
0
DMSO
0.5 uM
1 uM
10 uM
100 uM
LNCaP

Figure 3. Kaplan Meier analyses comparing pathological Gleason Score versus CHD8.

Biochemical recurrence after radical prostatectomy was examined in patient samples stained for CHD8. ***A,*** Nuclear CHD8 significantly separates patients into risk categories for PSA recurrence using a Log rank analysis (P = 0.048). ***B,*** Gleason score provides insignificant separation of patients for PSA recurrence using a Log rank analysis (P = 0.163). ***C,*** Nuclear CHD8 is superior to pathological Gleason score when Gleason score was stratified into low versus high CHD8. The median value for nuclear CHD8 staining was 0.04025 in all benign and cancer samples. This value was subsequently used as a cut point to define high versus low nuclear CHD8 expression for the Log rank analysis.

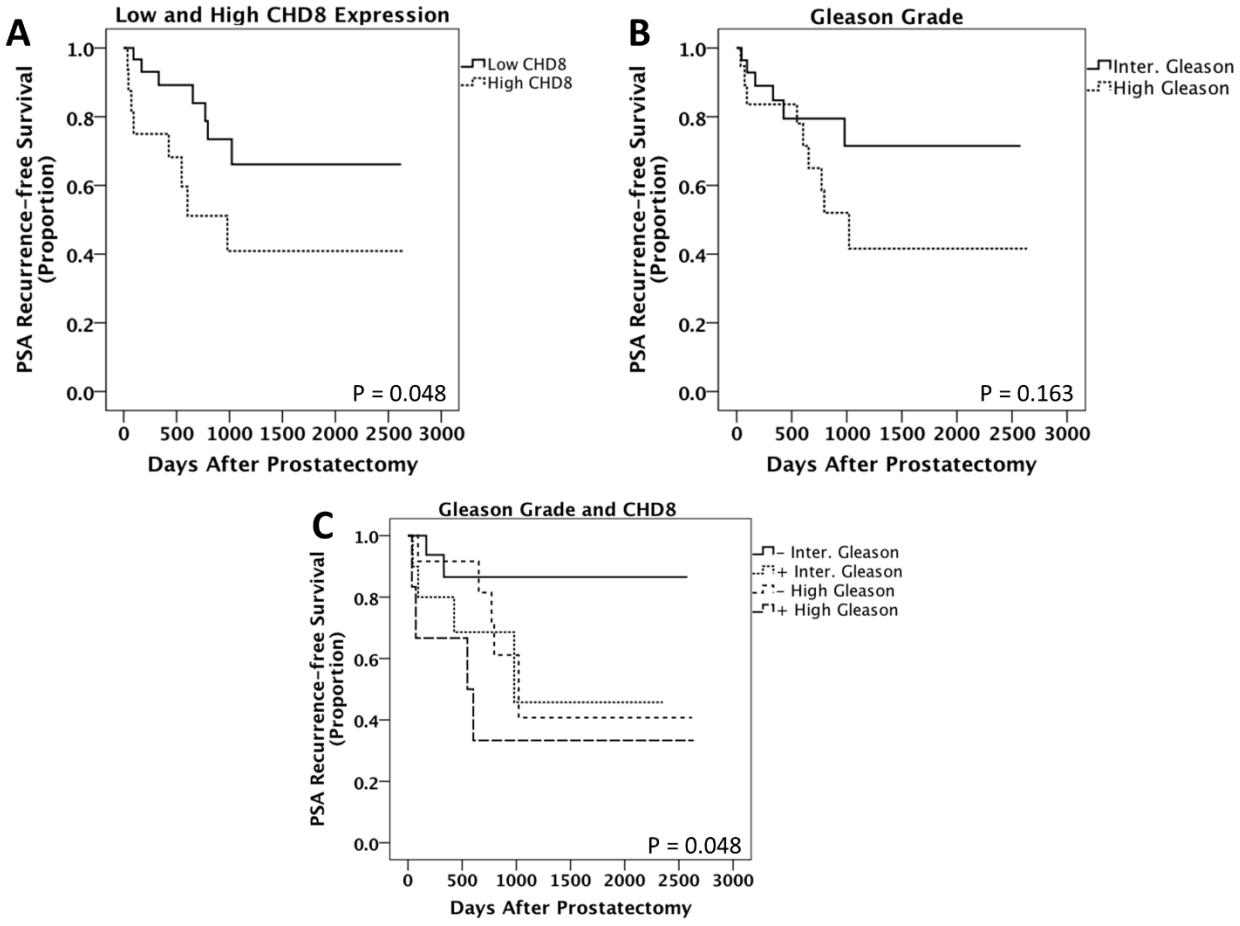
A
Low and High CHD8 Expression
PSA Recurrence-free Survival (Proportion)
1.0
0.8
0.6
0.4
0.2
0.0
0 500 1000 1500 2000 2500 3000
Days After Prostatectomy
Low CHD8
High CHD8
P = 0.048
B
Gleason Grade
PSA Recurrence-free Survival (Proportion)
Days After Prostatectomy
Inter. Gleason
High Gleason
P = 0.163
C
Gleason Grade and CHD8
PSA Recurrence-free Survival (Proportion)
Days After Prostatectomy
- Inter. Gleason
+ Inter. Gleason
- High Gleason
+ High Gleason
P = 0.048

Figure 4. Quantitative analysis of CTCF and BORIS expression in human PCa.

A, Nuclear CTCF significantly decreases in metastases cores ($P < 0.001$). ***B,*** BORIS nuclear expression significantly increased in cancer cores ($P = 0.002$); nuclear and cytoplasmic expression increased in HGPIN cores compared to benign (both $P < 0.001$). ***C,*** The ratio of BORIS to CTCF expression was analyzed for differences among cores. Significant increases in the BORIS/CTCF ratio are seen among cancer and metastases cores compared to benign ($P = 0.031$ and $P = 0.006$ respectively). ***D,*** Comparing the BORIS/CTCF ratio among cancer cores, high Gleason grade cancers have significantly higher BORIS/CTCF ratio than both benign and intermediate Gleason cores ($P = 0.006$ and $P = 0.024$ respectively).

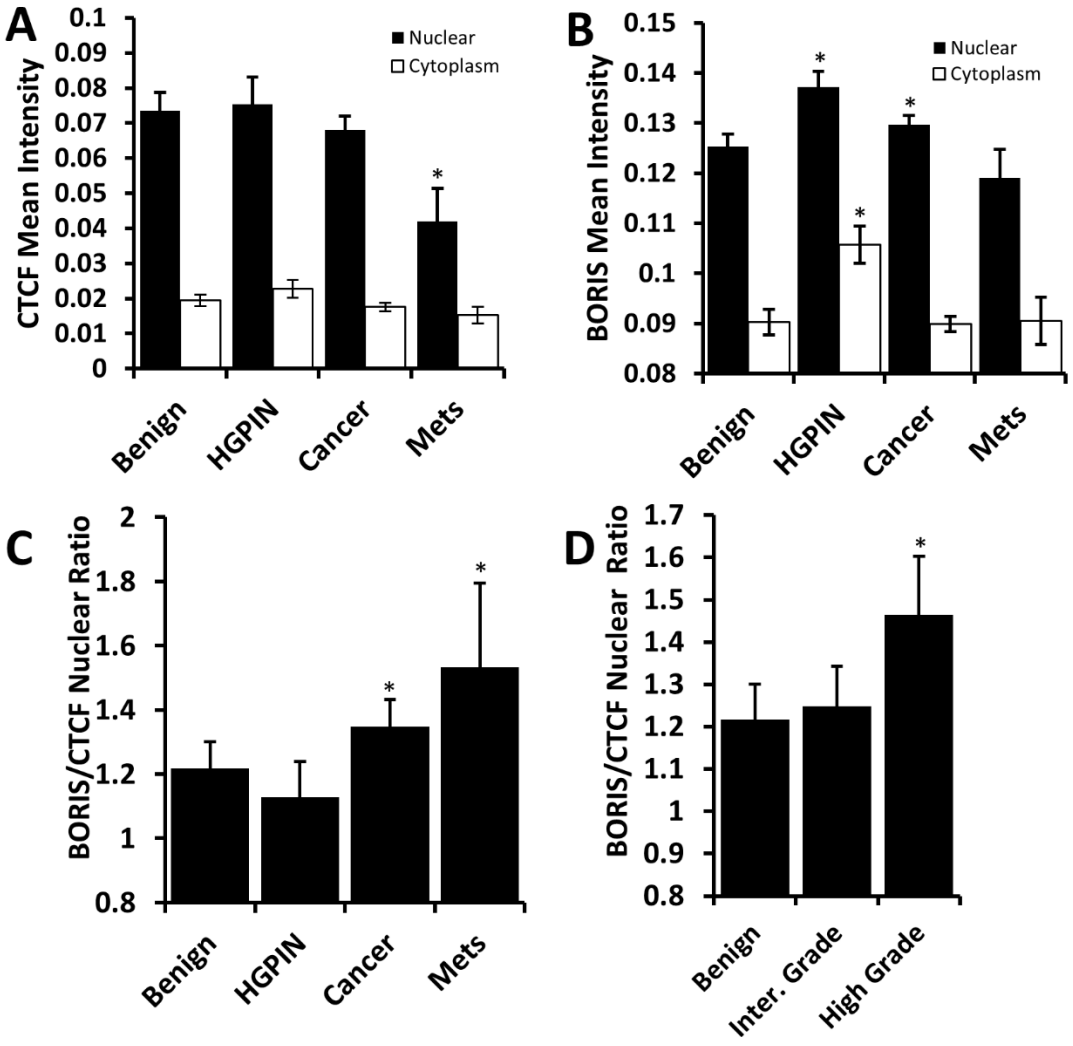
A
CTCF Mean Intensity
0.1
0.09
0.08
0.07
0.06
0.05
0.04
0.03
0.02
0.01
0
Nuclear
Cytoplasm
*
Benign
HGPIN
Cancer
Mets
B
BORIS Mean Intensity
0.15
0.14
0.13
0.12
0.11
0.1
0.09
0.08
Nuclear
Cytoplasm
*
*
*
Benign
HGPIN
Cancer
Mets
C
BORIS/CTCF Nuclear Ratio
2
1.8
1.6
1.4
1.2
1
0.8
*
*
Benign
HGPIN
Cancer
Mets
D
BORIS/CTCF Nuclear Ratio
1.7
1.6
1.5
1.4
1.3
1.2
1.1
1
0.9
0.8
*
Benign
Inter. Grade
High Grade

Figure 5. CHD8 and BORIS expression alterations are exclusive and exhibit significantly greater heterogeneity in malignant cores.

A, Using expression of all cores, the expression data for CHD8 and BORIS was divided into quartiles. Each column box-pair represents a primary tumor sample (total 73). When cancer cores are separated into quartiles of protein expression, CHD8 is frequently decreased (26/73; 36%) while BORIS is frequently increased (19/73; 26%) in primary cancer. Rare cancers (12%) exhibited both alterations in concert indicating that these pathway alterations infrequently occur in concert. An analysis of heterogeneity of cores was performed using the Simpson's Diversity Index (SI). BORIS ***(B)***, CHD8 ***(C)***, and CTCF ***(D)*** all had significantly higher heterogeneity of protein expression in cancer and metastases cores compared to benign (all $P < 0.005$) as measured by Simpson's Diversity Index.

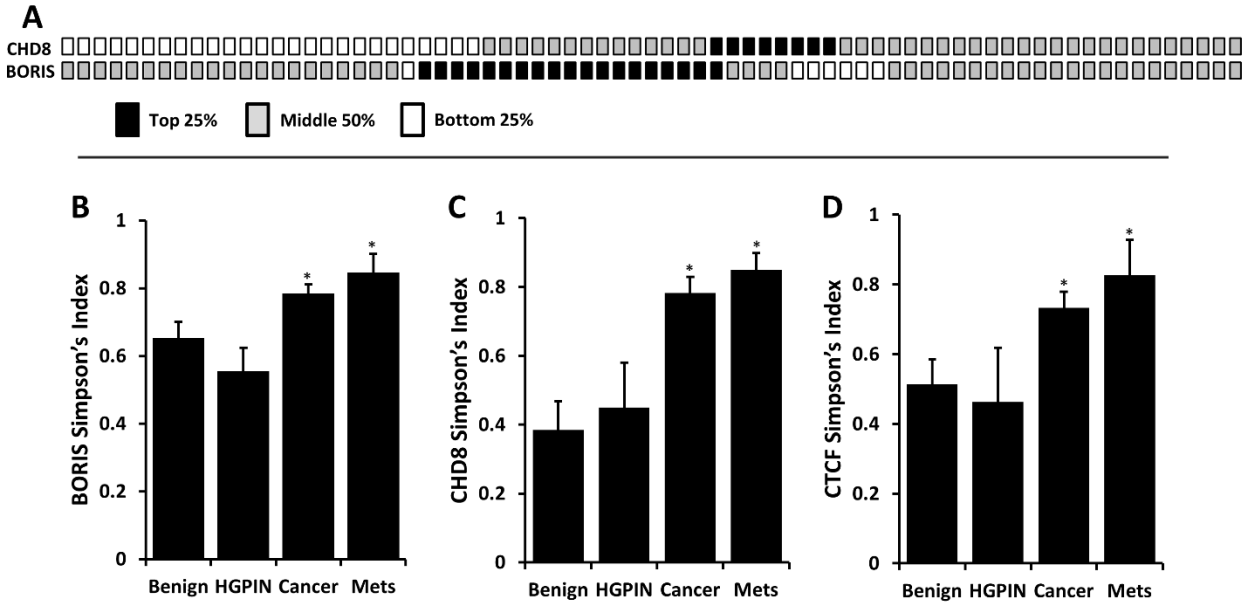
A
CHD8
BORIS
Top 25%
Middle 50%
Bottom 25%
B
BORIS Simpson's Index
C
CHD8 Simpson's Index
D
CTCF Simpson's Index
0
0.2
0.4
0.6
0.8
1
Benign HGPIN Cancer Mets
*

Supplementary Table S1: Clinicopathological Characteristics of Cancer Samples

Variable	Average	Number (%)
Age	58.9	
PSA	10.24	
Tumor Volume (cc)	0.19	
Gleason Grade		
6		13 (19.4%)
7		28 (41.8%)
8		15 (22.4%)
9		11 (16.4%)
Stage		
II		39 (58.2%)
III		11 (16.4%)
IV		17 (25.4%)
Metastastic		
No		50 (74.6%)
Yes		16 (23.9%)
No Data		1 (1.5%)
Extraprostatic Extension		
No		42 (62.7%)
Yes		23 (34.3%)
No Data		2 (3%)
SV Involvement		
No		48 (71.6%)
Yes		15 (22.4%)
No Data		4 (6%)
Biochemical Recurrence		
No		33 (49.3%)
Yes		18 (26.9%)
No Data		16 (23.9%)

Supplementary Table S2. Association of BORIS/CTCF Expression Ratios With Patient Pathological Features

		Nucleus		Cytoplasm		Total	
Variable	***Patient #***	**Mean Intensity (SD)**	**p-value**	**Mean Intensity (SD)**	**p-value**	**Mean Intensity (SD)**	**p-value**
Gleason							
3+3 or 3+4	38	1.22 (0.41)	**0.024***	2.96 (1.21)	**0.019***	1.59 (0.54)	**0.021***
4+3 or 4+4 or 4+5	28	1.53 (0.64)		3.88 (2.06)		2.03 (0.93)	
Stage							
T2	39	1.40 (0.65)	0.931	3.49 (1.99)	0.868	1.85 (0.91)	0.935
T3	11	1.28 (0.32)		3.31 (1.22)		1.70 (0.45)	
T4	17	1.29 (0.39)		3.07 (1.14)		1.68 (0.53)	
Tumor Volume							
<5	9	0.96 (0.38)	**0.020***	2.28 (0.89)	**0.029***	1.25 (0.49)	**0.022***
5-20	31	1.38 (0.67)		3.35 (2.13)		1.82 (0.97)	
>20	24	1.36 (0.42)		3.54 (1.38)		1.81 (0.58)	
SV involvement							
Absent	48	1.40 (0.64)	0.551	3.51 (1.99)	0.559	1.86 (0.90)	0.551
Present	15	1.25 (0.30)		3.06 (0.97)		1.64 (0.41)	
Margins Positive							
No	42	1.23 (0.42)	**0.027***	3.12 (1.31)	0.204	1.63 (0.56)	**0.041***
Yes	24	1.56 (0.69)		3.78 (2.24)		2.06 (1.00)	
Extracapsular							
No	42	1.40 (0.63)	0.525	3.52(1.97)	0.513	1.86 (0.89)	0.515
Yes	23	1.25 (0.30)		3.06 (0.97)		1.64 (0.41)	
Metastasis							
No	50	1.33 (0.46)	0.925	3.30 (1.31)	0.628	1.75 (0.61)	0.868
Yes	16	1.29 (0.43)		3.09 (1.21)		1.68 (0.56)	

*1 patient GS 3+5 not analyzed

Supplementary Table S3. Rates of genetic alteration in CTCF/BORIS/CHD8 genes in various cancers

Cancer Type	CTCF	BORIS	CHD8	2 or more genes
Uterine	45/240 (19%)	17/240 (7%)	20/240 (8%)	15/240 (6%)
Ovarian	13/311 (4%)	35/311 (11%)	19/311 (6%)	3/311 (1%)
Lung	3/129 (2%)	16/129 (12%)	8/129 (6%)	1/129 (0.7%)
Colorectal	9/212 (4%)	25/212 (12%)	6/212 (3%)	4/212 (2%)
Breast	30/962 (3%)	69/962 (7%)	21/962 (2%)	6/962 (0.6%)

Supplementary Figure 1. Methylation of Cancer Cell Lines at CHD8 Regulatory Regions.

Despite no significant changes in CHD8 expression in DU145 with 5-azadC treatment ***(A)***, methylation levels were similar to LNCaP and HELA. ***B,*** Methylation analyses by quantitative pyrosequencing at a CpG region spanning from the promoter into exon 1 exhibited moderate methylation. ***C,*** Methylation analyses at a CpG region 600 BPs upstream of the TSS revealed heavy methylation across all three cell lines with DU145 and LNCaP exhibiting slightly greater methylation.

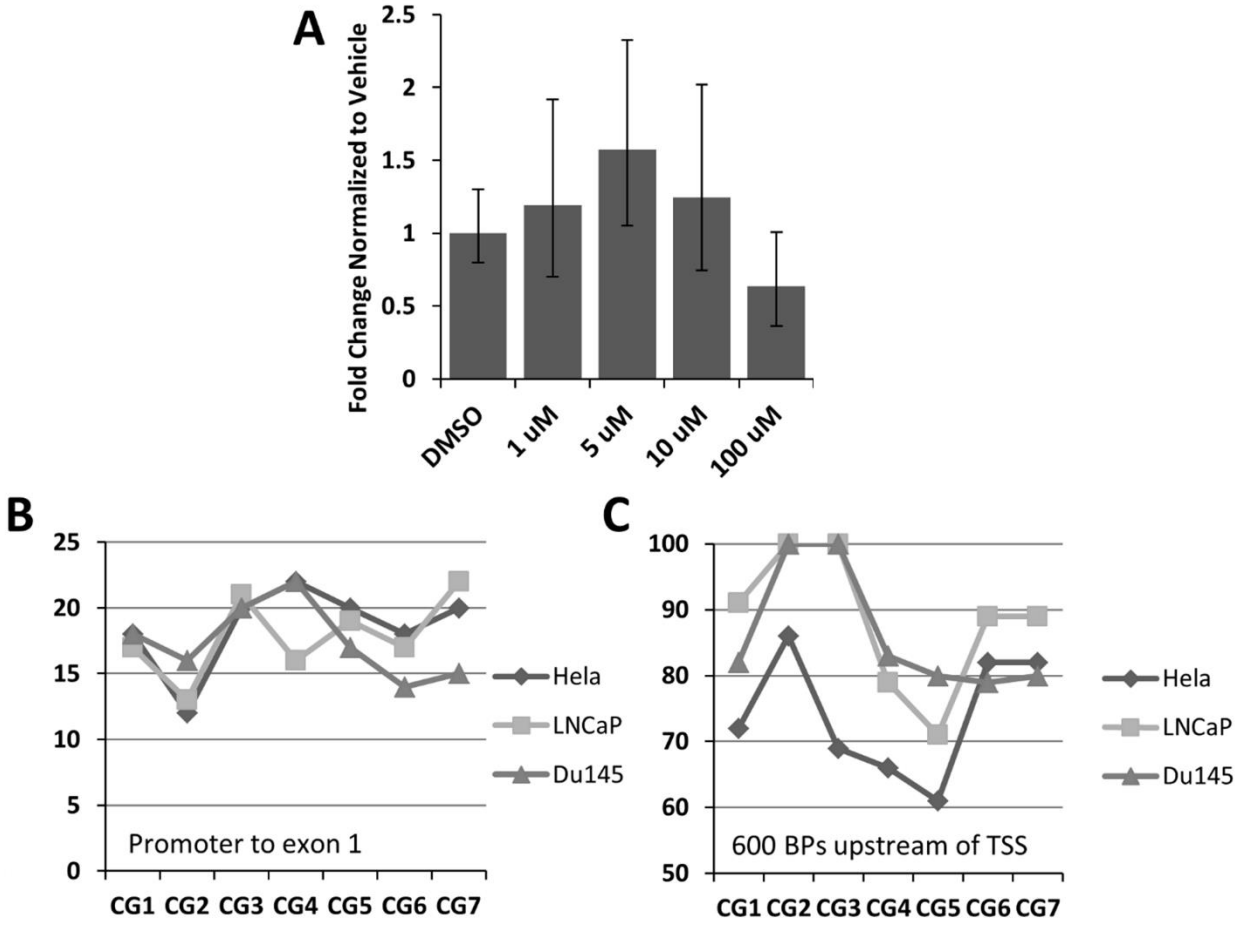
A
Fold Change Normalized to Vehicle
2.5
2
1.5
1
0.5
0
DMSO
1 uM
5 uM
10 uM
100 uM
B
25
20
15
10
5
0
Promoter to exon 1
CG1 CG2 CG3 CG4 CG5 CG6 CG7
Hela
LNCaP
Du145
C
100
90
80
70
60
50
600 BPs upstream of TSS
CG1 CG2 CG3 CG4 CG5 CG6 CG7
Hela
LNCaP
Du145

Chapter IV

Decreased CTCF Expression Directs DNA Hypermethylation Events in Cancer

Nathan A. Damaschke and David F. Jarrard

NA Damaschke, B Yang, M Avilla, JP Svaren, A Roopra, JH Luo, YP Yu, S Keles, and DF Jarrard. Preparing for Submission.

Abstract

CTCF is a highly conserved, ubiquitously expressed, chromatin insulator known to participate in a variety of genome regulation events. Early research established its role in transcriptional regulation and enhancer blocking insulator functions; more recently, genomic profiling has elucidated CTCF's role in long range chromosome interactions. CTCF exhibits methylation sensitive binding and is thought to protect epigenetic states through barrier insulation. Despite these observations, the impact of CTCF loss on genome-wide DNA methylation has not yet been determined in human cancers. Here we demonstrate human tumors of The Cancer Genome Atlas (TCGA) exhibit DNA hypermethylation at CTCF binding sites with loss of CTCF. Through the use of DNA methylation and transcriptome profiling *in vitro*, we demonstrate forced downregulation of CTCF widely alters DNA methylation and gene expression, and these events are associated with CTCF binding sites. In prostate cells, decreased CTCF expression mediates resistance to oxidative and hypoxia induced stress. These results indicate CTCF loss in human tissues mediate DNA methylation alterations associated with cancer development.

Introduction

Epigenetic changes, including altered DNA methylation, underlie the development and progression of cancer. Prostate cancer specifically, which presents low overall mutation rates compared to other cancers (1) relies on epigenetic alterations to overcome barriers to neoplastic development. Tumor progression is accompanied by changes to cytosine methylation at CpG dinucleotides. The tumor specific DNA methylation landscape is marked by frequent hypermethylation of CpG dinucleotides often at normally unmethylated CpG islands, presenting a repressive effect on gene transcription while DNA hypomethylation typically occurs on a global scale (2).

Technological advances have enabled in depth characterization of DNA methylation alterations common to cancer development. Despite the discovery of these frequent alterations, an instructive mechanism of why these site-specific events are common to specific cancers is not well understood. Recently, it has been postulated that gene silencing precedes DNA hypermethylation (2,3), where evacuation of activating transcription factors results in alterations to chromatin structure. In support of this hypothesis, it was shown that nucleosome presence is required for *de novo* methylation by DNA methyltransferases (4), indicating active transcription start sites depleted of nucleosomes lack the substrate for *de novo* methylation (2). These advancements in our understanding demonstrate the crucial role that chromatin organization plays in mediating epigenetic regulation.

CCCTC-binding factor (CTCF) is an 11-zinc finger DNA binding protein originally characterized for its activating and repressive effects on gene expression (5,6), but has since been established as the main vertebrate insulator protein (7) exhibiting methylation-sensitive DNA binding activity (8,9). Many recent studies have focused on the role of CTCF

in the organization of chromatin, highlighting the methylation sensitive binding of CTCF and further demonstrating its role as a boundary element (10-12). Initially, the presence of CTCF was thought to be sufficient for maintaining unmethylated states by physical protection of DNA, however, recent research provides a mechanistic link in which CTCF actively inhibits local DNA methyltransferase-1 (DNMT1) activity through PARP-1 activation (13).

These findings provide a backdrop for a putative role for CTCF in the genome-wide regulation of DNA methylation. In the prostate, the CTCF regulated *Igf2-H19* locus frequently experiences DNA methylation alterations specifically at a series of intergenic CTCF sites resulting in loss of imprinting during both aging and cancer development (14,15). Other mechanisms resulting in downregulation of CTCF protein levels include cellular senescence and oxidative stress (16,17). CTCF binding sites, numbering from 55,000 to 65,000 in human cells (18), are found throughout the genome generally located in linker regions as a boundary between surrounding nucleosomes (19,20). Given these findings, we postulated that a reduction of CTCF levels would mediate DNA methylation throughout the genome and preferentially at CTCF sites. We further postulated that these changes would contribute to disease development.

Herein, we show that loss of CTCF is a common alteration in primary prostate and other cancers and is associated with a distinctive hypermethylation profile that occurs near CTCF binding sites. Genome-wide profiling of methylation and transcription after CTCF reduction in prostate cells supports these findings. Extended CTCF knockdown demonstrates that a reduction in CTCF levels is sufficient to induce transcriptional change and an associated alteration of DNA methylation. These findings underscore the importance of CTCF as a tumor suppressor that is required for epigenome stability.

Furthermore, they provide a potential connection between CTCF mediated DNA methylation alterations in cancer development during aging.

Methods

TCGA Analysis and CTCF Chip-Seq in LNCaP

Level 3 RNA-sequencing, GISTIC2 copy number alterations, and HM450 methylation data was downloaded for 333 primary prostate adenocarcinomas previously documented by the TCGA Network (21). Samples were divided by CTCF copy number alteration status to compare RNA expression and DNA methylation. Analyses were conducted in R using TCGAbiolinks package from Bioconductor. Boxplots and volcano plots created using ggplot2 (Bioconductor) in R.

Cell lines, plasmids, and antibodies

Prostate cancer cell lines PPC-1 and LNCaP were obtained from American Type Culture Collection (ATCC). 293FT cells were used in Lentiviral packaging. Cells were maintained in DMEM with 4.5g/L glucose (293FT, PPC-1) or 1g/L glucose (LNCaP) with 10% FBS and 1% Penicillin/Streptomycin in a humidified incubator at $37^{O}C$ and 5% CO_2. E6/E7 is one of a series of nontumorigenic, HPV E6/E7 immortalized cell lines derived from human prostate epithelial cells (22).

Lentiviral pTRIPz empty vector and non-silencing control (NSC) was purchased from Open Biosystems. Multiple CTCF shRNA sequences were cloned into pTRIPz and tested for efficacy in 293FT cells, two separate vectors targeting CTCF displaying consistent knockdown by western blot were carried forward (shCTCF1 and shCTCF2). Lentiviral particles were produced by co-transfecting 293FT cells with TransLentiviral shRNA Packaging system and either shCTCF1 (Sequence), shCTCF2 (Sequence), or non-silencing control (NSC) shRNA according to manufacturer's protocol. Transduction was performed according to manufacturer's protocols with PPC-1, LNCaP, or E6/E7 cells.

Stable cell lines were generated via puromycin selection and shRNA was induced using 2 ug/mL Doxycycline. CTCF shRNA and controls were analyzed by western blotting using anti-CTCF rabbit monoclonal antibody (Cell Signaling #3418) to verify knockdown.

Cell counting assays were performed as previously described (23) to measure response to oxidative stress (H_2O_2; Fisher) and chemically induced hypoxia ($CoCl_2$; Fisher). Briefly, cells were seeded at 100 cells/well in a 96-well tissue culture plate. CTCF knockdown was induced for 48 hrs prior to chemical administration, CTCF knockdown was continued throughout chemical administration of 3 or 5 days. Plates were collected and analyzed as described (23). Average intensity of replicate wells are generated from each plate.

Methylated DNA Immunoprecipitation and Array Profiling (MeDIP-chip)

The MeDIP-chip approach was adapted from previous studies utilizing methylated DNA immunoprecipitation followed by application to an Affymetrix copy number array (24,25). Biological triplicates grown for 5 days of immortalized HPECs containing either shNSC, uninduced shCTCF1 (-Dox), or induced shCTCF1 (+Dox) were used for methylation profiling. Genomic DNA depleted of RNA was prepared using DNeasy tissue and blood DNA extraction kit (Qiagen, Hilden, Germany) according to manufacturer's protocols.

For each DNA sample, 1ug of genomic DNA was digested with Nsp1 at 37^{O}C for 2 hours followed by adapter ligation at 16^{O}C for 16 hours. Adapter-ligated DNAs were purified using an Amicon Ultra-centrifugation filter (Millipore, Darmstadt, Germany). Purified DNA was then denatured to single strands by heating at 95^{O}C for 10 minutes, followed by rapid cooling on ice.

Methylated DNA was immunoprecipitated with 5ug of anti-5-methylcytosine antibody (Cat. #A3001-200, Zymo Research, Irvine, CA) in IP buffer overnight at 4^{O}C with rotation.

Antibody-DNA complexes were captured with Pierce ChIP-grade Protein A/G magnetic beads (Cat. #26162, ThermoFisher Scientific, Waltham, MA) by rotating at 4^{O}C for 2 h. Three washes were performed with 0.5 mL of immunoprecipitation buffer. DNA was eluted from the beads with 50 uL of elution buffer (TE + 1% SDS) for 10 min at 65^{O}C, elution was performed a total of two times, combining eluates. Eluates were Proteinase K treated at 50^{O}C for 2 h, and purified by PCR purification kit (Qiagen).

Whole genome amplification of eluates, fragmentation, array hybridization, and array scanning were performed according to manufacturer's instructions. CEL files generated from the scanned array image files by Affymetrix GeneChip Command Console Software were processed using Affymetrix Power Tools. Background subtraction and RMA normalization was performed to obtain normalized log2 transformed raw intensity values. Input subtraction was performed for each IP-input pair for normalization of copy number differences. Statistical analysis was performed on input subtracted values using Limma (R; Bioconductor). Methylation validation was performed using MeDIP-qPCR and COBRA assays of selected regions (Supplemental Figure S2)

Quantitative pyrosequencing of Bisulfite DNA and Combined Bisulfite Restriction Analysis (COBRA)

RNA-depleted genomic DNA was isolated using DNeasy DNA isolation kit (Qiagen). 1ug of gDNA was used for bisulfite conversion as previously described (26). Regions surrounding *LTBP2* gene region were analyzed to verify meDIP-qPCR results. Primer sequences listed in supplementary table S5. COBRA analysis was performed as previously described (27) to validate meDIP-chip result (Supplemental Figure S2). Briefly, significant DMRs were analyzed for sequences appropriate for COBRA analysis (TaqI - TCGA or BstUI - CGCG sequence, Supplemental Table S2). Primers (Supplemental Table S4) were

designed targeting bisulfite converted DNA, after PCR amplification, restriction digest was performed and products were analyzed by agarose gel electrophoresis. Results were quantified using ImageJ (28).

Transcriptional profiling and validation

Total RNA was isolated from immortalized HPECs using PerfectPure RNA Isolation kit (5prime, Hilden, Germany). Sample preparation, quality control, and Human Transcriptome 2.0 Microarray profiling were performed according to manufacturer's protocol (Affymetrix). Affymetrix GeneChip Comman Console was used to extract raw data. Transcriptome Analysis Console (v3.0 Affymetrix) was used for RMA normalization and statistical analysis. Genes with FDR < 10% were considered significant. Biological validation of significant genes was performed in biological replicates in both independent vectors targeting CTCF (shCTCF1 and shCTCF2) as well as non-silencing shRNA by qPCR (Supplemental Figure 3).

Heat maps were created using Z-score transformation of normalized intensity values using ggplot2 (Bioconductor) in R. Gene ontology was performed using DAVID (Nature protocols 2009 citation – see website). Pathway analyses were performed using Gene Set Enrichment Analysis v2.2.3 (29).

Chromatin immunoprecipitation (ChIP)

Decreases in CTCF binding after shCTCF induction were verified by chromatin immunoprecipitation. Potential CTCF binding sites were identified using ENCODE CTCF ChIP-Seq data from UCSC for highly conserved CTCF binding sites, and LNCaP CTCF ChIP-Seq data for potential prostate specific CTCF binding sites. The ChIP assay was performed as previously described (16). Briefly, 1x10^7 cells were used for each IP with

5ug of anti-CTCF antibody (Cell Signaling #3418) at 4C overnight. Negative controls performed using anti-Rabbit IgG antibody (Cell Signaling #3900). Immunoprecipitation complexes were purified with Protein A/G magnetic beads (Cat. #26162, ThermoFisher Scientific) at 4C for two hours, followed by washing. Elution was performed twice, using 75uL elution buffer (1% SDS, 100mM NaHCO3), combining eluates for a total of 150uL. Crosslink reversal was performed overnight at 67C, followed by RNase and Proteinase K treatment. DNA was purified using PCR purification kit (Qiagen). Purified DNA was analyzed by qPCR.

Methylated DNA Immunoprecipitation (meDIP) Analyzed by qPCR

For meDIP-qPCR experiments, meDIP was performed as described in meDIP-chip methods with only slight deviations. For meDIP-qPCR experiments, gDNA was sonicated to obtain fragments <1000 base pairs. 4ug of gDNA was used for each IP using 5ug of anti-5mC antibody. Purified DNA was analyzed by qPCR.

Quantitative Polymerase Chain Reaction (qPCR)

For gene expression analysis, DNase treated total RNA from cultured cells was isolated using PerfectPure RNA isolation kit (5prime). A total of 2ug of RNA was used for reverse transcription using qScript cDNA Synthesis Kit (Quantabio, Beverly, MA). For ChIP and meDIP analysis, column purified DNA was used for analysis. Quantitative PCR was performed using PerfeCTa SYBR Green FastMix (Quantabio, Beverly, MA) on a Bio-Rad CFX96 (Bio-Rad, Hercules, CA) using experimental samples including no reverse transcriptase and cDNA free negative controls.

Bioinformatic Analysis

MeDIP-chip

We followed guidelines for analysis as outlined previously for meDIP-chip analysis using Affymetrix genotyping and copy number arrays (24,25). Using Affymetrix Cytoscan HD probe annotation data, we matched array probes to their predicted *NspI* digested fragments to predict enrichment regions. Analysis was restricted only to those fragments containing CpG sequences. We considered P-values < 0.01 as significant, several probe regions identified by this cut point were further validated using combined bisulfite restriction analysis (COBRA) assay and MeDIP-qPCR (Supplemental Figure S2).

Motif Finding

Searching methylated sequences for known transcription factor binding sites (TFBS) was performed using the HOMER package (30). Significant hypermethylated or hypomethylated sequences were searched for known TFBS using the *de novo* motif finding parameters. Cytoscan HD array targeted *NspI* fragments containing CpG sequences were used as background sequences.

Annotation Data

Hg19 genome annotation data was obtained from Ensembl. CTCF binding sites for prostate cells were obtained from CTCF ChIP-Seq in LNCaP cells (GEO: GSE33213). For breast cancer data, CTCF binding sites were obtained from CTCF ChIP-Seq in MCF7 cells (GSE30263). Transcribed regions including introns, exons and untranslated regions, CpG island locations, and CTCF binding sites were matched to Cytoscan HD array *NspI* fragment or Illumina 450k Methylation array probe genomic location using BedTools.

Results

CTCF Copy Number Alterations Are Frequently Found in Prostate and Breast Cancers

To determine the relevance of CTCF loss *in vivo* we first queried prostate cancer samples within the publicly available The Cancer Genome Atlas (TCGA) datasets. In a 333 primary PCa sample set previously annotated by the TCGA Research Network, 27% (90/333) of samples exhibit genomic copy number (CN) loss of *CTCF* (Figure 1A) with no mutations of *CTCF* detected in the cohort. Samples with CN loss express significantly lower levels of *CTCF* mRNA than tumors diploid for genomic *CTCF*. We analyzed other cancers of the TCGA in a similar fashion. In breast cancer samples, we noted a pronounced deletion and expression pattern, (513/816 (62.9%) - *CTCF* CN loss/Total; Figure 1D). These data confirm CTCF alterations are a common finding in primary cancers with 1/3 of prostate and 3/5 of breast samples harboring loss of CTCF.

DNA Hypermethylation Is Frequently Found at Putative CTCF Binding Sites *In Vivo*

Publicly available Illumina Infinium HumanMethylation450 (HM450) data of prostate TCGA specimens were analyzed for common DNA methylation alterations in CTCF copy number alteration (CNA) samples. To minimize confounding variables, quality control procedures were followed as outlined in the initial characterization of these samples by TCGA Research Network (21). Samples were grouped based on CTCF CN, combining deep and shallow deletion samples versus CTCF diploid prostate tumors. CTCF CN gain samples occur rarely (n=5) and were not included in this analysis.

In prostate tumors, a comparison of absolute mean methylation (β-values) in *CTCF* CNA versus *CTCF* diploid tumors demonstrated 1,786 differentially methylated probesets

using a restrictive cut-point (Fold Change (FC): absolute value log2 *CTCF* CNA/*CTCF* Diploid β-values > 0.5; FDR $q < 0.01$). A volcano plot demonstrates a predominance of hypermethylation events (1,684 significant DMRs; 94.2%) in tumors harboring loss of *CTCF* CNA (Figure 1B). In addition, this demonstrates the significantly greater degree of hypermethylation events in *CTCF* CNA tumors (Mean absolute value log2 FC in β-value, 0.55 hypomethylated vs. 0.69 hypermethylated; $P = 1.26e\text{-}13$) compared to diploid tumors.

In addition, CTCF binding sites seem to be a target of altered epigenetic enzymes, as seen in the case of *IDH* mutant gliomas, which exhibit hypermethylation at CTCF-Cohesin binding sites (11). Therefore, we sought to determine whether decreased CTCF expression via CN loss in prostatic tumors was principally associated with hypermethylation at CTCF binding sites. Publicly available CTCF ChIP-Seq data in LNCaP was used to define putative CTCF binding sites (GEO: GSE33213). Comparing CTCF binding sites identified by ChIP-Seq against HM450 methylation data of TCGA samples demonstrated a significant enrichment for differentially methylated regions at putative CTCF binding sites (Fig 1C). Nearly half of all significant hypermethylation (*CTCF* CN loss/*CTCF* Diploid) events were located near these sites (889/1786, 49.8%; $\pm$2kb) (Supplemental Figure S1A). We extended this analysis to profile TCGA breast tumors in a similar fashion, over half of breast tumors exhibit CTCF CN loss (Figure 1D). In BCa, out of 670 detected DMRs in CTCF CN loss tumors versus CTCF diploid tumors, 476 (476/670; 71%) were hypermethylation events (Figure 1E). A similar association was seen with altered methylation and hypermethylation events concentrated near CTCF binding sites (MCF7 Chip-Seq; GSE30263) (10) in CTCF CNA tumors (Figure 1F; Supplemental Figure S1B). These data indicate decreased CTCF expression is associated with aberrant DNA methylation at CTCF binding sites in human tumors.

CTCF Knockdown in Prostate Cells Leads to Widespread Changes in DNA Methylation

Recent observations have indicated CTCF binding sites are sensitive to altered epigenetic states and a target of altered epigenetic enzymes (11). The analysis of TCGA prostate and breast tumors suggests a significant association with methylation at CTCF binding sites. CTCF hemizygous deletion in mouse models led to genome-wide destabilization of DNA methylation, in this model CTCF binding site disruption by DNA methylation was not investigated thoroughly (31). Decreased CTCF expression in the prostate is linked to a variety of physiologic events associated with cancer development including aging (14), senescence (32), and oxidative stress (16).

The above findings demonstrate a correlation between DNA methylation and CTCF levels in human breast and prostate cancer samples. We sought to determine whether decreased CTCF expression is causal in methylation targeting and cell phenotype. A performed a genome-wide methylation analysis was performed using methylated DNA immunoprecipitation followed by application to the CytoScan HD copy number variation array (MeDIP-chip Flowchart; Figure 2A). Methylation profiling was performed on non-tumorigenic immortalized human prostate epithelial cells (HPECs) with a doxycycline-inducible shRNA targeting CTCF, verified by western blot (Figure 2B). This approach was used in a non-tumorigenic cell line in an effort to capture changes associated with transformation. Methylation profiling in HPECs yielded 9640 differentially methylated regions (DMRs) between CTCF knockdown and controls ($P < 0.01$) (Figure 2C). Similar to human tumors with CTCF copy number loss, DMRs in CTCF knockdown genome demonstrated preferential hypermethylation with 58.8% of significant probes

hypermethylated (0.55 hypomethylated vs. 0.63 hypermethylated; P = 3.5E-37; mean absolute value, log2 FC) albeit less dramatically than intact tumors (Figure 2C).

Genome-wide distribution of DMRs across gene features including exons, intron, shores and promoters mirrored the total DMR distribution, favoring hypermethylation. We detected a high number of DMRs within gene transcribed regions (Figure 2D), potentially due to denser CytoScan HD coverage in transcribed regions. Overall, there was no significant enrichment for specific gene features compared to the array distribution of probes.

We questioned whether significant associations with other transcription factor binding motifs could be found in the DMRs of CTCF knockdown cells. A *de novo* motif finding approach of known transcription factor binding sites was performed using the DNA sequence of *NspI* fragments detected by the array probes using HOMER (30). Significant enrichment for CTCF binding sites was only seen in hypermethylated DMRs (Figure 2E). *CTCFL/BORIS*, a CTCF paralogue, was also identified. The NFκB-p65 motif was also significantly enriched.

Alterations in Gene Transcription Associate with CTCF Binding Sites and Correlate with Differentially Methylated Regions

In an effort to associate changes in DNA methylation with gene transcription, CTCF knockdown HPECs were profiled by Affymetrix Human Transcriptome 2.0 arrays. Compared to control, 1308 gene level transcripts were significantly altered (FDR q < 0.1) with CTCF knockdown corresponding to 608 downregulated and 700 upregulated transcripts (46.5% and 53.5%, respectively) (Figure 3A). Using CTCF LNCaP ChIP-Seq data, CTCF binding sites near ($\pm$2kb) the transcription start site (TSS) of altered genes were

significantly enriched, validating the function of CTCF as a locally acting transcription factor. This enrichment represented 39.2% of significantly altered genes compared to only 24% of genes covered by the array (Chi-square $P < 1e\text{-}4$).

To examine the overlap of differentially expressed genes and differential methylation marks, gene sets were compared by mapping the MeDIP-chip probe fragments to the 33,801 unique RefSeq coding transcripts, containing well-established annotation, profiled by the transcriptional array. Of the DMRs, over half (5877/9640) were found in transcribed or promoter (<2kb downstream and <5kb upstream) associated regions, representing 3,773 unique genes to contrast with 1065 differentially expressed annotated genes (243 genes lacking annotation). Without respect to transcriptional direction, 216 differentially expressed genes were found to contain a DMR ($P < 0.0001$; hypergeometric distribution) (Figure 3C). Suggesting an association between gene transcription and methylation with CTCF knockdown.

CTCF Knockdown Increases Cell Survival After Stress Exposure

We applied Gene Ontology (GO) and Gene Set Enrichment Analysis (GSEA) to analyze phenotypic associations with genes significantly altered with CTCF knockdown. Gene ontology analysis using all differentially expressed genes indicated an enrichment of genes associated with cell motion, oxygen levels and/or hypoxia, and response to hormone stimulus (Figure 3D). GSEA results specified genes associated with a variety of inflammation/oxidative stress pathways altered in response to CTCF knockdown (Figure 4A and 4B). Interestingly, negative enrichment scores were noted for inflammation and hypoxia related gene sets suggesting genes positively associated with these pathways are negatively associated with CTCF knockdown (Figure 4C and 4D).

Given these results, we investigated the effects of CTCF knockdown on stress pathways by performing cell growth assays in the presence of chemically-induced oxidative stress (Figure 4E) and hypoxia (Figure 4F) after 48 hours of CTCF shRNA induction in multiple cell lines. For both conditions, CTCF knockdown in immortalized HPECs (Figure 4E and 4F) and the cancer cell line PPC-1 (Supplemental Figure S4) results in increased cell survival after 96h of stress induction. These increased cell numbers could not be explained by CTCF knockdown-induced proliferation, as no significant difference in proliferation by cell growth assays were noted after 3 or 5 days of CTCF knockdown under normal conditions (not shown). Therefore, cells with decreased CTCF appear to have better survival under stressful conditions.

DNA Hypermethylation Occurs at CTCF Binding Sites of Downregulated Genes

We tested whether CTCF knockdown would lead to promoter-CTCF binding site (pCBS) associated gains of DNA methylation within transcriptionally silenced genes. We queried silenced genes in the above observed stress response pathways (Figure 4) after CTCF knockdown. Furthermore, genes to examine were chosen based on a greater extent of expression downregulation and the presence of a CTCF binding site within the promoter, identified from LNCaP ChIP-Seq and ENCODE conserved transcription factor binding sites (UCSC Genome Browser). Initial studies included *LTBP2* (latent transforming growth factor β binding protein 2), a gene previously linked to promoter hypermethylation in cancer (33,34). After verifying *LTBP2* transcriptional silencing (Figure 5A), we characterized CTCF binding at the *LTBP2* pCBS, and demonstrate a significant reduction in CTCF binding in knockdown cells (Figure 5B). DNA methylation in this region was examined by two independent methods, quantitative pyrosequencing of bisulfite DNA (Figure 5C; expanded results Supplemental Figure S5) and MeDIP-qPCR (Figure 5D). Both methods detected

marked increases in DNA methylation at pCBS of CTCF knockdown cells compared to controls.

We applied this analysis to other candidate genes identified as transcriptionally silenced stress response associated genes containing a pCBS. *TNFAIP3, FGF5, EPHA3, AMIGO2* and *IL7R* all demonstrated significantly decreased expression following CTCF knockdown (Figure 5E). Decreased CTCF binding activity at identified pCBS's was discovered for all genes (Figure 5F; expanded results Supplemental Figure S6), with the exception of *IL7R,* which remained below the detection limit. MeDIP-qPCR demonstrated pCBS-associated increases in DNA methylation (Figure 5G; expanded results Supplemental Figure S6). These data confirm that sustained transcriptional silencing via CTCF downregulation results in DNA methylation gains at CTCF associated promoters.

Discussion

CTCF is a critical regulator of chromatin organization and cell-type specific gene expression. Recently, a haploinsufficient mouse model suggested a tumor suppressive function for CTCF by finding increased tumor growth after chemotherapy in deficient mice (31). Despite this characterization, the extent and contribution of CTCF in disease development is not well understood. We demonstrate that loss of CTCF expression plays a pivotal role in directing DNA hypermethylation in human tumors to critical regions of the genome containing CTCF binding sites. Furthermore, the cell-type specific chromatin landscape dictated by CTCF and likely other chromatin modulators might explain the variation in tumor suppressor and oncogene function across different tissues and cancer types. Previous reports have documented that normal CTCF binding is crucial for loci-specific maintenance of epigenetic marks at specific critical genes (35-38). These data suggest epigenetic deregulation by altered CTCF is a crucial mediator of cancer formation and progression.

In the current work, a query of human cancer samples highlights the frequency (27% PCa; 62% BCa) of CTCF copy number alteration in primary samples (Figure 1). Adaptation of other publicly available data demonstrates that CTCF copy number status has functional consequences on the DNA methylation landscape, specifically associated with CTCF binding sites in breast and prostate tumors. *In vitro* we demonstrate that genome-wide DNA methylation alterations occur with short term reductions (~5d) in CTCF protein levels. Drawing comparisons between *in vivo* and *in vitro* results, CTCF downregulation was associated with an increase in hypermethylation events and that these hypermethylation events specifically were enriched for CTCF binding sites in both analyses (Figure 1C and Figure 2E).

Previous data have demonstrated a role for CTCF as a tumor suppressor (31,39), however the mechanisms by which CTCF achieves these effects are diverse and not well understood. Inflammation can induce a decrease in CTCF levels mediated by NFκB activation and binding to the CTCF promoter (16). GSEA results of CTCF knockdown cells in the current study indicate loss of CTCF negatively regulates a number of pathways, including inflammatory response associated genes. Using functional enrichment analyses and phenotypic tests we demonstrate in prostate cells CTCF knockdown confers a resistance to hypoxia and oxidative stress-induced reduction in cell growth (Figure 5; Supplemental Figure S3). Together, these data suggest a novel role for CTCF in the response to cell stress, and provides a novel tumor suppressive activity of CTCF in the prostate.

To date, an instructive mechanism for aging and cancer associated DNA hypermethylation events has yet to be elucidated. It has been proposed that the evacuation of transcription factors leaves DNA vulnerable to *de novo* DNA methyltransferase activity (3). In addition to physical protection of DNA, CTCF has been shown to play an active role in inhibiting DNMT activity through PARP-1 activation (40), indicating CTCF reduction results in a loss of protection from DNMTs contributing to methylation gain. In this study, we show extended loss of CTCF binding results in transcriptional silencing and a gain of DNA methylation (Figure 5). Given the ubiquitous nature of CTCF binding throughout the genome, these data strongly suggest CTCF may be an important factor in mediating the development of a cancer specific DNA methylation landscape.

In conclusion, decreases in CTCF expression alters the DNA methylation landscape in two of the most common human tumors, prostate and breast, both strongly linked to aging. These findings may be of critical importance in explaining epigenetic alterations in

other tissues and tumor types since CTCF function can be altered through other mechanisms. Proteins identified as CTCF binding partners, including CHD8 (41) and Cohesin (42-45), may alter CTCF attachment patterns when their expression is disturbed, a feature that has been noted in primary prostate cancer (46). In addition, Katinen *et al*. recently demonstrated CTCF/cohesin binding sites are frequently mutated in cancer, disrupting CTCF genome regulation by inhibiting CTCF recognition at specific DNA binding sites (47). Although the mutational frequency of *CTCF* is low in prostate and breast samples (1-2%), mutation of *CTCF* occurs at higher rates in other cancers (e.g. 20% in uterine tumors of the TCGA) and may reduce CTCF binding and contribute to alterations in the epigenetic landscape.

In summary, characterization of human tumors demonstrates genetic alteration of CTCF induces changes to genomic DNA methylation. *In vitro*, short term reduction of CTCF levels suggests other mechanisms that regulate short term changes in CTCF expression may contribute to accumulated epigenetic change. Further research will be crucial to understand the effects of short term CTCF reduction on accumulated epigenetic alterations with aging and cancer initiation.

References

1. Grasso CS, Wu YM, Robinson DR, Cao X, Dhanasekaran SM, Khan AP*, et al.* The mutational landscape of lethal castration-resistant prostate cancer. Nature **2012**;487:239-43
2. Jones PA. Functions of DNA methylation: islands, start sites, gene bodies and beyond. Nat Rev Genet **2012**;13:484-92
3. Clark SJ, Melki J. DNA methylation and gene silencing in cancer: which is the guilty party? Oncogene **2002**;21:5380-7
4. Ooi SK, Qiu C, Bernstein E, Li K, Jia D, Yang Z*, et al.* DNMT3L connects unmethylated lysine 4 of histone H3 to de novo methylation of DNA. Nature **2007**;448:714-7
5. Baniahmad A, Steiner C, Köhne AC, Renkawitz R. Modular structure of a chicken lysozyme silencer: involvement of an unusual thyroid hormone receptor binding site. Cell **1990**;61:505-14
6. Lobanenkov VV, Nicolas RH, Adler VV, Paterson H, Klenova EM, Polotskaja AV*, et al.* A novel sequence-specific DNA binding protein which interacts with three regularly spaced direct repeats of the CCCTC-motif in the 5'-flanking sequence of the chicken c-myc gene. Oncogene **1990**;5:1743-53
7. Bell AC, West AG, Felsenfeld G. The protein CTCF is required for the enhancer blocking activity of vertebrate insulators. Cell **1999**;98:387-96
8. Kanduri C, Pant V, Loukinov D, Pugacheva E, Qi CF, Wolffe A*, et al.* Functional association of CTCF with the insulator upstream of the H19 gene is parent of origin-specific and methylation-sensitive. Curr Biol **2000**;10:853-6
9. Maurano MT, Wang H, John S, Shafer A, Canfield T, Lee K*, et al.* Role of DNA Methylation in Modulating Transcription Factor Occupancy. Cell Rep **2015**;12:1184-95
10. Wang H, Maurano MT, Qu H, Varley KE, Gertz J, Pauli F*, et al.* Widespread plasticity in CTCF occupancy linked to DNA methylation. Genome Res **2012**;22:1680-8
11. Flavahan WA, Drier Y, Liau BB, Gillespie SM, Venteicher AS, Stemmer-Rachamimov AO*, et al.* Insulator dysfunction and oncogene activation in IDH mutant gliomas. Nature **2016**;529:110-4
12. Vietri Rudan M, Barrington C, Henderson S, Ernst C, Odom DT, Tanay A*, et al.* Comparative Hi-C reveals that CTCF underlies evolution of chromosomal domain architecture. Cell Rep **2015**;10:1297-309
13. Zampieri M, Guastafierro T, Calabrese R, Ciccarone F, Bacalini MG, Reale A*, et al.* ADP-ribose polymers localized on Ctcf-Parp1-Dnmt1 complex prevent methylation of Ctcf target sites. Biochem J **2012**;441:645-52
14. Fu VX, Dobosy JR, Desotelle JA, Almassi N, Ewald JA, Srinivasan R*, et al.* Aging and Cancer-Related Loss of Insulin-like Growth Factor 2 Imprinting in the Mouse and Human Prostate. Cancer Res **2008**;68:6797-802
15. Damaschke NA, Yang B, Bhusari S, Svaren JP, Jarrard DF. Epigenetic susceptibility factors for prostate cancer with aging. Prostate **2013**;73:1721-30
16. Yang B, Wagner J, Damaschke N, Yao T, Wuerzberger-Davis SM, Lee MH*, et al.* A novel pathway links oxidative stress to loss of insulin growth factor-2 (IGF2) imprinting through NF-κB activation. PLoS One **2014**;9:e88052

17. Fu Vx SSRKMLLSSJJDF. A loss of insulin-like growth factor-2 imprinting is modulated by CCCTC-binding factor down-regulation at senescence in human epithelial cells. J Biol Chem **2004**;279:52218-26
18. Chen H, Tian Y, Shu W, Bo X, Wang S. Comprehensive identification and annotation of cell type-specific and ubiquitous CTCF-binding sites in the human genome. PLoS One **2012**;7:e41374
19. Ong CT, Corces VG. CTCF: an architectural protein bridging genome topology and function. Nat Rev Genet **2014**;15:234-46
20. Cuddapah S, Jothi R, Schones DE, Roh TY, Cui K, Zhao K. Global analysis of the insulator binding protein CTCF in chromatin barrier regions reveals demarcation of active and repressive domains. Genome Res **2009**;19:24-32
21. Network CGAR. The Molecular Taxonomy of Primary Prostate Cancer. Cell **2015**;163:1011-25
22. Jarrard DF, Sarkar S, Shi Y, Yeager TR, Magrane G, Kinoshita H*, et al.* p16/pRb pathway alterations are required for bypassing senescence in human prostate epithelial cells. Cancer Res **1999**;59:2957-64
23. Rago R, Mitchen J, Wilding G. DNA fluorometric assay in 96-well tissue culture plates using Hoechst 33258 after cell lysis by freezing in distilled water. Anal Biochem **1990**;191:31-4
24. Luo JH, Ding Y, Chen R, Michalopoulos G, Nelson J, Tseng G*, et al.* Genome-wide methylation analysis of prostate tissues reveals global methylation patterns of prostate cancer. Am J Pathol **2013**;182:2028-36
25. Aryee MJ, Liu W, Engelmann JC, Nuhn P, Gurel M, Haffner MC*, et al.* DNA methylation alterations exhibit intraindividual stability and interindividual heterogeneity in prostate cancer metastases. Sci Transl Med **2013**;5:169ra10
26. Yang B, Bhusari S, Kueck J, Weeratunga P, Wagner J, Leverson G*, et al.* Methylation profiling defines an extensive field defect in histologically normal prostate tissues associated with prostate cancer. Neoplasia **2013**;15:399-408
27. Xiong Z, Laird PW. COBRA: a sensitive and quantitative DNA methylation assay. Nucleic Acids Res **1997**;25:2532-4
28. Schneider CA, Rasband WS, Eliceiri KW. NIH Image to ImageJ: 25 years of image analysis. Nat Methods **2012**;9:671-5
29. Mootha VK, Lindgren CM, Eriksson KF, Subramanian A, Sihag S, Lehar J*, et al.* PGC-1alpha-responsive genes involved in oxidative phosphorylation are coordinately downregulated in human diabetes. Nat Genet **2003**;34:267-73
30. Heinz S, Benner C, Spann N, Bertolino E, Lin YC, Laslo P*, et al.* Simple combinations of lineage-determining transcription factors prime cis-regulatory elements required for macrophage and B cell identities. Mol Cell **2010**;38:576-89
31. Kemp CJ, Moore JM, Moser R, Bernard B, Teater M, Smith LE*, et al.* CTCF haploinsufficiency destabilizes DNA methylation and predisposes to cancer. Cell Rep **2014**;7:1020-9
32. Fu VX, Schwarze SR, Kenowski ML, LeBlanc S, Svaren J, Jarrard DF. A Loss of Insulin-like Growth Factor-2 Imprinting Is Modulated by CCCTC-binding Factor Down-regulation at Senescence in Human Epithelial Cells. J Biol Chem **2004**;279:52218-26
33. Chan SH, Yee Ko JM, Chan KW, Chan YP, Tao Q, Hyytiainen M*, et al.* The ECM protein LTBP-2 is a suppressor of esophageal squamous cell carcinoma tumor

formation but higher tumor expression associates with poor patient outcome. Int J Cancer **2011**;129:565-73
34. Chen H, Ko JM, Wong VC, Hyytiainen M, Keski-Oja J, Chua D*, et al.* LTBP-2 confers pleiotropic suppression and promotes dormancy in a growth factor permissive microenvironment in nasopharyngeal carcinoma. Cancer Lett **2012**;325:89-98
35. De La Rosa-Velázquez IA, Rincón-Arano H, Benítez-Bribiesca L, Recillas-Targa F. Epigenetic regulation of the human retinoblastoma tumor suppressor gene promoter by CTCF. Cancer Res **2007**;67:2577-85
36. Rodriguez C, Borgel J, Court F, Cathala G, Forné T, Piette J. CTCF is a DNA methylation-sensitive positive regulator of the INK/ARF locus. Biochem Biophys Res Commun **2010**;392:129-34
37. Soto-Reyes E, Recillas-Targa F. Epigenetic regulation of the human p53 gene promoter by the CTCF transcription factor in transformed cell lines. Oncogene **2010**;29:2217-27
38. Witcher M, Emerson BM. Epigenetic silencing of the p16(INK4a) tumor suppressor is associated with loss of CTCF binding and a chromatin boundary. Mol Cell **2009**;34:271-84
39. Fiorentino FP, Giordano A. The tumor suppressor role of CTCF. J Cell Physiol **2012**;227:479-92
40. Guastafierro T, Cecchinelli B, Zampieri M, Reale A, Riggio G, Sthandier O*, et al.* CCCTC-binding factor activates PARP-1 affecting DNA methylation machinery. J Biol Chem **2008**;283:21873-80
41. Ishihara K, Oshimura M, Nakao M. CTCF-dependent chromatin insulator is linked to epigenetic remodeling. Mol Cell **2006**;23:733-42
42. Wendt KS, Yoshida K, Itoh T, Bando M, Koch B, Schirghuber E*, et al.* Cohesin mediates transcriptional insulation by CCCTC-binding factor. Nature **2008**;451:796-801
43. Rubio ED, Reiss DJ, Welcsh PL, Disteche CM, Filippova GN, Baliga NS*, et al.* CTCF physically links cohesin to chromatin. Proc Natl Acad Sci U S A **2008**;105:8309-14
44. Stedman W, Kang H, Lin S, Kissil JL, Bartolomei MS, Lieberman PM. Cohesins localize with CTCF at the KSHV latency control region and at cellular c-myc and H19/Igf2 insulators. EMBO J **2008**;27:654-66
45. Parelho V, Hadjur S, Spivakov M, Leleu M, Sauer S, Gregson HC*, et al.* Cohesins functionally associate with CTCF on mammalian chromosome arms. Cell **2008**;132:422-33
46. Damaschke NA, Yang B, Blute ML, Jr., Lin CP, Huang W, Jarrard DF. Frequent disruption of chromodomain helicase DNA-binding protein 8 (CHD8) and functionally associated chromatin regulators in prostate cancer. Neoplasia **2014**;16:1018-27
47. Katainen R, Dave K, Pitkänen E, Palin K, Kivioja T, Välimäki N*, et al.* CTCF/cohesin-binding sites are frequently mutated in cancer. Nat Genet **2015**;47:818-21

Figure 1. Primary Tumors of the TCGA Harboring CTCF Copy Number Alterations Exhibit a Distinct DNA Methylation Profile.

A, Primary Prostate Tumors from TCGA (n = 333) segregated by *CTCF* CN status, boxplots of RNA-Seq expression data for *CTCF* mRNA. Deep Deletion, n = 10; Shallow Deletion, n = 80; Diploid, n = 238; Gain, n = 5. ***B,*** A volcano plot of Illumina Methylation 450k Array data for *CTCF* CN loss tumors versus *CTCF* diploid tumors identifying significant differences in DNA methylation. Dots represent individual probes detected by HM450 array; Black – Above cut point, Grey – Below cut point. Cut point: Absolute Log2FC > 0.5, Adjusted P-value < 0.01. ***C,*** Prostate cancer cell line LNCaP CTCF ChIP-Seq (GSE33213) identified putative CTCF binding sites. The percentage of differentially methylated probes and percentage of total probes were calculated with respect to proximity to CTCF binding sites. ***D,*** Primary Breast Tumors from the TCGA (TCGA BRCA, n=816) segregated by CTCF CN status, boxplots of RNA-Seq expression data for CTCF mRNA. ***E,*** Volcano plot of Illumina Methylation 450k Array for BRCA tumors, CTCF CNA (n=513) vs. CTCF Diploid (n=230) tumors. Dots represent individual probes detected by HM450 array; Black – Above cut point, Grey – Below cut point. Cut point: Absolute Log2FC > 0.5, Adjusted P-value < 0.01. ***F,*** Breast cancer cell line MCF7 CTCF ChIP-Seq (GSE30263) identified putative CTCF binding sites for BRCA samples. The percentage of differentially methylated probes and percentage of total probes were calculated with respect to proximity to CTCF binding sites.

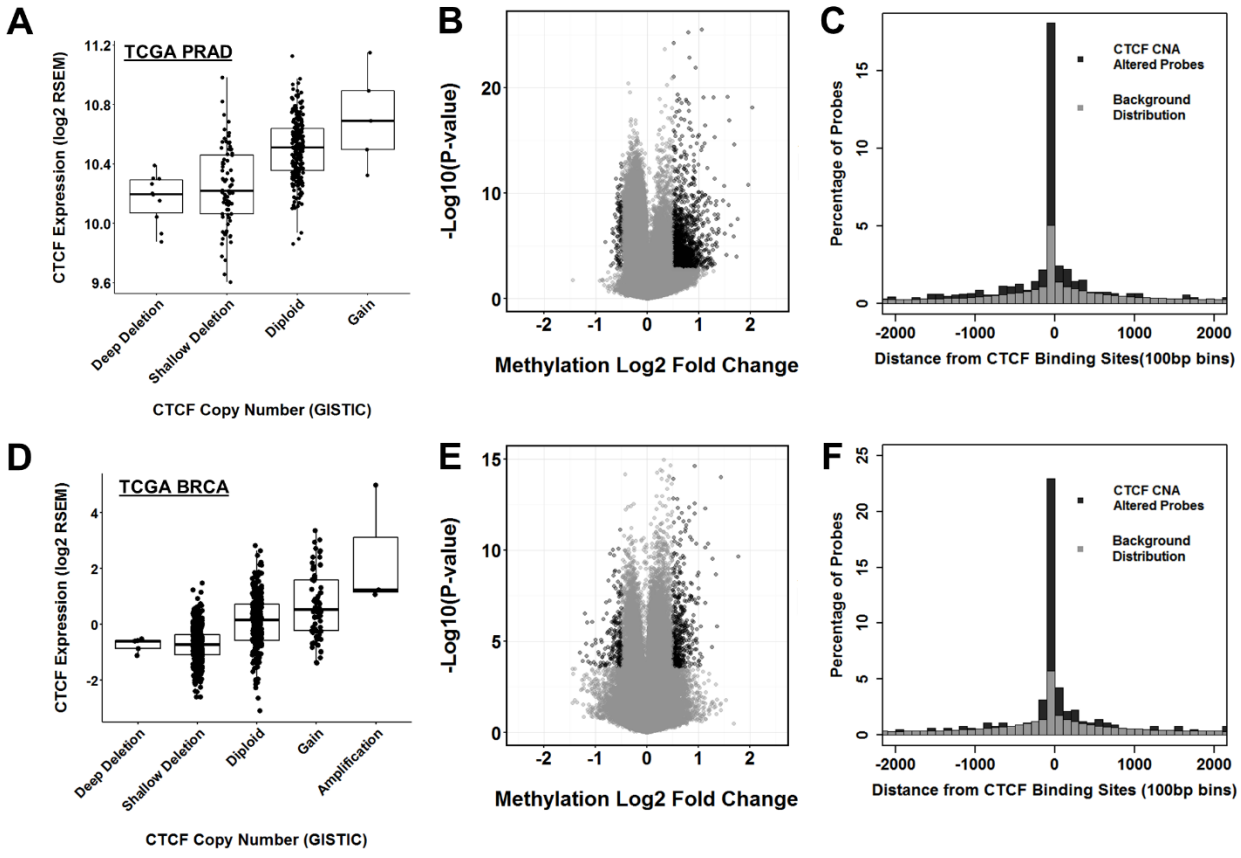
A
TCGA PRAD
CTCF Expression (log2 RSEM)
11.2
10.8
10.4
10.0
9.6
Deep Deletion
Shallow Deletion
Diploid
Gain
CTCF Copy Number (GISTIC)
B
-Log10(P-value)
20
10
0
-2
-1
0
1
2
Methylation Log2 Fold Change
C
Percentage of Probes
15
10
5
0
CTCF CNA Altered Probes
Background Distribution
-2000
-1000
0
1000
2000
Distance from CTCF Binding Sites(100bp bins)
D
TCGA BRCA
CTCF Expression (log2 RSEM)
4
2
0
-2
Deep Deletion
Shallow Deletion
Diploid
Gain
Amplification
CTCF Copy Number (GISTIC)
E
-Log10(P-value)
15
10
5
0
-2
-1
0
1
2
Methylation Log2 Fold Change
F
Percentage of Probes
25
20
15
10
5
0
CTCF CNA Altered Probes
Background Distribution
-2000
-1000
0
1000
2000
Distance from CTCF Binding Sites (100bp bins)

Figure 2. Knockdown of CTCF protein results in a wide range of DNA methylation alterations.

A, Workflow of methylated DNA immunoprecipitation followed by copy number array application (MeDIP-chip) for detecting methylation alterations. ***B,*** Short hairpin mediated CTCF knockdown in two separate shRNA targeting CTCF verified by western blotting after 3 and 5 days of shRNA induction including shRNA non-silencing control (shNSC). Data shown are one representative of 3 independent experiments using immortalized HPECs. Percentage knockdown compared to shCTCF -Dox control, quantified by ImageJ. ***C,*** Volcano plot of detected methylation changes in CTCF knockdown HPECs (Cut-point: Abs. Methylation Fold-change > 1.25, $P < 0.01$). ***D,*** Genomic distribution of differentially methylated (DM) probes with respect to gene features. ***E,*** *De novo* motif analysis results of top 3 transcription factor motifs. Enrichment of CTCF, BORIS, and NFκB-p65 were found in hypermethylated sequences compared to background distribution of array (All $P < 0.001$).

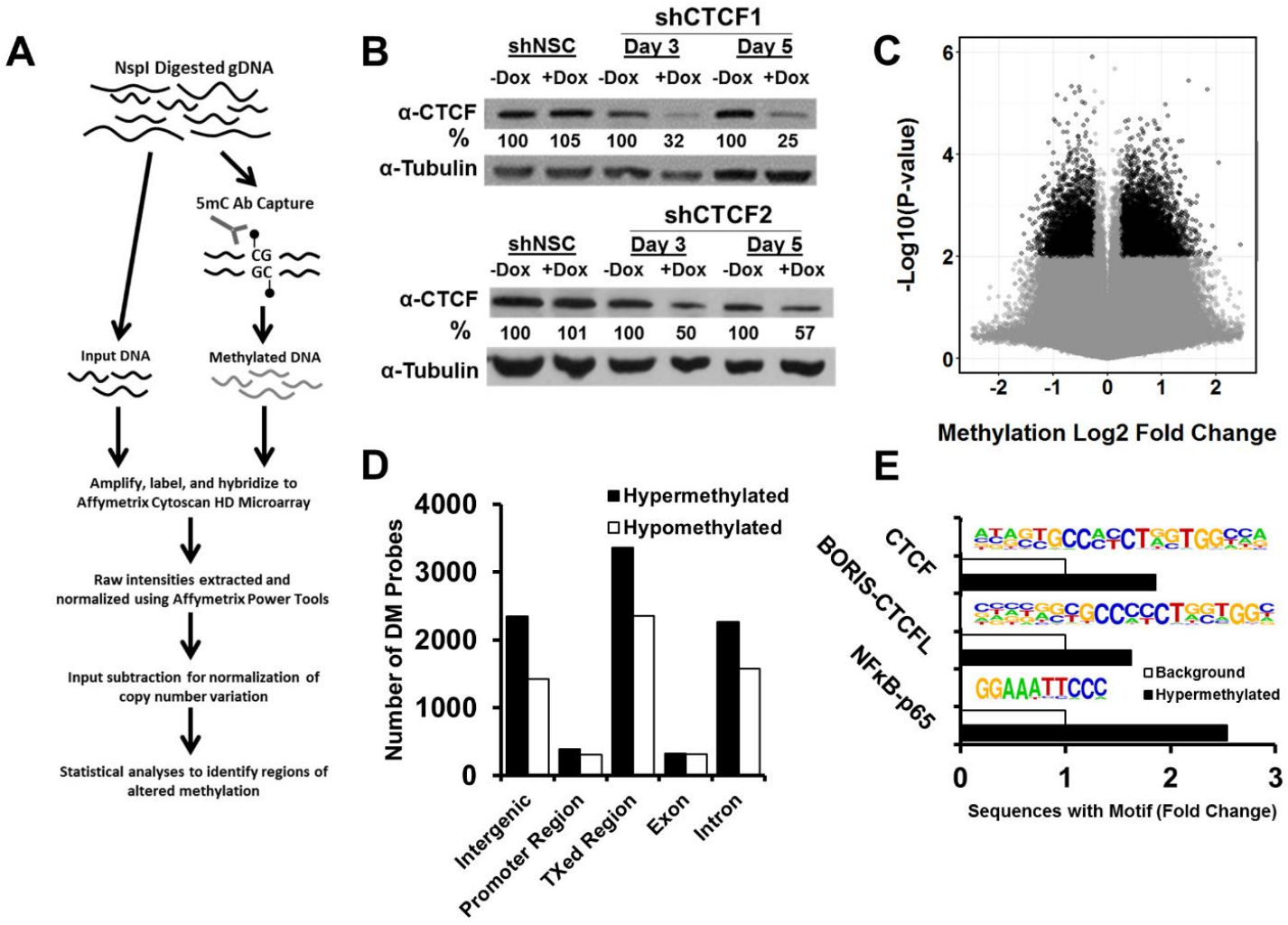
A
NspI Digested gDNA
5mC Ab Capture
CG
GC
Input DNA
Methylated DNA
Amplify, label, and hybridize to Affymetrix Cytoscan HD Microarray
Raw intensities extracted and normalized using Affymetrix Power Tools
Input subtraction for normalization of copy number variation
Statistical analyses to identify regions of altered methylation
B
shCTCF1
shNSC
Day 3
Day 5
-Dox +Dox -Dox +Dox -Dox +Dox
α-CTCF
%
100 105 100 32 100 25
α-Tubulin
shCTCF2
shNSC
Day 3
Day 5
-Dox +Dox -Dox +Dox -Dox +Dox
α-CTCF
%
100 101 100 50 100 57
α-Tubulin
C
-Log10(P-value)
Methylation Log2 Fold Change
D
Hypermethylated
Hypomethylated
Number of DM Probes
Intergenic
Promoter Region
TXed Region
Exon
Intron
E
CTCF
BORIS-CTCFL
NFκB-p65
Background
Hypermethylated
Sequences with Motif (Fold Change)

Figure 3. Transcriptional Profiling of Genes Altered with CTCF Knockdown

A, Heatmap of DE genes following 5 days of CTCF shRNA induction. CTCF knockdown in Immortalized HPECs lead to 1308 significantly altered gene transcripts (*FDR* < 0.1). ***B,*** Prostate cell CTCF binding sites are enriched near DE genes transcription start sites (LNCaP ChIP-Seq) (*P* = 0.0001; ±2kb from TSS). ***C,*** Detected DMRs represented found within a promoter or transcribed region represented 3,883 genes. Compared with 1065 genes (1065/1308 with gene annotation data) significantly DE, 216 genes were DE and contained a DMR (*P* = 1.1e-5; hypergeometric test). ***D,*** Gene ontology analysis of DE genes, pathways with FDR *q-value* < 0.05.

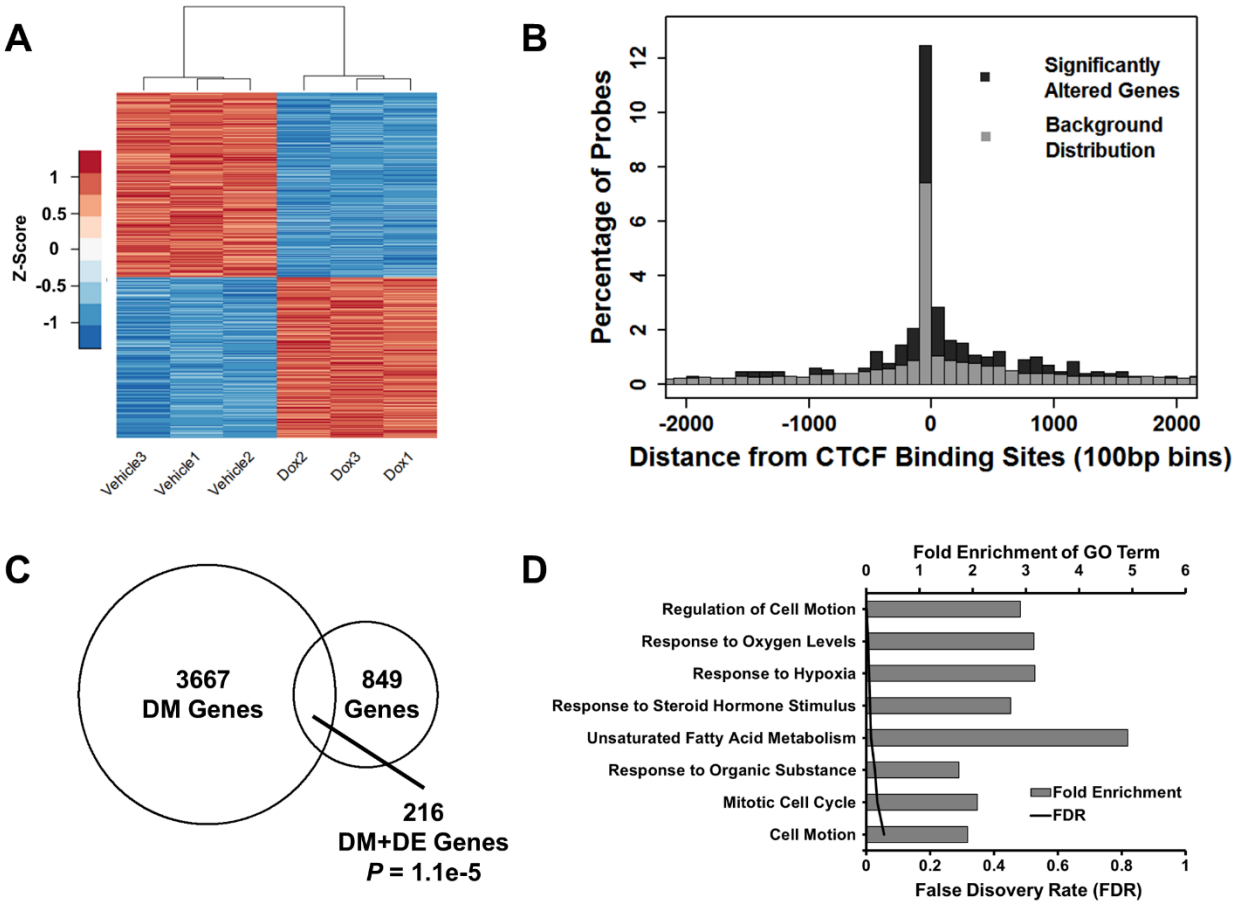
A
Z-Score
1
0.5
0
-0.5
-1
Vehicle3
Vehicle1
Vehicle2
Dox2
Dox3
Dox1
B
Percentage of Probes
0
2
4
6
8
10
12
Significantly Altered Genes
Background Distribution
-2000
-1000
0
1000
2000
Distance from CTCF Binding Sites (100bp bins)
C
3667 DM Genes
849 Genes
216 DM+DE Genes
P = 1.1e-5
D
Fold Enrichment of GO Term
0
1
2
3
4
5
6
Regulation of Cell Motion
Response to Oxygen Levels
Response to Hypoxia
Response to Steroid Hormone Stimulus
Unsaturated Fatty Acid Metabolism
Response to Organic Substance
Mitotic Cell Cycle
Cell Motion
Fold Enrichment
FDR
0
0.2
0.4
0.6
0.8
1
False Disovery Rate (FDR)

Figure 4. Functional Analysis of CTCF Knockdown DE Genes Reveals Alterations in Stress Response Pathways.

A, Pathways positively associated with CTCF knockdown identified by Gene Set Enrichment Analysis (GSEA). ***B,*** Pathways negatively associated with CTCF knockdown phenotype identified by GSEA. ***C,*** Genes positively associated with inflammatory response demonstrated negative enrichment with CTCF knockdown. ***D,*** Genes positively associated with hypoxia demonstrate negative enrichment with CTCF knockdown. ***E,*** In vitro response to 96h of oxidative stress by hydrogen peroxide after 48h of CTCF knockdown. Data normalized to -Dox or +Dox (H_20_2 vehicle) control cells. (+SD, *P < 0.05). ***F,*** In vitro response to 96h of chemically induced hypoxia by cobalt dichloride (CoCl2) administration after 48h of CTCF knockdown. Data normalized to -Dox or +Dox (CoCl2 vehicle) control cells (Mean+SD, *P < 0.05)

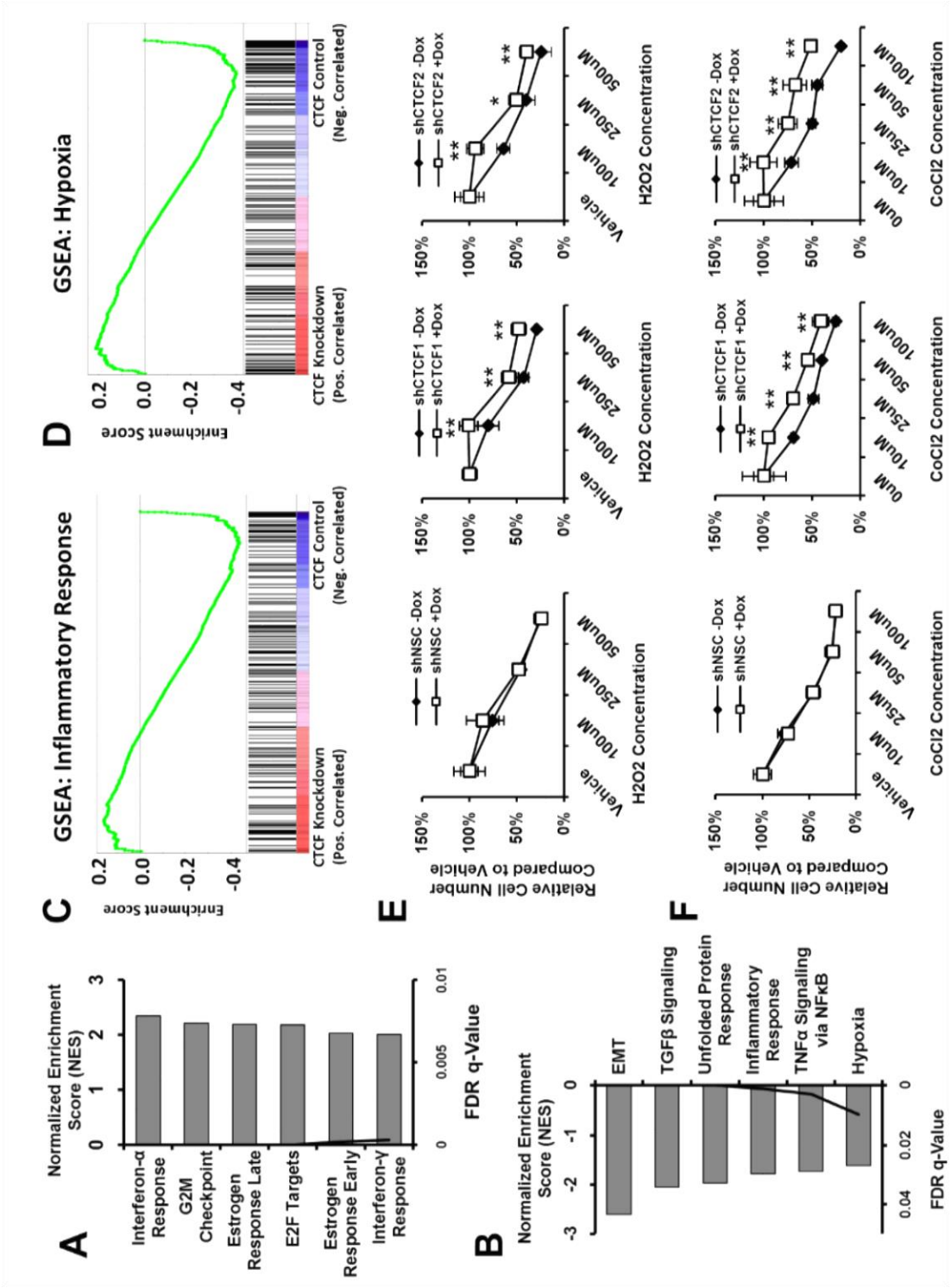
A
Normalized Enrichment Score (NES)
0
1
2
3
Interferon-α Response
G2M Checkpoint
Estrogen Response Late
E2F Targets
Estrogen Response Early
Interferon-γ Response
FDR q-Value
0
0.005
0.01
B
Normalized Enrichment Score (NES)
-3
-2
-1
0
EMT
TGFβ Signaling
Unfolded Protein Response
Inflammatory Response
TNFα Signaling via NFκB
Hypoxia
FDR q-Value
0.04
0.02
0
C
GSEA: Inflammatory Response
Enrichment Score
0.2
0.0
-0.2
-0.4
CTCF Knockdown (Pos. Correlated)
CTCF Control (Neg. Correlated)
D
GSEA: Hypoxia
Enrichment Score
0.2
0.0
-0.2
-0.4
CTCF Knockdown (Pos. Correlated)
CTCF Control (Neg. Correlated)
E
Relative Cell Number Compared to Vehicle
150%
100%
50%
0%
shNSC -Dox
shNSC +Dox
shCTCF1 -Dox
shCTCF1 +Dox
shCTCF2 -Dox
shCTCF2 +Dox
Vehicle
100uM
250uM
500uM
H2O2 Concentration
**
*
F
Relative Cell Number Compared to Vehicle
150%
100%
50%
0%
shNSC -Dox
shNSC +Dox
shCTCF1 -Dox
shCTCF1 +Dox
shCTCF2 -Dox
shCTCF2 +Dox
Vehicle
10uM
25uM
50uM
100uM
CoCl2 Concentration
**

Figure 5. DNA Methylation Alterations Occur at CTCF Binding Sites After Extended CTCF Knockdown *In Vitro*

A, Validation of *LTBP2* transcriptional silencing after 10 days of shCTCF induction by qPCR. Data are shown mean ± SD of technical triplicates from one representative experiment of three. ***B,*** ChIP-qPCR for CTCF at *LTBP2* promoter associated CTCF binding site (pCBS) ~400 bp upstream of *LTBP2* transcription start site. Showing a reduction in CTCF binding after 10 days of shCTCF induction. Data shown are mean ± SD of technical triplicates from one representative experiment of three. $*P < 0.05$ and $*P < 0.01$. ***C,*** Quantitative pyrosequencing of *LTBP2* promoter CTCF binding site (pCBS) following 10 days of shCTCF induction. Data represent mean±SE of two independent experiments. ***D,*** MeDIP-qPCR demonstrating increased methylation at *LTBP2* promoter CTCF binding site after 10 days of shCTCF induction. Data shown are mean ± SD of technical triplicates from one representative experiment of three. $*P < 0.05$ and $*P < 0.01$. ***E,*** Validation of *TNFAIP3*, *FGF5*, *EPHA3*, and *AMIGO2* transcriptional silencing after 10 days of CTCF knockdown. Data are shown mean ± SD of technical triplicates from one representative experiment of three. ***F,*** ChIP-qPCR for CTCF demonstrating decreased binding activity at promoter associated CTCF binding sites of candidate genes after 10 days of CTCF knockdown. ***G,*** MeDIP-qPCR of promoter associated CTCF binding sites exhibiting loss of CTCF binding. Methylation increases were detected accompanying reduced CTCF binding.

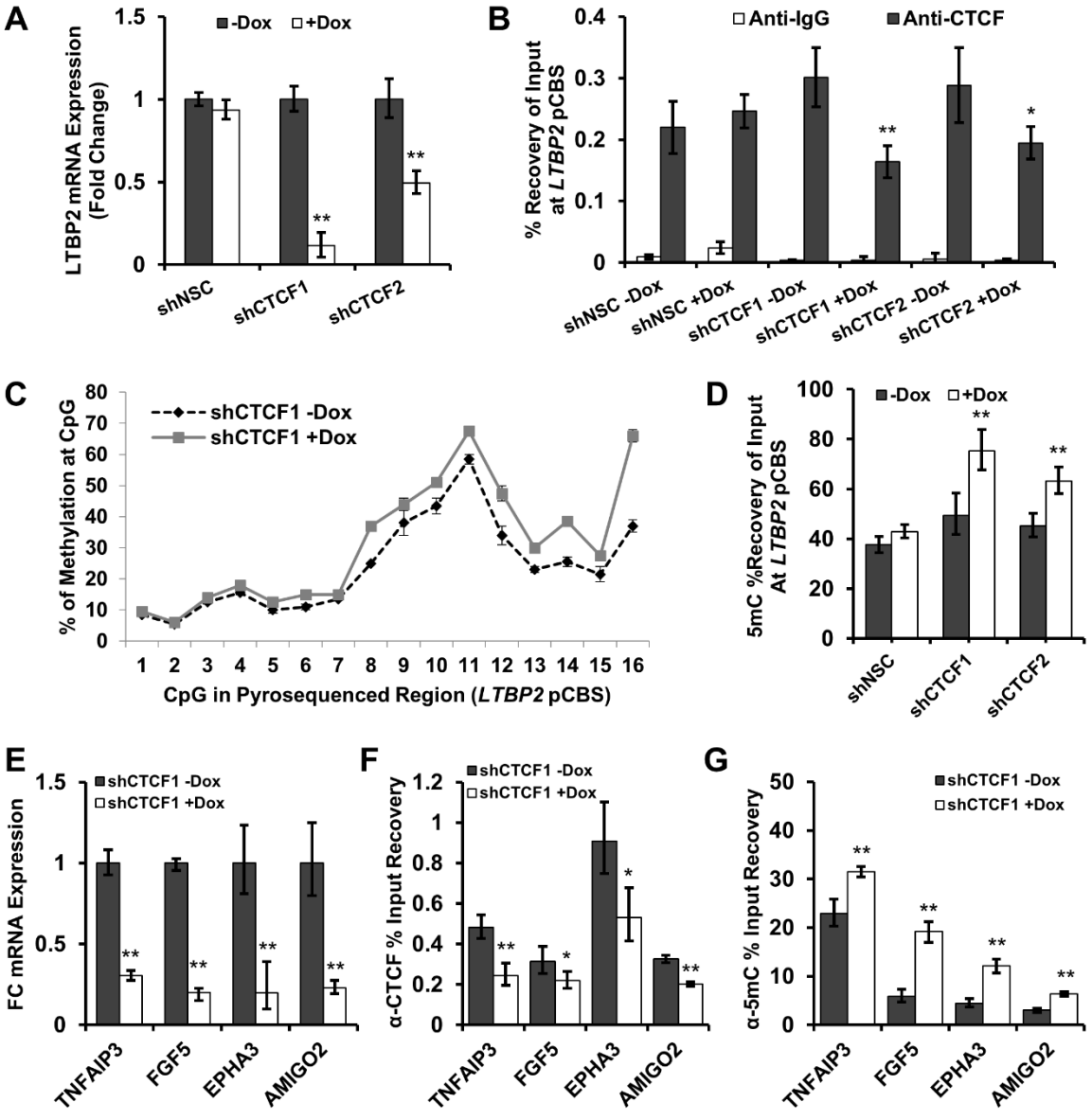
A
LTBP2 mRNA Expression (Fold Change)
-Dox
+Dox
shNSC
shCTCF1
shCTCF2
B
% Recovery of Input at LTBP2 pCBS
Anti-IgG
Anti-CTCF
shNSC -Dox
shNSC +Dox
shCTCF1 -Dox
shCTCF1 +Dox
shCTCF2 -Dox
shCTCF2 +Dox
C
% of Methylation at CpG
shCTCF1 -Dox
shCTCF1 +Dox
CpG in Pyrosequenced Region (LTBP2 pCBS)
D
5mC %Recovery of Input At LTBP2 pCBS
E
FC mRNA Expression
F
α-CTCF % Input Recovery
G
α-5mC % Input Recovery
TNFAIP3
FGF5
EPHA3
AMIGO2

Supplemental Figure 1. Comparison of hypermethylated versus hypomethylated probes with proximity to CTCF binding sites in TCGA tumor samples

Hypermethylated probes in CTCF CN loss tumors dominate the distribution in both PCa and BCa samples, clustering around CTCF binding sites. ***A,*** Prostate cancer cell line LNCaP CTCF ChIP-Seq (GSE33213) identified putative CTCF binding sites. The percentage of hypermethylated probes (CTCF CN loss > CTCF Diploid) and percentage of hypomethylated probes (CTCF CN loss < CTCF Diploid) were calculated with respect to proximity to CTCF binding sites (CTCF CN loss > CTCF Diploid). ***B,*** Breast cancer cell line MCF7 CTCF ChIP-Seq (GSE30263) identified putative CTCF binding sites. The percentage of hypermethylated probes and percentage of hypomethylated probes were calculated with respect to proximity to CTCF binding sites.

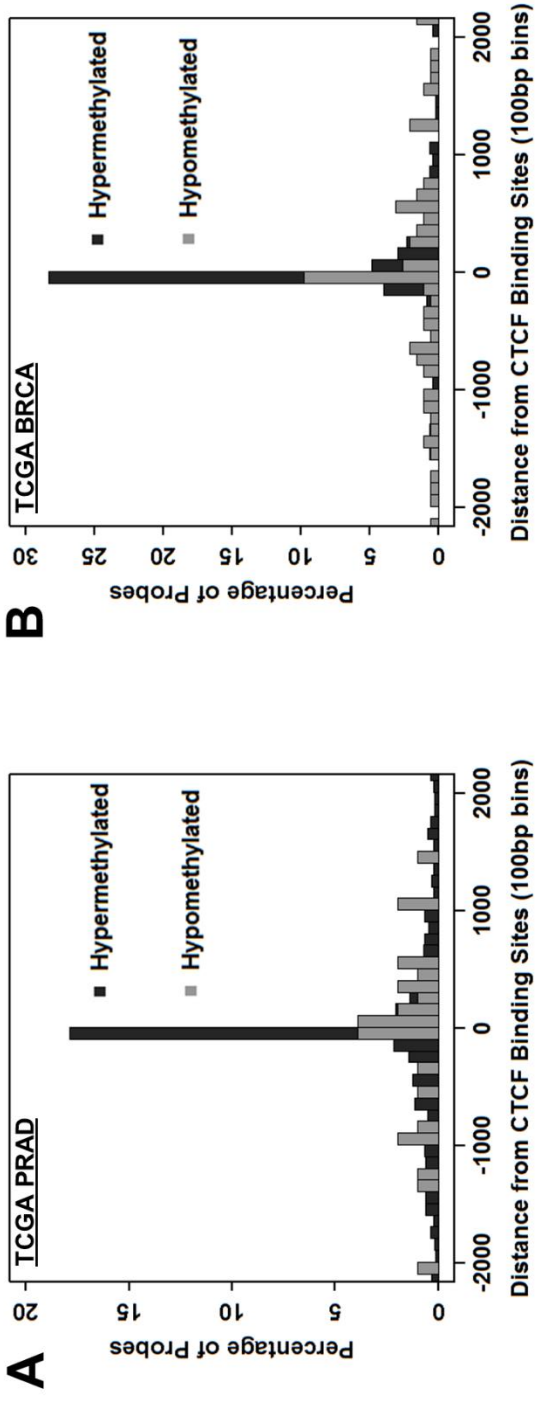
A
TCGA PRAD
Hypermethylated
Hypomethylated
Percentage of Probes
0
5
10
15
20
-2000
-1000
0
1000
2000
Distance from CTCF Binding Sites (100bp bins)
B
TCGA BRCA
Hypermethylated
Hypomethylated
Percentage of Probes
0
5
10
15
20
25
30
-2000
-1000
0
1000
2000
Distance from CTCF Binding Sites (100bp bins)

Supplemental Figure 2. Combined Bisulfite Restriction Analysis (COBRA) and MeDIP-qPCR Validation of Differentially Methylated Identified Probes

Two different methods were used to validate probes identified by MeDIP-chip analysis in biological replicates of 5 day shRNA induction. Detailed information of array probes (Supplementary Table 1), COBRA characteristics (Supplementary Table 2), and MeDIP-chip vs. MeDIP-qPCR comparisons (Supplementary Table 3) are provided. MeDIP-qPCR results are presented as mean±SD of technical triplicates (***P*<0.01, **P*<0.05). Arrows denote uncut bands. ***A,*** COBRA using *TaqI* (left) and MeDIP-qPCR (right) of Cytoscan HD probe C-4QPFF region. ***B,*** COBRA using *TaqI* (left) and MeDIP-qPCR (right) of Cytoscan HD probe C-6LWFW region. ***C,*** COBRA using *TaqI* (left) and MeDIP-qPCR (right) of Cytoscan HD probe C-4QXQN region. ***D,*** COBRA using *TaqI* (left) and MeDIP-qPCR (right) of Cytoscan HD probe C-3GEQV region. ***E,*** COBRA using *BstUI* restriction enzyme of Cytoscan HD probe C-3GEQV region. ***F,*** COBRA using *TaqI* (left) and MeDIP-qPCR (right) of Cytoscan HD probe C-6XOOB region.

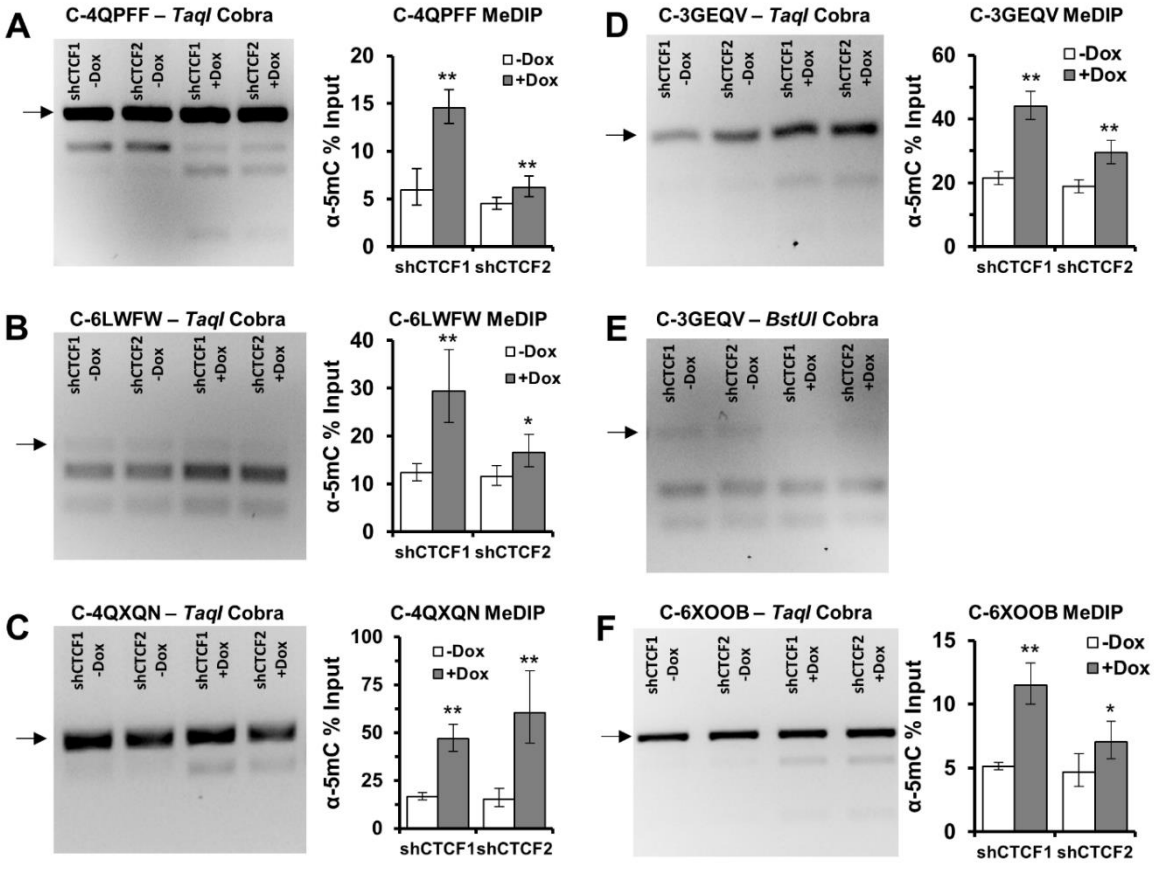
A
C-4QPFF – TaqI Cobra
shCTCF1 -Dox
shCTCF2 -Dox
shCTCF1 +Dox
shCTCF2 +Dox
C-4QPFF MeDIP
α-5mC % Input
-Dox
+Dox
shCTCF1 shCTCF2
B
C-6LWFW – TaqI Cobra
C-6LWFW MeDIP
C
C-4QXQN – TaqI Cobra
C-4QXQN MeDIP
D
C-3GEQV – TaqI Cobra
C-3GEQV MeDIP
E
C-3GEQV – BstUI Cobra
F
C-6XOOB – TaqI Cobra
C-6XOOB MeDIP

Supplemental Figure 3. Quantitative PCR Validation of Differentially Expressed Genes Identified by Transcriptional Array Following CTCF Knockdown

A, Six genes identified by transcriptional array profiling as down regulated following CTCF knockdown were validated using qPCR in biological replicates. Significant downregulation was confirmed in two independent shRNAs targeting CTCF following 5 days of doxycycline induction. Data show are mean±SD of technical triplicates representative of multiple experiments (**$P < 0.01$, *$P < 0.05$). ***B,*** Three genes identified by transcriptional array profiling as up regulated following CTCF knockdown were validated using qPCR in biological replicates. Significant upregulation was confirmed in two independent shRNAs targeting CTCF following 5 days of doxycycline induction. Data show are mean±SD of technical triplicates representative of multiple experiments (**$P < 0.01$, *$P < 0.05$).

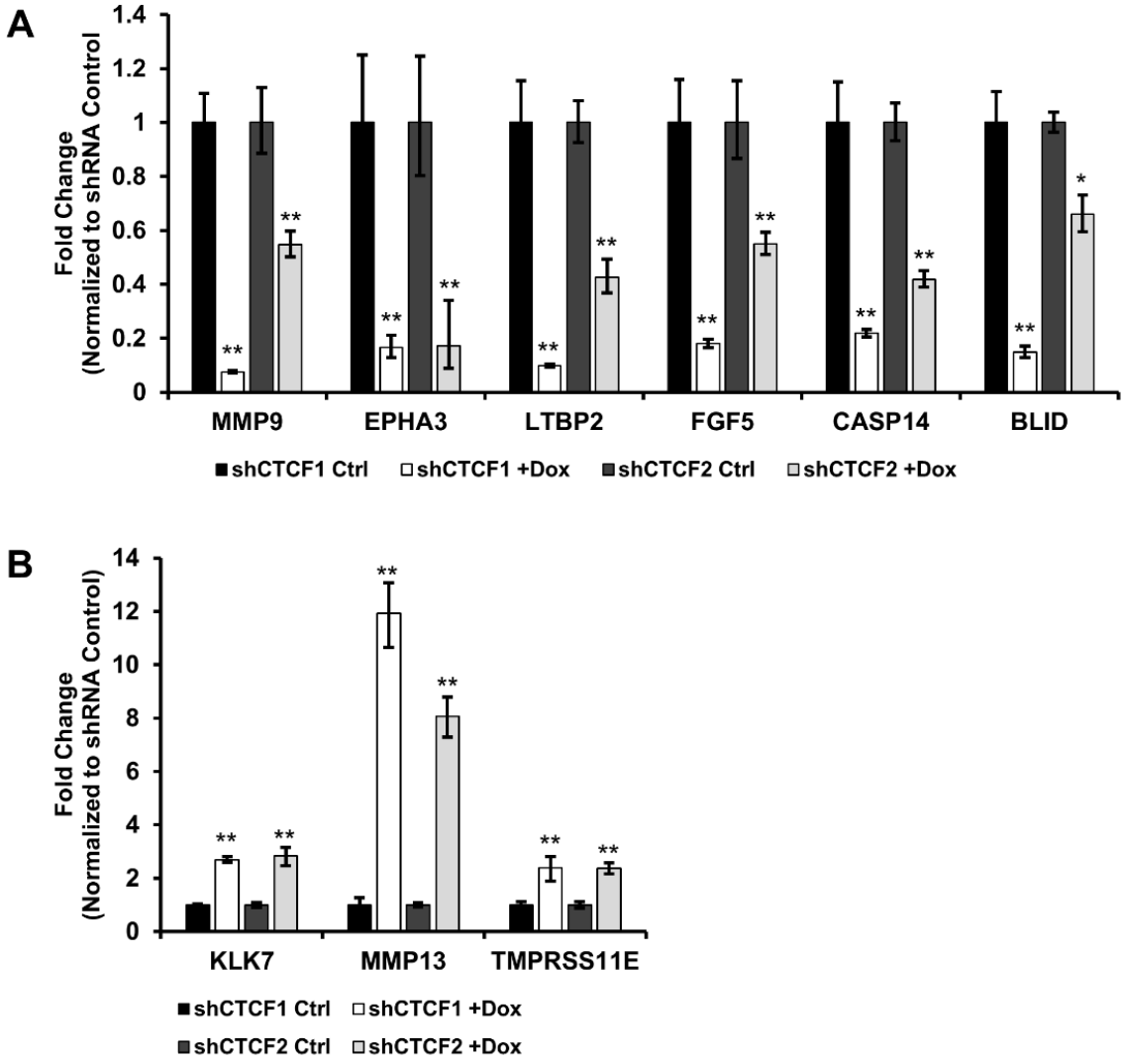
A
Fold Change
(Normalized to shRNA Control
1.4
1.2
1
0.8
0.6
0.4
0.2
0
MMP9
EPHA3
LTBP2
FGF5
CASP14
BLID
shCTCF1 Ctrl
shCTCF1 +Dox
shCTCF2 Ctrl
shCTCF2 +Dox
B
Fold Change
(Normalized to shRNA Control)
14
12
10
8
6
4
2
0
KLK7
MMP13
TMPRSS11E
shCTCF1 Ctrl
shCTCF1 +Dox
shCTCF2 Ctrl
shCTCF2 +Dox

Supplemental Figure 4. Response to Oxidative Stress and Hypoxia in Prostate Cancer Cell Line PPC-1

A, *In vitro* response to 96h of oxidative stress by hydrogen peroxide after 48h of CTCF knockdown in PPC-1 cells. Data normalized to -Dox or +Dox (H_20_2 vehicle) control cells. (Mean±95% CI, ***P* < 0.01, **P* < 0.05). ***B,*** *In vitro* response to 96h of chemically induced hypoxia by cobalt dichloride ($CoCl_2$) administration after 48h of CTCF knockdown in PPC-1 cells. Data normalized to -Dox or +Dox (CoCl2 vehicle) control cells (Mean±95% CI, ***P* < 0.01, **P* < 0.05).

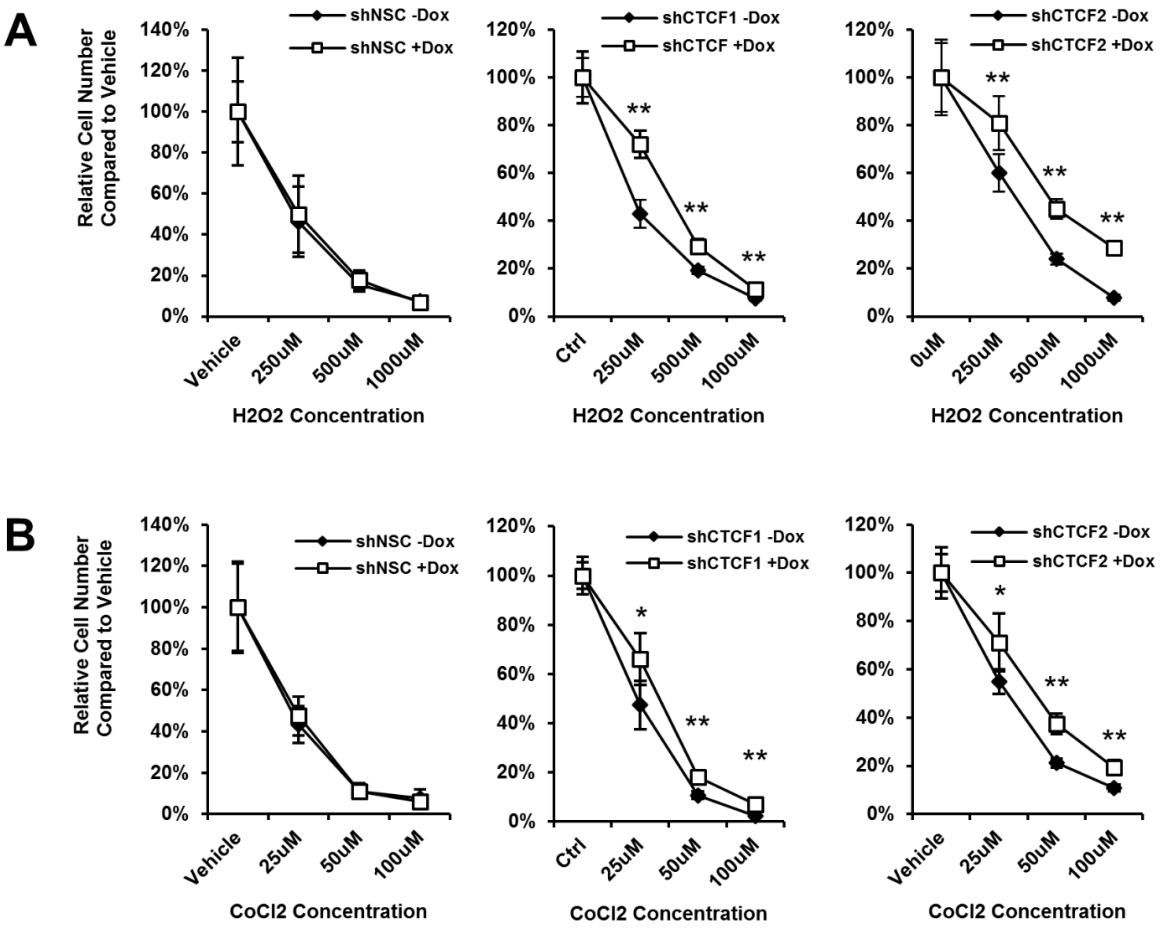
A
Relative Cell Number Compared to Vehicle
shNSC -Dox
shNSC +Dox
140%
120%
100%
80%
60%
40%
20%
0%
Vehicle
250uM
500uM
1000uM
H2O2 Concentration
shCTCF1 -Dox
shCTCF +Dox
Ctrl
250uM
500uM
1000uM
H2O2 Concentration
**
shCTCF2 -Dox
shCTCF2 +Dox
0uM
250uM
500uM
1000uM
H2O2 Concentration
B
Relative Cell Number Compared to Vehicle
shNSC -Dox
shNSC +Dox
Vehicle
25uM
50uM
100uM
CoCl2 Concentration
shCTCF1 -Dox
shCTCF1 +Dox
Ctrl
25uM
50uM
100uM
CoCl2 Concentration
*
shCTCF2 -Dox
shCTCF2 +Dox
Vehicle
25uM
50uM
100uM
CoCl2 Concentration

Supplemental Figure S5. Methylation Quantification of *LTBP2* Promoter CTCF binding site by Quantitative Pyrosequencing of Bisulfite Converted DNA, to Validate MeDIP-qPCR Results

A, Methylation quantification of HPECs ±Dox in shCTCF1 after 10 days of shRNA induction (Data represent mean±SE of two independent experiments). ***B,*** Methylation quantification of HPECs ±Dox in shCTCF2 after 10 days of shRNA induction (Data represent mean±SE of two independent experiments). ***C,*** Methylation quantification of HPECs ±Dox in shNSC after 10 days of shRNA induction (Data represent mean±SE of two independent experiments).

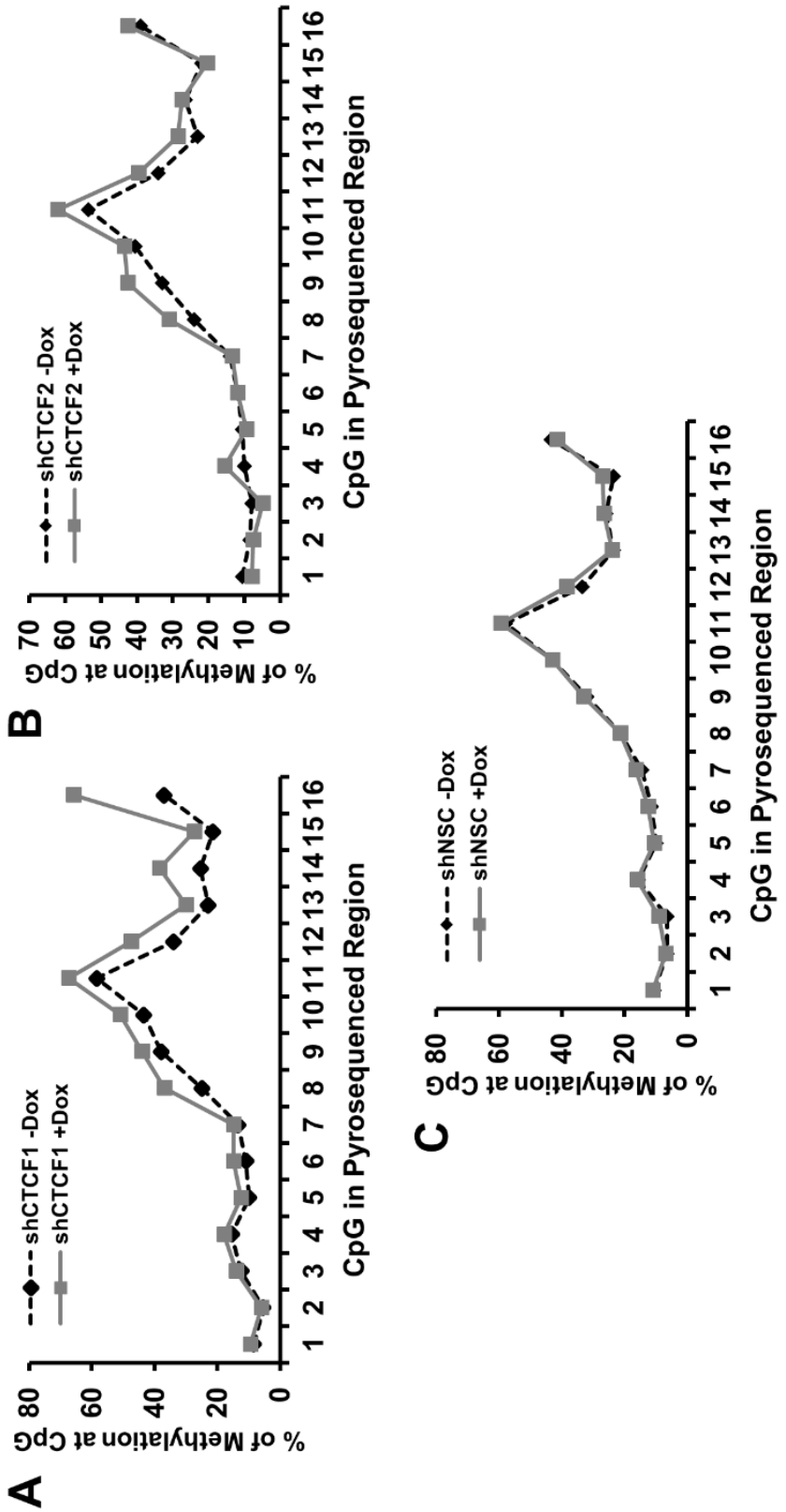
A
% of Methylation at CpG
shCTCF1 -Dox
shCTCF1 +Dox
CpG in Pyrosequenced Region
B
% of Methylation at CpG
shCTCF2 -Dox
shCTCF2 +Dox
CpG in Pyrosequenced Region
C
% of Methylation at CpG
shNSC -Dox
shNSC +Dox
CpG in Pyrosequenced Region

Supplemental Figure S6. Expanded Results of ChIP-qPCR and meDIP-qPCR in Immortalized HPECs Following 10 days of shRNA Induction. CTCF knockdown was conducted for 10 days by shRNA induction in Immortalized HPECs. CTCF binding was analyzed by chromatin immunoprecipitation quantified by qPCR (ChIP-qPCR). DNA methylation was analyzed by immunoprecipitation with an anti-5-methylcytosine antibody and quantified by qPCR (MeDIP-qPCR). The same primers were used for ChIP-qPCR and MeDIP-qPCR to analyze CTCF binding and DNA methylation of the same regions. ChIP-qPCR results for **(A)** *TNFAIP3* promoter CTCF binding site, **(B)** *FGF5* promoter CTCF binding site, **(C)** *AMIGO2* promoter CTCF binding site, and **(D)** *EPHA3* promoter CTCF binding site. MeDIP-qPCR Results for **(E)** *TNFAIP3* promoter CTCF binding site, **(F)** *FGF5* promoter CTCF binding site, **(G)** *AMIGO2* promoter CTCF binding site, and **(H)** *EPHA3* promoter CTCF binding sites. All data are presented mean$\pm$SD of technical triplicates, one representative of two independent experiments. *$P < 0.05$ and **$P < 0.01$.

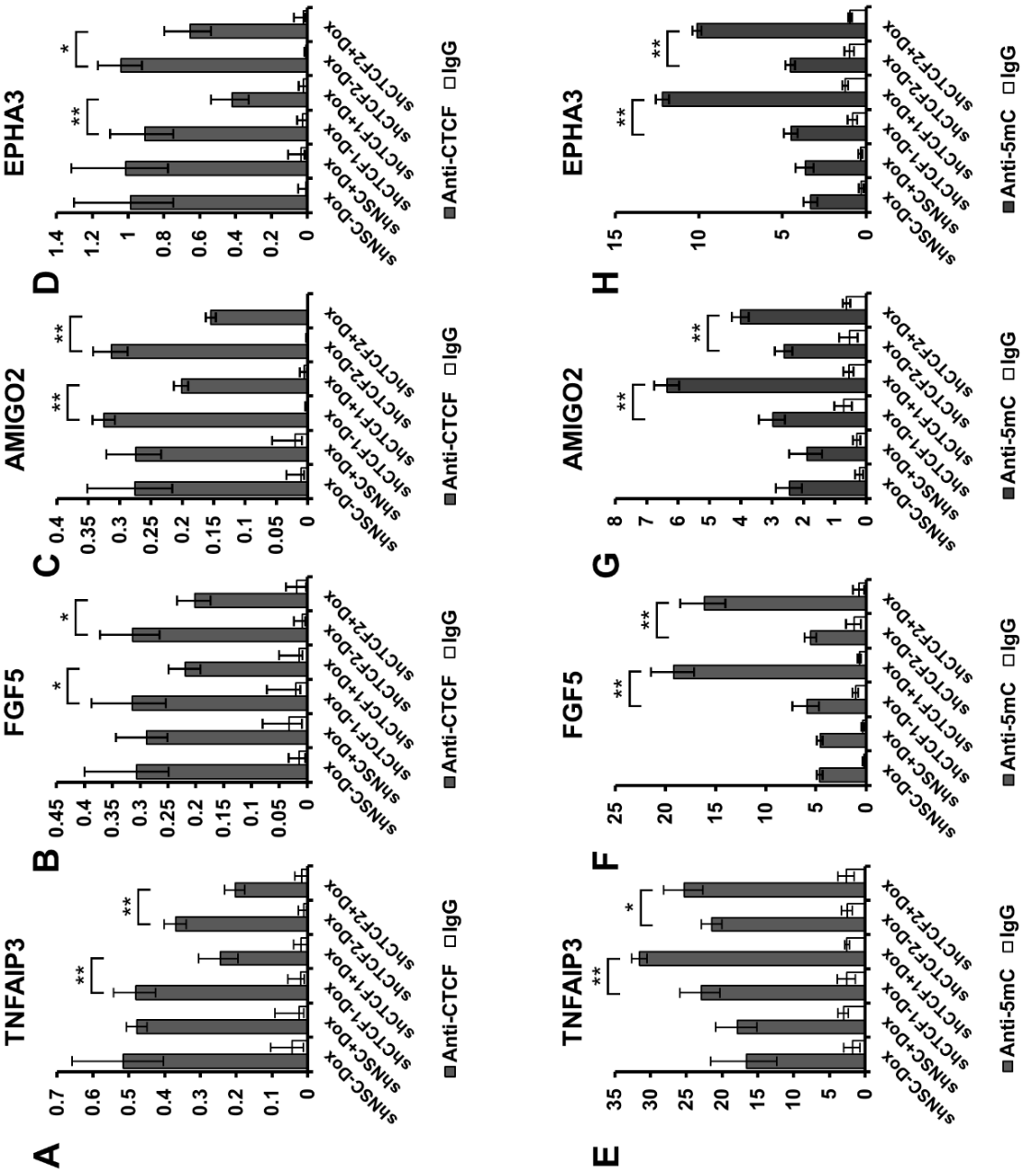
A
TNFAIP3
B
FGF5
C
AMIGO2
D
EPHA3
E
TNFAIP3
F
FGF5
G
AMIGO2
H
EPHA3
shNSC-Dox
shNSC+Dox
shCTCF1-Dox
shCTCF1+Dox
shCTCF2-Dox
shCTCF2+Dox
Anti-CTCF
IgG
Anti-5mC
IgG

Table S1: Cytoscan Probe Characteristics Used in Array Validation (COBRA and MeDIP-qPCR)

Cytoscan Probe	*NspI* Fragment Chr:Start-Stop	Methylation Fold Change	*P*-value	CpG Percentage
C-4QPFF	Chr8:67782483-67782995	1.85	0.01	4.29
C-6LWFW	Chr5:141184952-141185538	2.34	2.7E-04	1.02
C-4QXQN	Chr7:28893607-28894301	1.71	1.7E-03	6.62
C-3GEQV	Chr4:118569881-118570276	2.08	1.12E-05	1.01
C-6XOOB	Chr6:12289044-12289931	1.71	0.016	1.24

Table S2: Combined Bisulfite Restriction Analysis (COBRA) Assay Characteristics (Related to Supplemental Figure S2)

Cytoscan Probe	Bisulfite Converted Sequence	Amplicon Size; Enzyme Cut Site(s)
C-4QPFF	**5'-** **GGGAATATTGGAATGTTTTTTA**AAGTGATTAGATATTTTGTA TTTTTTGAAGTAGCGTTTTGAATTTTTTAAATATAATATTATTT GTTTGAGATAATAATAAAAATTAAACGTAGATTTATTTTTTTT TTGTT**TCGA**TGGGAGGGAGTAAGAGTGAAGTTATTAAAACG TAAGGGAATAAGTTCGGTTAGTTTTTTTGTTGAT**TCGA**GGG CGCGGGCGGTTTCGGTAGGTTTCGCGACGTAGTTAACGGT CGGGACGTGCGCGTATGCGCGTTAGGATTTCGTTTCGTTTA CGTTGTAGGCGGAGAGTAATC**GTTAAGTTTGGTGGGAGTT AAG** **-3'**	335bp; *TaqI*; 135, 205
C-6LWFW	**5'-** **ATTTTTGGTTGTATTTGAGTAAAA**TTTTAGGAAGGGACGTA TAGTTTGATTGTGTTGGAAGGAAGGTAGAAGGATGGATAGG GAGATTTTGAAGATGTTTTCGTAGGATTAGAGAAGGAGGTA GCGGAGGTATAGTAGTTTTTTT**TCGA**GGTTTTTTTTGAGATT TATTTTTTGGAGGTTTTGTCGGAATTTACGGTGATT**TTGAAG TAGGGGTTATGTTTT** **-3'**	222bp; *TaqI*; 146
C-4QXQN	**5'-** **GAAGGAGGTAGTTTTGGTAGTT**AGGGAAGGTGCGGTGTTC GTGTCGGGGTCGCGGGGCGTGCGGGAGTTTTGGGCGTCG TCGTATTTGTCGGTTTTTTTTGGGAGTTTTGGG**TCGA**ATTTT TAGTTCGGGCGTTTTTTGGCGTCGTCGTGGGGAAATTATTC GGCGTTAGGCGTTATGTCGTATAATATTGTGGAGTAGTTTT GTCGGCGGGGTGGGTGTTTTTTATTTAAGGTATTGGATTAG GGGTTTTGTTAGTAAATATGGTTTTTTTATTAGCGTGTCGGG GT**TGTAGAATTTTAGGGTATGGTTT** **-3'**	311bp; *TaqI*; 113
C-3GEQV	**5'-** **TTGGAGTTTTTTTTTTAGTTTTT**TGTTTTGATGATTCGTTTAA TGTTGTTAG**CGCG**TG**TCGA**AGTTTTTTATTATTATTATGTTG TTGTTTAAGTTGTTTTATAGGTTAAGAAGAATTTGTTTTATGA TT**TTGGGTATTTTAATGTT** **-3'**	147bp; *BstUI* – 54; *TaqI* – 59
C-6XOOB	**5'-** **ATTGTTTTGTGTGTATTTTAGG**GGGGGATTTTAAGGTTAGAT AGATAGGAAATTGTTTTGAAAATGTAAATATATTATTAAATGT GAAGTATTATTTGATTTTTTGT**TCGA**ATGGTATTTTTTTTTTA GTATTATTTTTTTTGTATATTTATTTAATTTTGTATAAGAATAT TTTTTTGTTTTAAATGAAGATATTTTTTTAAAAAAAAGAGTTTT AGAAAATATGTTTTTGTTTGTGCGGGGAATAAATAGAATATT TTGAGGTGTATTTTTTTTTTTTATGTTAGGTAATATTTTTTGA TTTTTTTCGGTTTTTAAGTTAGGTTGCGTTT**TTTTTTGTTATT TAGAAGGGTT** **-3'**	354bp; *TaqI*; 108

Table S3: MeDIP-qPCR Cytoscan Array Validation of Biological Replicates (Related to Supplemental Figure S2)

Cytoscan Probe	MeDIP-qPCR Region	shCTCF1 FC; *P*-value	shCTCF2 FC; *P*-value
C-4QPFF	chr7:28,893,861-28,894,158	2.44 Fold; 6.9E-04	1.38 Fold; 4.3E-03
C-6LWFW	chr5:141185284-141185572	2.37 Fold; 2.5E-05	1.44 Fold; 0.023
C-4QXQN	chr8:67782856-67783073	2.79 Fold; 3.6E-05	3.92 Fold; 7.0E-04
C-3GEQV	chr4:118570146-118570346	2.05 Fold; 1.0E-04	1.56 Fold; 1.4E-03
C-6XOOB	chr6:12289526-12289797	2.23 Fold; 6.6E-05	1.51 Fold; 8.0E-3

Table S4: Primers Used for Validation of Cytoscan Array (Related to Supplemental Figure S2)

Cytoscan Probe	Method	Primer Sequence (5'->3')
C-4QPFF	COBRA	For – GGGAATATTGGAATGTTTTTTA Rev – CTTAACTCCCACCAAACTTAAC
C-4QPFF	MeDIP-qPCR	For – TTTCTCTGCTTCGCTGGGAG Rev – CACTCACCTTGACTCCCACC
C-6LWFW	COBRA	For – ATTTTTGGTTGTATTTGAGTAAAA Rev – AAAACATAACCCCTACTTCAA
C-6LWFW	MeDIP-qPCR	For – GCAACAACAGGCCTAGTCCT Rev – AATAGAGCTGTGGCCCAGTG
C-4QXQN	COBRA	For – GAAGGAGGTAGTTTTGGTAGTT Rev – AAACCATACCCTAAAATTCTACA
C-4QXQN	MeDIP-qPCR	For – CTTGGTAGCCAGGGAAGGTG Rev – AACCATGCCCTGAGGTTCTG
C-3GEQV	COBRA	For – TTGGAGTTTTTTTTTTAGTTTTT Rev – AACATTAAAATACCCAAAATCA
C-3GEQV	MeDIP-qPCR	For – TCTGCCCTGATGATCCGTCT Rev – AGAAGGGCAAAGAAGGACATT
C-6XOOB	COBRA	For – ATTGTTTTGTGTGTATTTTAGG Rev – AACCCTTCTAAATAACAAAAAA
C-6XOOB	MeDIP-qPCR	For – TGCCCTAAATGAAGACACCCC Rev – GGTCGGTGCCACCAATCTTA

Table S5: LTBP2 Pyrosequencing Primers (Related to Figure 5)

Primer	Sequence (5' -> 3')
Forward	GATAGGGGGATTTAGGTTGTAGTTTTGTA
Reverse (Biotinylated)	(Biotin)-AAAAAAAAAACCCCTCTTCTACC
Sequence	GGAGAGTAGGGAGGT

Table S6: Primers Used for ChIP-qPCR and MeDIP-qPCR in Extended Knockdown Studies (Related to Figure 5)

Gene of pCBS; Genome Location (hg19)	Sequence (5' -> 3')	Amplicon Length
LTBP2 Chr14:75079440-75079547	For – GGAGCGCAGGGAGGTCC Rev – AGGGGATTGAGATCCAGAGC	108bp
TNFAIP3; Chr6:138190414-138190862	For – GCTGTGCCACAAAGGAAAGG Rev – TGCTGGGAAAGGCATAGTGG	139bp
FGF5; Chr4:81188069-81188400	For – TGGAGCAGAGCAGTTTCCAG Rev – ATTGACTTTGCCATCCGGGT	110bp
EPHA3; Chr3:89148142-89148548	For – AAGTTAAGCGAACACGAGCG Rev – GTCCAGGTGGCAAGGAGTAC	95bp
AMIGO2; Chr12:47473167-47473554	For – TCCGTGTCTGTCACTCTTGC Rev – CGGCTGCTTGAAACTCCTCA	103bp

Chapter V

General Discussion and Future Directions

General Discussion

In this thesis we characterized the effects of decreased CTCF expression in the prostate. We examined the effects of *Igf2* loss of imprinting in the mouse prostate, a change seen with aging and known to be mediated by loss of CTCF expression, demonstrating its functional impact in prostatic neoplasia. We evaluated, for the first time, the protein expression of CTCF, CHD8, and BORIS/CTCFL in human prostate tissues, showing altered regulation of these proteins and their potential as biomarkers for diagnosis and prognosis. Finally, we examined the alterations to genome-wide regulation of DNA methylation and gene transcription experienced with CTCF knockdown in prostate cells. In addition, using novel combinations of publically available data, we definitively demonstrate human tumors with CTCF loss experience an epigenetic signature of DNA hypermethylation at CTCF binding sites.

In chapter two, we presented a role for *Igf2* in early prostatic disease development. *IGF2* LOI has been known to occur in both normal and cancerous human prostate tissues for over two decades (1). However, prior to the studies presented here, an in depth determination of the *IGF2* loss of imprinting impact on disease development had not yet been performed in the prostate. In part, progression on this research was inhibited by an incomplete understanding of *IGF2* imprinting regulation. Understanding the role of CTCF in mediating imprinting regulation was pivotal for the development of animal models that physiologically mimic the effects of LOI seen with aging and cancer development (2,3). In this study we adapted these animal models for the study of *Igf2* LOI in the prostate.

We demonstrated, for the first time, *Igf2* LOI increases rates of prostatic disease development as represented by prostatic intraepithelial neoplasia (PIN) in mouse prostate tissues. The specific finding of more individual foci of PIN, within mouse prostates

containing LOI, is an interesting finding as it may explain why prostates affected by cancer often have multiple distinct tumor foci. Our results indicate that organ-wide LOI, commonly experienced in the human prostate, can increase rates of proliferation in histologically normal prostate tissues. The impact of IGF2 on p-ERK and p-AKT signaling has been previously demonstrated (4), we found both of these signaling pathways may be upregulated by *Igf2* LOI in the prostate in a context dependent manner with *Nkx3.1* loss of function. Interestingly, we are not the first to demonstrate this distinct difference between *Nkx3.1*$^{+/+}$/*Nkx3.1*$^{+/-}$ and *Nkx3.1*$^{-/-}$ prostates (5). These results indicate IGF2 signaling may impact both p-ERK and p-AKT during disease development. Using benign and cancerous human prostate tissues, we further establish a positive relationship between IGF2 and these pathways, supporting the findings of our animal model analyses.

Prostate cancer is a disease that is notoriously difficult to prognosticate. Men at risk for prostate cancer identified by non-invasive screening techniques often undergo prostate biopsies to detect cancer. However, many men with positive screening tests will present negative biopsy findings. These patients often enter a viscous cycle of repeated screenings and biopsies until cancer is found, causing significant physical and emotional hardship. Our studies indicate *IGF2* LOI and elevated IGF2 levels may be a positive predictor of cancer development. Because this alteration is experienced in normal tissues, screening can potentially make use of negative biopsy samples, further identifying patients who are at increased risk of prostate cancer detection. These findings may also provide opportunities for early therapeutic intervention, potentially at the stage preceding cancer development.

In chapter three, we analyzed the expression of CTCF and two associated cofactors, CHD8 and BORIS/CTCFL, in human prostate samples. Prior to our studies, CTCF had previously been analyzed in only a few cell lines and tissue samples and none had utilized

automated IHC analysis which permits more objective quantification. Most frequently in breast cancer samples, where tissue staining demonstrated reductions in CTCF levels in lobular carcinoma *in situ* of the breast compared to normal tissues samples (6), however, a previous study noted a reduction in apoptosis in breast cancer cell lines presenting heightened CTCF expression (7). Our study found a non-significant reduction in CTCF levels from benign to cancer samples, and significant reductions in metastatic prostate cancer samples. Supporting a role for CTCF in the development of advanced prostate cancer.

This study also investigated the protein expression of the known CTCF cofactors BORIS/CTCFL and CHD8. *BORIS* is the mammalian paralog of *CTCF*, the 11 zing-finger DNA binding domains of CTCF and BORIS share almost 100% sequence identity, leading to almost identical DNA target recognition (8). Despite its similarity to the important chromatin insulator CTCF, BORIS function has remained elusive. It has been classified as a cancer testis antigen (CTA), expressed at low or undetectable levels in many adult tissues but is reactivated in many tumors and cancer cell lines (9,10). This reactivation is thought to be a result of CTCF and/or p53 loss in tumors, shown to negatively regulate *BORIS* expression (11). Ultimately, the consequence of BORIS binding to CTCF target sites is relatively unknown, but at specific sites, BORIS and CTCF have been shown to elicit opposite epigenetic responses (9,10). We detected significant increases in BORIS expression in prostate cancer tissues compared to benign. By comparing the ratio of BORIS and CTCF expression in human tissues, we also demonstrated increased BORIS compared to CTCF in both localized and metastatic cancer tissues. Further research is required to understand how increased BORIS versus CTCF may affect epigenetic marks

genome-wide, however, research suggests increased BORIS expression may have similar effects to CTCF decreases.

Similar to BORIS, changes in CHD8 expression may also modulate CTCF function. Ishihara *et al.* found CHD8 and CTCF interact at known CTCF target sites including the *IGF2-H19* region, *β-globin* locus control region, and promoter regions of *BRCA1* and *c-myc*. Further, loss of CHD8 expression leads to epigenetic changes similar to those seen with CTCF loss (12). The interaction between these two proteins is understudied, however a recent report compared ChIP-seq data for CTCF and CHD8 in T47D human breast cancer cells and noted 16.5% of CHD8 binding sites are enriched for CTCF while, representing only 4.4% of CTCF sites (13). We noted CHD8 expression was decreased in all disease states (HGPIN, localized cancer, metastases) compared to benign tissues. While CHD8 has been documented to influence epigenetic change, it remains unclear what role it plays at CTCF binding sites genome-wide. However, the changes in expression noted in our studies correlated with both disease progression and disease recurrence. Taken together, chapter three demonstrates CTCF regulation has an important role in prostate cancer, through changes in both CTCF expression and other factors that modulate its activity.

In chapter four, we further investigated the effects of decreased CTCF in prostate cancer. Building on the results of chapter three, we further looked at the status of *CTCF* in a large publicly available database of human prostate cancer samples from The Cancer Genome Atlas (TCGA). Copy number alterations and CTCF downregulation is frequent in these samples, further demonstrating a role for CTCF in prostate cancer. Methylation data identified hypermethylation at CTCF binding sites as a common event in these tumors. We modeled CTCF decreases *in vitro* showing similar results. Using bioinformatics analysis, we identified stress response pathways being particularly altered with CTCF decreases, we

further demonstrated these effects *in vitro*. This work demonstrates the effects of CTCF losses on the epigenome *in vitro* and in human tumors (TCGA data). Indicating that CTCF may be a major factor in mediating the focal hypermethylation events seen with cancer development. This work also demonstrates that short term reductions in CTCF levels can lead to DNA methylation alterations. An important finding as increasing research suggests factors such as inflammation, hormone signaling, and cellular stress pathways can modulate CTCF expression and function (14-18).

Taken together, these results suggest short term reductions of CTCF during acute and chronic stressors experienced with aging may be a main mediator of age-related epigenetic change. We found *IGF2* LOI impacts proliferation and neoplasia in the mouse prostate, and is a direct consequence of CTCF downregulation. Given this tight link, it is likely that *IGF2* LOI is a result of repeated CTCF expression alterations, and further, may be symptomatic of genome-wide epigenetic change in histologically normal tissues acting as a driver for cancer initiation. We initially hypothesized CTCF mediated epigenetic change is important for prostate cancer initiation, however, the studies presented here in breast and other cancers clearly point to a larger role in cancer progression than we originally thought. This role is demonstrated by the large number of primary tumors harboring CTCF copy number losses (Chapter IV) and significant loss of CTCF expression in metastatic tumor samples (Chapter III). It is likely, yet unclear, whether CTCF expression changes in cancer work through altering DNA methylation or through other CTCF mediated genomic regulation events.

Future directions

While several key questions have been answered in this thesis, many more questions have been raised as a result of the work presented here. New challenges have materialized with each chapter individually in addition to this work as a whole. First, while Chapter II is a culmination of over a decade of research by the Jarrard lab into *IGF2* LOI, key questions remain about *IGF2* as a biomarker, and its effects on intracellular signaling in the human prostate. Our studies found *Igf2* LOI increased p-ERK signaling in wild-type mouse prostates, but in the presence of other genetic alterations (*Nkx3.1*), p-AKT was increased. Meanwhile, human prostate tissues analyzed showed a stronger correlation between IGF2/p-AKT than IGF2/p-ERK. It is unclear whether this is a physiologic difference between mouse and human prostate tissues or if the benign tissues, harvested from prostates containing cancer, harbor as of yet undiscovered alterations in *Nkx3.1* function.

NKX3.1 loss is prevalent in prostate disease progression and is noted at very early stages of neoplastic development (19,20), therefore, it is reasonable to hypothesize *NKX3.1* alterations may be present in some non-tumor human tissues analyzed in our study. Analyzing NKX3.1 expression of the tissue microarray used for IGF2/p-AKT/p-ERK staining may provide insight into the IGF2 signaling axis as it pertains to these tissues. NKX3.1 is known to negatively regulate AKT signaling, a potentially confounding factor in this analysis, however, finding tissues with intact NKX3.1 and elevated IGF2 levels may shed light on the preference towards p-ERK or p-AKT signaling in human prostate tissues. To further study prostate changes with aging progression, our lab has developed tissue microarrays containing prostate tissue from non-tumor prostate specimens of men ranging from 27 to 86 years old, removed for other reasons besides cancer. A majority of these tissues show

no evidence of cancer, and can be used to further define the relationship between IGF2 and downstream signaling markers in benign human prostate tissues.

Investigating IGF2 signaling in the human prostate is also a question that could be modelled *in vitro*. Prostate cancer cell lines exhibit a range of *NKX3.1* expressions (21). Established relative levels of *NKX3.1* expression in these cell lines could then be correlated with either p-ERK or p-AKT increases following IGF2 administration. To further examine this relationship, *NKX3.1* levels can be manipulated through overexpression or knockdown techniques to examine the change in IGF2 mediated signaling. These studies would elucidate both the role of IGF2 and the effects of *NKX3.1* status on p-ERK and p-AKT signaling in human prostate cells.

Our studies previously published and those presented in Chapter II point to a role for *IGF2* LOI in clinical applications. Specifically, *IGF2* LOI determination may provide further clinical use for patients presenting negative biopsies. The difficulty of utilizing *IGF2* imprint status in clinical applications will be in determining the best assay method. IHC staining has proved difficult to translate to clinical applications, while transcriptional analysis is also often challenging to standardize across patients. The most promising method may be using allele-specific (AS) mRNA quantification methods. We have previously described, in detail, using different methods for AS quantification (22). These methods are not without their own set of challenges, however, a retrospective study using negative biopsy samples could be used to correlate *IGF2* AS expression with subsequent cancer development. This assay could help better stratify patient risk and aid providers in follow-up decisions.

Chapters III and IV were focused more specifically on CTCF decreases, therefore their results taken together dictate future studies. Firstly, our results from Chapters III and IV confirm CTCF downregulation is a common finding in prostatic disease. However,

several questions remain with respect to changes in CTCF and cofactor expression. Specifically, our studies revealed CHD8 was significantly downregulated with PCa progression. The relationship between CHD8 and CTCF is largely understudied, with a single study showing CHD8 interacts with CTCF, and that CHD8 is required for CTCF-dependent insulator activity at specific target sites (12). This study also showed that loss of CHD8 leads to changes in DNA methylation and other epigenetic marks at CTCF target sites. Therefore, it is reasonable to hypothesize that CHD8 decreases in human prostate tissues modifies CTCF epigenetic regulation genome-wide. Investigation of this relationship could be modeled after Chapter IV studies, in which CHD8 knockdown would be performed *in vitro* followed by subsequent analysis of epigenetic regulation at CTCF target sites. It will be important to identify areas in which CTCF and CHD8 co-bind DNA, as ChIP-Seq studies have identified CHD8 does not bind all CTCF target sites (13).

Our results *in vitro* demonstrate CTCF knockdown results in DNA methylation changes at specific CTCF binding sites throughout the genome. Following 10 days of CTCF knockdown in HPECs, we have shown CTCF sites exhibiting a loss of CTCF binding experience increases in DNA methylation. These results and our methylation array, performed after 5 days of CTCF knockdown, demonstrate these DNA methylation changes can occur in a relatively short period of time. The results of these studies raise the possibility that transient reductions in CTCF levels may be responsible for age-related epigenetic alterations in the prostate. Dr. Bing Yang in our lab has shown CTCF expression is reduced following oxidative stress mediated by NFκB binding to the CTCF promoter (23). Leading to the question, can repeated environmental exposures induce CTCF-mediated alterations in DNA methylation and other epigenetic marks?

This question can first be modeled *in vitro* using oxidative stress administration in prostate cells. We would model these tests similar to what may be experienced *in vivo*, with multiple exposures with and without oxidative stress induction. Short term, low dose exposures will also help to minimize oxidative stress mediated cell death which can be seen with high levels or extended exposure. Our knockdown studies have elucidated genes that are sensitive to CTCF levels, and will provide a starting point for the analysis of gene transcription and DNA methylation analysis. One important question to answer prior to these tests is: How long is CTCF downregulated post oxidative stress? This can be robustly determined via time course experiments using differing levels of oxidative stress induced via H_2O_2 and western blotting for CTCF. These results would aid in modeling how repeated reductions in CTCF levels mediate epigenetic change with environmental stress, which may be one path to age-related DNA methylation alterations in the prostate.

One area that our group and others have not yet studied in depth is how CTCF influences other epigenetic marks in the prostate besides DNA methylation, such as histone modifications. Early research demonstrated CTCF mediated gene repression is accompanied by histone deacetylase recruitment (24). More recently, it was shown that depletion of CTCF is associated with increases in H3K27me3 at CTCF binding sites, resulting in gene silencing (25). Further research, has demonstrated this association may be dependent on CTCF influencing histone variant incorporation at local CTCF binding sites (26). In the work of others, site specific increased H3K27me3 and reduced H3K4me1 have been shown to occur with CTCF knockdown (25,27). Our current CTCF knockdown model could be used to investigate these relationships in prostate cells, using H3K27me3 and H3K4me1 ChIP-qPCR to interrogate genes influenced by CTCF knockdown. Interestingly, H3K27me3 has only one known methyltransferase, EZH2 (28), thought to be an epigenetic

driver protein in prostate cancer (29), which may provide a role for EZH2 and CTCF cooperation in driving prostate cancer development and progression. These studies could also help define whether CTCF mediated DNA methylation alterations depend on histone modifications or *vice versa*.

Finally, it will be important to determine whether CTCF loss or CTCF mediated changes can be used as a diagnostic or prognostic tool, or as a potential target for therapy. An important question to answer is: Do decreases of CTCF impact disease progression? We conducted a preliminary analysis using TCGA PCa samples, comparing samples with genomic copy number loss of CTCF versus tumors diploid for CTCF. Using disease free survival data, patients with CTCF loss tumors experience disease recurrence at a significantly faster rate than those patients with CTCF diploid tumors (Figure 1). These preliminary results indicate CTCF loss significantly impacts patient disease-free survival. Loss of CTCF genomic copy number in specific lesions could be an important risk indicator for patients with cancer. Therefore, it is possible that a CTCF related gene signature, either mRNA or methylation-based, develops impacting disease progression rates. A potential mRNA gene signature could be developed from our *in vitro* and *in vivo* analyses. For example, we could identify genes which are altered with CTCF knockdown *in vitro*, and genes that are altered in tumors with loss of CTCF copy number, and combine these results to generate a list of genes that are associated with CTCF loss. This gene signature could then be applied to external data sets, attempting to correlate a CTCF gene signature with patient prognosis. These results could be important for early prognosis of both disease development and progression. Importantly, this would definitively show that CTCF acts as a driver of cancer progression further emphasizing its clinical significance. Ultimately, the

work demonstrated in this thesis has opened numerous potential avenues for research that show immense promise for understanding and treating prostate cancer.

References

1. Jarrard DF, Bussemakers MJ, Bova GS, Isaacs WB. Regional loss of imprinting of the insulin-like growth factor II gene occurs in human prostate tissues. Clin Cancer Res **1995**;1:1471-8
2. Kanduri C, Pant V, Loukinov D, Pugacheva E, Qi CF, Wolffe A*, et al.* Functional association of CTCF with the insulator upstream of the H19 gene is parent of origin-specific and methylation-sensitive. Curr Biol **2000**;10:853-6
3. Pant V, Mariano P, Kanduri C, Mattsson A, Lobanenkov V, Heuchel R*, et al.* The nucleotides responsible for the direct physical contact between the chromatin insulator protein CTCF and the H19 imprinting control region manifest parent of origin-specific long-distance insulation and methylation-free domains. Genes Dev **2003**;17:586-90
4. Sachdev D, Yee D. The IGF system and breast cancer. Endocr Relat Cancer **2001**;8:197-209
5. Magee JA, Abdulkadir SA, Milbrandt J. Haploinsufficiency at the Nkx3.1 locus. A paradigm for stochastic, dosage-sensitive gene regulation during tumor initiation. Cancer Cell **2003**;3:273-83
6. Green AR, Krivinskas S, Young P, Rakha EA, Paish EC, Powe DG*, et al.* Loss of expression of chromosome 16q genes DPEP1 and CTCF in lobular carcinoma in situ of the breast. Breast Cancer Res Treat **2009**;113:59-66
7. Docquier F, Farrar D, D'Arcy V, Chernukhin I, Robinson AF, Loukinov D*, et al.* Heightened expression of CTCF in breast cancer cells is associated with resistance to apoptosis. Cancer Res **2005**;65:5112-22
8. Loukinov DI, Pugacheva E, Vatolin S, Pack SD, Moon H, Chernukhin I*, et al.* BORIS, a novel male germ-line-specific protein associated with epigenetic reprogramming events, shares the same 11-zinc-finger domain with CTCF, the insulator protein involved in reading imprinting marks in the soma. Proc Natl Acad Sci U S A **2002**;99:6806-11
9. Hong JA, Kang Y, Abdullaev Z, Flanagan PT, Pack SD, Fischette MR*, et al.* Reciprocal binding of CTCF and BORIS to the NY-ESO-1 promoter coincides with derepression of this cancer-testis gene in lung cancer cells. Cancer Res **2005**;65:7763-74
10. Vatolin S, Abdullaev Z, Pack SD, Flanagan PT, Custer M, Loukinov DI*, et al.* Conditional expression of the CTCF-paralogous transcriptional factor BORIS in normal cells results in demethylation and derepression of MAGE-A1 and reactivation of other cancer-testis genes. Cancer Res **2005**;65:7751-62
11. Renaud S, Pugacheva EM, Delgado MD, Braunschweig R, Abdullaev Z, Loukinov D*, et al.* Expression of the CTCF-paralogous cancer-testis gene, brother of the regulator of imprinted sites (BORIS), is regulated by three alternative promoters modulated by CpG methylation and by CTCF and p53 transcription factors. Nucleic Acids Res **2007**;35:7372-88
12. Ishihara K, Oshimura M, Nakao M. CTCF-dependent chromatin insulator is linked to epigenetic remodeling. Mol Cell **2006**;23:733-42
13. Ceballos-Chávez M, Subtil-Rodríguez A, Giannopoulou EG, Soronellas D, Vázquez-Chávez E, Vicent GP*, et al.* The chromatin Remodeler CHD8 is required

for activation of progesterone receptor-dependent enhancers. PLoS Genet **2015**;11:e1005174
14. Yang B, Wagner J, Damaschke N, Yao T, Wuerzberger-Davis SM, Lee MH*, et al.* A novel pathway links oxidative stress to loss of insulin growth factor-2 (IGF2) imprinting through NF-κB activation. PLoS One **2014**;9:e88052
15. Wang Y, Lu L. Activation of oxidative stress-regulated Bcl-3 suppresses CTCF in corneal epithelial cells. PLoS One **2011**;6:e23984
16. Del Campo EP, Márquez JJ, Reyes-Vargas F, Intriago-Ortega MD, Quintanar-Escorza MA, Burciaga-Nava JA*, et al.* CTCF and CTCFL mRNA expression in 17β-estradiol-treated MCF7 cells. Biomed Rep **2014**;2:101-4
17. Taslim C, Chen Z, Huang K, Huang TH, Wang Q, Lin S. Integrated analysis identifies a class of androgen-responsive genes regulated by short combinatorial long-range mechanism facilitated by CTCF. Nucleic Acids Res **2012**;40:4754-64
18. Chen J, Yao ZX, Chen JS, Gi YJ, Muñoz NM, Kundra S*, et al.* TGF-β/β2-spectrin/CTCF-regulated tumor suppression in human stem cell disorder Beckwith-Wiedemann syndrome. J Clin Invest **2016**;126:527-42
19. Iwata T, Schultz D, Hicks J, Hubbard GK, Mutton LN, Lotan TL*, et al.* MYC overexpression induces prostatic intraepithelial neoplasia and loss of Nkx3.1 in mouse luminal epithelial cells. PLoS One **2010**;5:e9427
20. Abate-Shen C, Shen MM, Gelmann E. Integrating differentiation and cancer: the Nkx3.1 homeobox gene in prostate organogenesis and carcinogenesis. Differentiation **2008**;76:717-27
21. Song H, Zhang B, Watson MA, Humphrey PA, Lim H, Milbrandt J. Loss of Nkx3.1 leads to the activation of discrete downstream target genes during prostate tumorigenesis. Oncogene **2009**;28:3307-19
22. Yang B, Wagner J, Yao T, Damaschke N, Jarrard DF. Pyrosequencing for the rapid and efficient quantification of allele-specific expression. Epigenetics **2013**;8:1039-42
23. Yang B, Wagner J, Damaschke N, Yao T, Wuerzberger-Davis SM, Lee MH*, et al.* A novel pathway links oxidative stress to loss of insulin growth factor-2 (IGF2) imprinting through NF-kappaB activation. PLoS One **2014**;9:e88052
24. Lutz M, Burke LJ, Barreto G, Goeman F, Greb H, Arnold R*, et al.* Transcriptional repression by the insulator protein CTCF involves histone deacetylases. Nucleic Acids Res **2000**;28:1707-13
25. Kim YJ, Cecchini KR, Kim TH. Conserved, developmentally regulated mechanism couples chromosomal looping and heterochromatin barrier activity at the homeobox gene A locus. Proc Natl Acad Sci U S A **2011**;108:7391-6
26. Weth O, Paprotka C, Günther K, Schulte A, Baierl M, Leers J*, et al.* CTCF induces histone variant incorporation, erases the H3K27me3 histone mark and opens chromatin. Nucleic Acids Res **2014**;42:11941-51
27. Handoko L, Xu H, Li G, Ngan CY, Chew E, Schnapp M*, et al.* CTCF-mediated functional chromatin interactome in pluripotent cells. Nat Genet **2011**;43:630-8
28. Kuzmichev A, Nishioka K, Erdjument-Bromage H, Tempst P, Reinberg D. Histone methyltransferase activity associated with a human multiprotein complex containing the Enhancer of Zeste protein. Genes Dev **2002**;16:2893-905
29. Yang YA, Yu J. EZH2, an epigenetic driver of prostate cancer. Protein Cell **2013**;4:331-41

Figure 1. Patients with tumors harboring CTCF copy number loss exhibit significantly faster disease recurrence.

Survival data matched to patient tumors of the TCGA analyzed by **(A)** Kaplan-Meier Survival Analysis demonstrated significantly shorter time to disease recurrence (Mean time to Disease Recurrence ±SEM; 132.2±3 months, CTCF CN loss; 161.7±1.2 months, CTCF Diploid; $P = 0.021$)

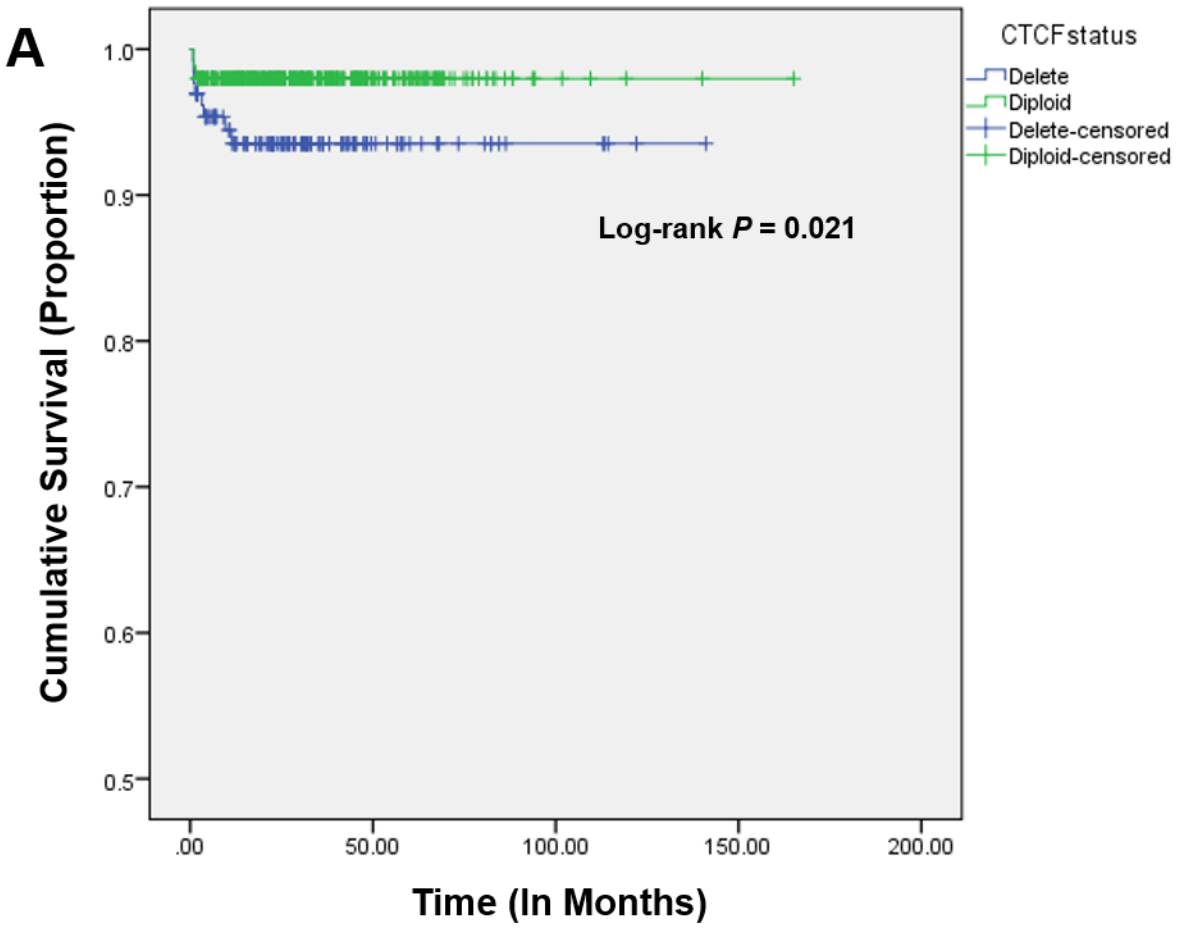
A
Cumulative Survival (Proportion)
1.0
0.9
0.8
0.7
0.6
0.5
.00
50.00
100.00
150.00
200.00
Time (In Months)
Log-rank P = 0.021
CTCFstatus
Delete
Diploid
Delete-censored
Diploid-censored